Short and Long Range Transport Effects in Salt Containing Solid-Liquid Composites

Von der Fakultät Chemie der Universität Stuttgart
zur Erlangung der Würde eines

Doktors der Naturwissenschaften
(Dr. rer. nat.)

genehmigte Abhandlung

Vorgelegt von
Christian Pfaffenhuber
aus Passau

Hauptberichter: Prof. Dr. J. Maier
Mitberichter: Prof. Dr. J. Bill

Tag der Einreichung: 04. März 2014
Tag der mündlichen Prüfung: 16. April 2014

Gewidmet
Meiner Frau Barbara und meiner Tochter Eva

Erklärung

Die vorliegende Doktorarbeit wurde vom Autor selbst in der Abteilung von Prof. J. Maier am Max-Planck-Institut für Festkörperforschung, im Zeitraum von Dezember 2009 bis Februar 2014 angefertigt. Der Inhalt ist die eigene Arbeit des Autors, Ausnahmen sind gekennzeichnet, und wurde noch nicht zur Erlangung einer Qualifizierung oder eines Titels an einer akademischen Institution eingereicht.

Stuttgart, 18. Februar 2014   Christian Pfaffenhuber

Declaration

The work described in this thesis was carried out by the author in the Department of Prof. J. Maier at the Max Planck Institute for Solid State Research from December 2009 to February 2014. The contents are the original work of the author except where indicated otherwise and have not been previously submitted for any other degree or qualification at any academic institution.

Stuttgart, February 18th 2014   Christian Pfaffenhuber

Contents

Abstract

This work is dedicated to the investigation of long-range and short-range ion transport in composite lithium battery electrolytes. In previous work it was shown that the addition of insulating oxide nanoparticles to liquid electrolytes consisting of lithium salt dissolved in a solvent with low dielectric constant can lead to a significant improvement of the electrical and mechanical properties. Furthermore, it was observed that the lithium transference number can be simultaneously increased. The effects were ascribed to the adsorption of the salt anions on the oxide particle surface coupled with enhanced dissociation of ion pairs resulting in the release of highly mobile lithium ions in the particle space charge zone. As the nanoparticles form networks due to their aggregation tendency the space charge zones eventually stretch throughout the electrolyte leading to an improved overall ionic transport.

The conductivity in these systems decreases over time due to unfavorable network restructuring, particularly in the case of rather high particle volume fractions. In this work it is shown that a conductivity increase is found in the course of time when the particle volume fraction in lithium perchlorate / tetrahydrofuran is low. As proven by different measurement techniques as well as by Monte Carlo simulation in combination with numerical FEM calculations, this can be assigned to the network formation process that is recorded in situ by means of ionic conductivity experiments. Furthermore, this system is used to successfully predict for the first time the expected conductivity and lithium transference number increase with help of literature data (such as association constant) based on the parallel switching model originating from solid-solid heterogeneous doping theory. Additionally, the already mentioned Monte Carlo simulation with adjacent numerical FEM calculation proved to be a good tool to investigate the relationship between the given particle characteristics such as its aggregation tendency and the resulting electrical properties of the composite electrolyte.

With respect to applied materials research, mesoporous materials with high specific surface areas are investigated as potential soggy-sand fillers. It is observed that such silica particles lead to a conductivity and lithium transference number increase that is comparable to the case when small nanoparticles are chosen for polyethylene glycol-150 system. The observed effects are ascribed to the additional ionic pathways provided by the highly porous materials. It was found that the beneficial electrical properties are here coupled with tunable mechanical

properties (gel-like materials) making such materials suitable candidates for the application as lithium battery electrolytes.

Filler materials are investigated with respect to their Ion Exchange Capacity allowing for more detailed insights in their capability to adsorb anions. Linked to this, it is shown that the ion adsorption on particles in composite leads to a decrease of the salt concentration in the bulk electrolyte resulting in a conductivity decrease therein. This effect of salt exhaustion especially plays a significant role for low lithium salt concentrations.

As ionic liquids have come into focus over the last years as potential battery electrolytes due to their high pristine room temperature ionic conductivity, heterogeneous doping of a model system is also investigated. Here, remarkably, the ionic conductivity can be kept constant in spite of the higher electrolyte viscosity.

With regard to measurements of the ionic diffusion in solid polymer electrolytes, as well as in pure liquid electrolytes, it has recently been proposed that also ion pairs contribute to the ionic conduction by means of a vehicular transport mechanism. In this work this effect is investigated for pure liquid electrolyte model system (lithium triflate in polyethylene glycol-150) which now allows for the determination of the contribution of individual ionic species to the overall ionic conductivity. The analysis is realized by the combination of results originating from tracer diffusion, AC and DC polarization experiments.

Zusammenfassung

Diese Arbeit widmet sich der Untersuchung des kurzreichweitigen und langreichweitigen Ionentransports in heterogenen Lithium-Batterie-Elektrolyten. In früheren Arbeiten wurde gezeigt, dass die Zugabe von nichtleitenden Oxidnanopartikeln zu flüssigen Elektrolyten, die aus gelöstem Lithiumsalz in einem Lösungsmittel mit niedriger Dielektrizitätskonstante bestehen, zu einer signifikanten Verbesserung der elektrischen und mechanischen Eigenschaften führen kann. Weiterhin wurde beobachtet, dass die Lithium-Überführungszahl dabei erhöht werden kann. Die Effekte wurden auf die Adsorption von Salzanionen an der Oxidpartikeloberfläche zurückgeführt, die den Dissoziationsgrad der Ionenpaare erhöht, was eine Freisetzung von sehr beweglichen Lithiumionen in der Raumladungszone der Partikel zur Folge hat. Da die Nanopartikel aufgrund ihrer Neigung zur Aggregation Netzwerke bilden, erstrecken sich die Raumladungszonen schließlich durch den gesamten Elektrolyten, was einen verbesserten Ionentransport ermöglicht.

Die Leitfähigkeit dieser Systeme sinkt mit der Zeit aufgrund der ungünstigen Netzwerkrestrukturierung, vor allem im Falle von relativ hohen Volumenanteilen der Partikel. In dieser Arbeit wird gezeigt, dass ein Leitfähigkeitsanstieg im Verlauf der Zeit registriert werden kann, wenn der Volumenanteil der Partikel in Lithiumperchlorat / Tetrahydrofuran gering ist. Wie mittels verschiedener Messtechniken sowie mit Hilfe einer Monte-Carlo-Simulation in Kombination mit numerischen Finite-Elemente-Berechnungen gezeigt wird, kann dies dem Netzwerkbildungsprozess zugeschrieben werden, der in situ unter Verwendung von Ionenleitfähigkeitsmessungen aufgenommen werden kann. Weiterhin wird dieses System dazu verwendet, zum ersten Mal den erwarteten Leitfähigkeits- und Lithium-Überführungszahlanstieg mit Hilfe von Literaturdaten (wie der Assoziationskonstante) vorherzusagen, basierend auf dem Modell der Parallelen Stränge, das seinen Ursprung in der Theorie der Heterogenen Dotierung in Festkörpern hat. Zusätzlich erweist sich die bereits erwähnte Monte-Carlo-Simulation mit nachfolgender FEM-Berechnung als ein nützliches Werkzeug, um die Beziehung zwischen gegebenen Partikelcharakteristiken wie der Neigung zur Aggregation und den daraus resultierenden elektrischen Eigenschaften des Kompositelektrolyten zu untersuchen.

Bezüglich der angewandten Materialforschung wurden mesoporöse Materialien mit hohen spezifischen Oberflächen als potentielle „Soggy-sand"-Füllstoffe untersucht. Es wurde beobachtet, dass solche Siliziumpartikel zu einem Leitfähigkeits- und Lithium-Überführungszahlanstieg führen, der mit denjenigen im Falle von deutlich kleineren Partikeln in einem Polyethylenglykol-150-System vergleichbar ist. Die Effekte werden den zusätzlichen Transportpfaden für Ionen zugeschrieben, die von den hochporösen Materialien zur Verfügung gestellt werden. Es wurde ermittelt, dass die guten elektrischen Eigenschaften mit veränderbaren mechanischen Eigenschaften einher gehen (gelartige Materialien), was diese Materialien als geeignete Kandidaten für die Anwendung in Lithium-Batterie-Elektrolyten auszeichnet.

Füllermaterialien werden hinsichtlich ihrer Ionenaustauschkapazität untersucht, womit tiefergehende Einblicke in ihre Fähigkeit zur Ionenadsorption gewonnen werden. Damit verbunden ist die Erkenntnis, dass die Ionenadsorption auf den Partikeln im Kompositelektrolyten zu einer Verringerung der Salzkonzentration im Volumen des Elektrolyten führt, was einen dortigen Leitfähigkeitsverlust zur Folge hat. Dieser Effekt der Salzverarmung spielt vor allem eine wichtige Rolle im Falle von geringen Salzkonzentrationen.

Da ionische Flüssigkeiten in den letzten Jahren als potentielle Batterieelektrolyte aufgrund ihrer hohen Ionenleitfähigkeit bei Raumtemperatur in den Fokus gerückt sind, wird die heterogene Dotierung eines Modellsystems ebenfalls untersucht. Bemerkenswerterweise kann die ionische Leitfähigkeit trotz der erhöhten Viskosität konstant gehalten werden.

Mit Bezug auf Messungen der ionischen Diffusion in festen Polymerelektrolyten sowie in reinen flüssigen Elektrolyten wurde jüngst postuliert, dass auch Ionenpaare zur Ionenleitfähigkeit mittels eines Vehikel-Transport-Mechanismus beitragen können. In dieser Arbeit wird dieser Effekt für das Modellsystem eines reinen flüssigen Elektrolyten (Lithiumtriflat in Polyethylenglykol 150) untersucht, wodurch nun die Bestimmung des Beitrages der individuellen ionischen Spezies zur Gesamtleitfähigkeit ermöglicht wird. Die Analyse wird durch eine Zusammenführung von Resultaten, die aus Tracer-Diffusions-, AC- und DC-Experimenten stammen, realisiert.

1 Introduction

1.1 Significance of Lithium-Based Batteries

A key factor in the modern world is electrical energy that is required not only in an increasing amount due to the permanent usage of devices in the industrial and private sector but also in terms of local storage flexibility. To fulfill the latter demand all possible ways of energy storage have to be taken into account. In that context, surprisingly, there are only limited possibilities for obtaining transportable energy in a sufficient quantity that are fundamentally distinct from each other. A classical way is offered by fossil fuels. They provide high energy densities and are still crucial in the field of automotive engineering for the realization of sufficient mobility ranges with satisfactory driving performances. Additionally, they play a major role for the continuous provision of electrical power in emergency power systems. In recent years their major drawbacks such as strongly limited disposability and resulting environmental impacts of their application led to fundamental political decisions treading new pathways for future energy storage. Key technologies for that purpose on which hopes are pinned are the fuel cell and battery technologies of which the latter is discussed in the following in more detail.

The demands for modern batteries are multifaceted and vary from each of their intended application sectors which are not only limited to electromobility but also comprise portable computers, mobile phones, cameras etc. They are expected to be of compact and light-weight design but still offering high energy and power densities. Furthermore, new developments in that field are supposed to aim at the usage of safer materials concerning their flammability and electrochemical stability.

In recent years the lithium ion battery technology became predominant in the handheld electronic device sector as it combines a high energy density at a high voltage and an impressive cycling stability apart from outstanding energy storage characteristics. The reason of the predominance of the lithium based technology originates in lithium's electrochemical superiority of fortunately being at the same time the most electropositive (-3.04 V versus SHE) and the lightest metal (equivalent weight of 6.94 g·mol^{-1}) leading to a high capacity.[1] Therefore, with the application of lithium ion batteries better performing devices can be

designed compared with lead-acid (1859, G. Planté) or nickel-cadmium batteries (W. Jungner, 1899). Some common battery types are presented in the volumetric energy density (Wh·l^{-1}) vs. specific energy density (Wh·kg^{-1}) plot by Tarascon and Armand [1] shown in Fig. 1.
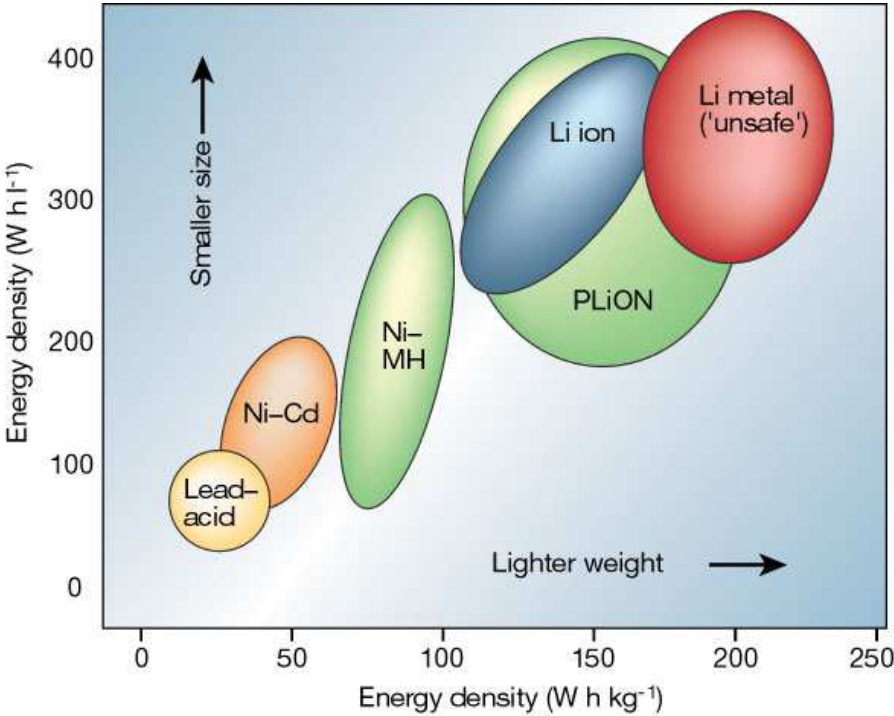
Fig. 1: Comparison of currently used battery technologies with respect to volumetric and specific energy density.[1]

Even though perceptible improvements of the respective energy densities are achieved which have led to the application of lithium ion batteries in portable devices in a predominant way increase of energy capacity is still required as it for instance sets a limit for the driving distance with an electric vehicle. Looking at the development of the specific energy density over the last decades for various battery technologies (Fig. 2) leads to the conclusion that Li ion batteries cannot keep pace with the improvements of electronic components which is often expressed by the Moore's law. Applied to the battery capacity, Moore's law would demand its doubling within 18 months.
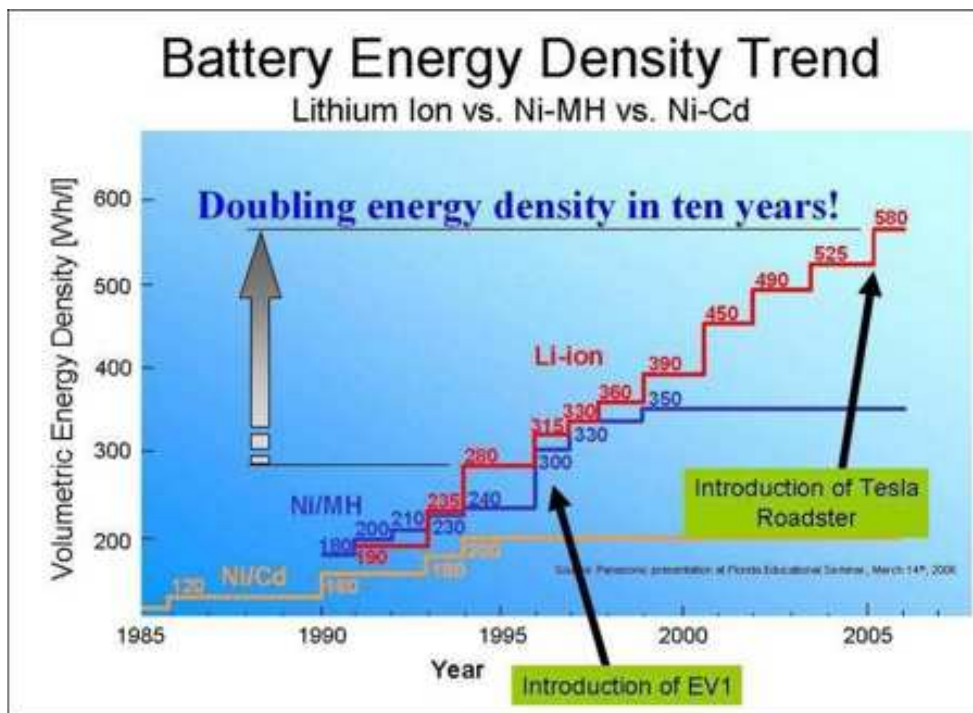
CPU Transistor Counts 1971-2008 & Moore's Law
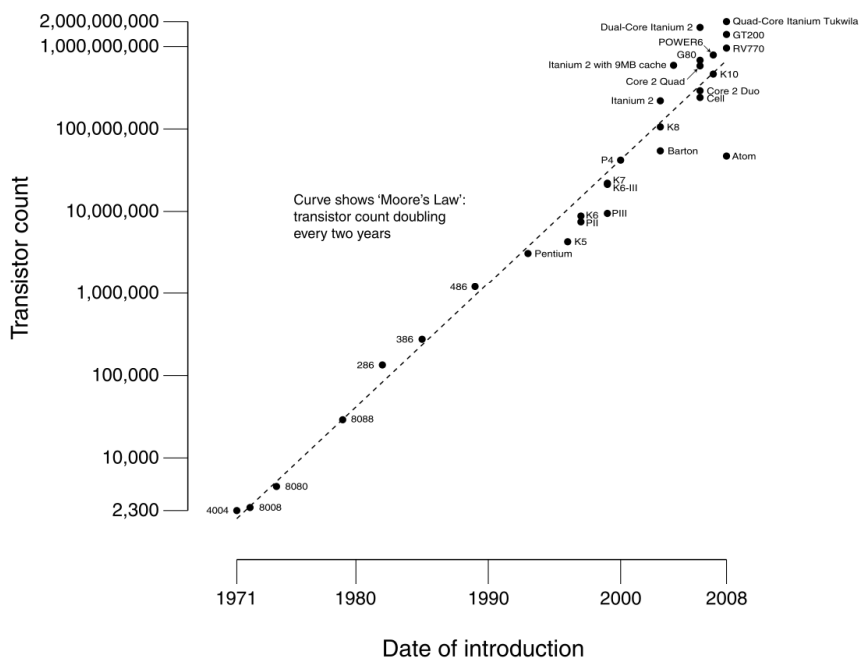
Fig. 2: Increase of energy density in batteries as a function of time (top)[2] compared with number of transistors on a microprocessor as a function of time (bottom).[3]

The reason for the slow improvement process is the complex and multi-facetted chemistry on which batteries are based. Thereby one key factor for further developments is the solution of

3

technical problems arising when solid and liquid materials are combined for energy storage under voltage.

The principle of the lithium battery is based on the reversible insertion and extraction of lithium ions into and out of active electrode materials – the anode and cathode – through electrochemical reactions (Fig. 3). Both electrodes are connected electrically to each other via a resistance through an outer circuit. The electrolyte often contains the lithium salt and serves to close the circuit and to efficiently transport the lithium ions whereas the separator avoids a direct contact between the electrodes which would lead to a short circuit.

The first commercial type of lithium batteries was introduced by M. S. Whittingham during his work for Exxon in the early 1970s based on experiments by G.N. Lewis in 1912.[4] In the full cell TiS_2 (cathode) and metallic lithium (anode) were used. Already in this approach one major problem occurred that still presents a major challenge in today's research. Due to chemical reactions at the anode with the organic liquid electrolyte a self-growing dendritic solid electrolyte interphase (SEI) is formed. The dendrites not only reduce the battery capacity during each charge/discharge cycle but also create short circuits between the electrodes resulting in ignitions and even explosions. As a result not only different electrode materials with better performance and safety have been investigated (e.g. the $LiCoO_2$ cathode at 4 V leading to the rocking-chair lithium battery proposed by J. Goodenough et. al. [5-7] presented in Fig. 3 which dominates today's battery technology) to circumvent this problem but also new types of electrolytes with less reactivity and high ionic conductivity have come into focus of interest.
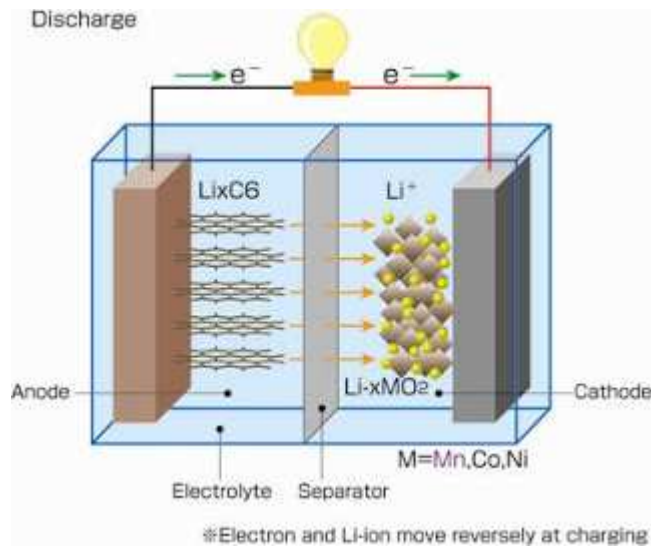
Fig. 3: Principal setup of a lithium-ion battery with negative graphite (Li_xC_6) and positive Li_xMO_2 (M = Mn, Co, Ni) electrode bordering the liquid non-aqueous electrolyte which contains a separator to avoid electrical short circuits. [8]

Due to the limited and locally unbalanced availability of lithium worldwide and its rather expensive exploitation the total price for a lithium-ion battery is still high. It achieved its commercial breakthrough by Sony Corporation in 1991. [1] The type of battery presented at that time is still the predominant lithium-ion battery setup in high-performance portable electronic devices. [1] It has an open circuit voltage of 3.6 V and a gravimetric density of 120-150 Wh·kg^{-1}. The performance is satisfactory for portable electronics but especially the low energy density leads to high weights in the sector of electric vehicles as large lithium-ion battery stacks are needed.

Therefore present research is focused on finding new battery materials providing promising electrochemical characteristics. Even though major efforts in lithium battery research are directed towards the search for new or further improved electrode materials like $LiFePO_4$ (~170 mAh/g at 3.5 V) [9, 10] and respective electrodes for the lithium-sulfur (500-600 Wh·kg^{-1} technically achievable) [11] or the more visionary lithium-oxygen battery (up to 15 times the energy density compared to lithium-ion batteries) [12], the electrolyte remains a crucial component as sufficient ionic transport combined with electrochemical stability of the whole system are key factors for the applicability of a battery system.

1.2 The Role of the Electrolyte in Lithium-Ion Batteries

While the energy and the voltage a lithium-ion battery can provide is determined by the cathode and anode materials and their morphologies, and it is their scientific development for a new battery that is most often emphasized, the influence of the applied electrolyte is not to be underestimated with respect to battery performance and safety. For instance in the lithium-ion batteries, mentioned above, the couple $LiCoO_2$ (cathode, high lithium potential) and graphite (anode, low lithium potential) gives rise to the beneficial high voltage of 4 V. Yet both electrodes are characterized by their thermodynamic instability against almost all electrolytes. Aqueous and protic electrolytes are unsuitable due to their immediate reaction with lithium causing immediate inflammation and hydrogen formation, but also many typical organic solvents decompose on the anode side when the battery is charged. Only for selected solvents the applicability of lithium-ion batteries is ensured by their kinetic stability. The latter is provided by the formation of the solid-electrolyte interphase (SEI), a layer on top of the electrode which is composed of products of the reaction between the electrode and whose structure is strongly dependent on the materials and still under investigation. SEI is electronically insulating but shows a perceptible ionic conductivity. This corresponds to an additional constant resistance for the battery but prevents the electrolyte decomposition after the first cycles. Yet under unfavorable operation conditions of the battery the problem of flammability is still crucial. The circumvention of this problem is therefore one of the key issues in the search for battery electrolytes.

As seen by means of the given examples, in general several demands are set to modern battery electrolytes that are sometimes even contradictory to each other. To lower the overall resistance of the battery cell it is important to ensure a high ionic conductivity within the electrolyte. [13] The desired chemical stability originating from the problem of uncontrolled SEI formation for new materials goes along with the demand for a good electrochemical stability. This means the reduction/oxidation insensitivity towards the large potential difference between the electrodes. Furthermore thermal stability of the electrolyte itself is required in the whole temperature range in which a battery is operating. Not least to reduce the costs for manufacturing lithium-ion batteries, naturally the materials used for creating a suitable electrolyte should be acquirable for a decent price.

To fulfill the practical requirements, the current scientific focus with respect to battery electrolytes covers the whole range from solid to liquid materials including intermediate stages.

1.3 Types of Electrolytes for Lithium-Ion Batteries

1.3.1 Pure Solid Electrolytes

Solid electrolytes often consist of polymeric matrices in which a lithium salt is incorporated. Thereby lithium is still able to move but with typically very low diffusivities resulting in low ionic conductivities. Their biggest advantage is their high mechanical and electrochemical stability. [14-18] However their contact area with the electrodes often is insufficient.

Plasticized gel electrolytes [19, 20] are – on the other hand – a materials class with which an attempt is made to create a solid polymer matrix in which a liquid component is contained to ensure a sufficient ionic conductivity with a satisfactory stability. Indeed they outmatch the classical solid polymer electrolytes (SPE's, e.g. $LiClO_4$ in high molecular weight polyethylene oxide) by orders of magnitude with respect to the ionic conductivity. However it is still under discussion if their chemical and electrochemical properties are sufficient to present a real improvement compared to the conventional liquid electrolytes that are described in the next chapter. [21] Instead of PEO also Polyacrylnitrile or Polyvinylidene fluoride are often used for gel electrolytes. With polymer electrolytes in general, one hopes for the simplification of battery cell manufacturing.

An additional fascinating class is represented by inorganic solid lithium ion conductors. Despite their comparatively lower conductivity their negligible electronic conductivity is a favorable asset; yet their grain boundary resistance as well as the electrode-electrolyte contact resistance may be critical. Popular examples are $Li_2S\text{-}SiS_2\text{-}Li_4SiO_4$ glasses [22] or $Li_{3.4}Si_{0.4}P_{0.6}S_4$.[23]

1.3.2 Pure Liquid Electrolytes

The ionic conductivity for salt containing liquid solvents in general – following the Stokes-Einstein Equation – is given as [24]

$$\sigma = \frac{z^2 e_0^2}{6\pi\eta r} \frac{N}{V} \tag{1}$$

with $z=1$ as the lithium ion is singly charged, e_0 being the elementary charge, η being the electrolyte viscosity, r being the ionic radius and $\frac{N}{V}$ being the amount of charge carriers per volume. According to Equation (1) the ionic conductivity is proportional to the number of charge carriers but inversely proportional to the overall viscosity. Hereby the problem of conflicting requirements for lithium battery electrolytes becomes evident. A suitable electrolyte needs to have a sufficiently high viscosity to reduce battery leakage and flammability which comes at the costs of a lower ionic conductivity. To still be able to use a certain electrolyte with a low viscosity, a separator (usually a polypropylene based membrane) within the battery is required which on its part reduces the ionic conductivity. Another approach is a solvent mixture such as the commercially widely-used combination of Ethylene Carbonate (EC) with Dimethylcarbonate (DMC) as solvent for a lithium salt such as LiPF$_6$. Especially the solid Ethylene Carbonate is characterized by a high dielectric constant $\varepsilon = 89$ [25] reflecting a principal strong ability to dissolve ion pairs which results in a large number of charge carriers. The latter aspect though is strongly dependent on the actual lithium salt as the dielectric constant does not make a statement on the specific solvent-salt interactions. To achieve an actual high conductivity, DMC is added for liquidating even though its own capability of ion pair dissociation and ionic transport is significantly lower.

When looking at more recently investigated types of liquid electrolytes a promising class is represented by ionic liquids [26] that are also addressed experimentally in this work (chapter 3.2.6). They consist of organic salts whose ions have delocalized charges and are bulky resulting in a reduced ability to form crystalline structures. As a consequence they are characterized by a wide liquid range. Typical examples for cations are imidazolium, ammonium or pyrrollidinium while for the anionic component often halides, trifluoroacetates or tosylates are applied. In the last years they came into focus for fuel cells, supercapacitors and batteries owing to their high ionic conductivity accompanied by a large electrochemical

window within which they remain stable versus redox reactions. Their salt-like properties provide good thermal stabilities but with contact to typical battery electrodes they show poor chemical stabilities which is one of the reasons for their limited applicability in the field of energy storage at present.

To summarize it depends on the actual application field whether liquid or solid electrolytes are preferable especially when the disclaimer of the battery separator is considered. In general the liquid electrolytes are beneficial to achieve high ionic conductivities. Additionally the equilibration of concentration gradients within the electrolyte occurs much faster owing to the higher diffusion coefficient. With use of liquid electrolytes the volume changes during electrochemical reactions within the battery hardly cause technical problems.[27] This is in particular important in the context of battery setups with the modern nanoelectrodes. They benefit from the ability of the electrolyte to penetrate well into the electrodes. On the other hand they require separators and the cell manufacturing has to be done with care due to leakage problems.

The ideal electrolyte would combine the advantageous properties of liquid and solid electrolytes. In the course of the research for such a material one is bound to concern oneself with the possibilities composite electrolytes offer. The investigations on these electrolyte mixtures and their properties to date are in the focus of the following chapter.

1.3.3 Solid-Liquid Composites as Electrolytes

All composite electrolytes have in common that they consist of a backbone material which is – to a certain extent – able to provide ionic conductivity. However this material does not exhibit enough mechanical/chemical stability or sufficient electrical performance which is the reason why further components are added to the basic material. As fillers typically electrically insulating metal oxide particles of different sizes and morphologies are chosen. Inspired by early work on composite ceramic systems, Weston and Steele were the first to report on composite electrolytes based on PEO and lithium perchlorate to which alumina (300 mesh) was added.[28] Surprisingly it has been shown that for certain material compositions in this work the conductivity could be maintained or even increased. As a result of following investigations on composite solid polymer electrolytes it has often been observed that the

filler particles are able to lower the tendency for the polymer matrix to form crystalline regions leading to amorphous areas which are obviously capable of quicker ionic transport. From this starting point intensive research has been done on composite electrolytes with different filler types and solvent/salt combinations.[29-31] In the case of liquid electrolytes the primary aim has often been to improve the mechanical and chemical properties for an expected decrease of ionic conductivity beforehand. However also here the ionic conductivity and also the lithium ion transference number were found to be increased. With knowledge of the principles for heterogeneous doping in ceramic systems that is briefly addressed in the next chapter, A. Chandra and J. Maier [32] presented a liquid-solid electrolyte, viz. AgCl filled with aqueous solution of $AgNO_3$, with a high conductivity combined with good mechanical properties.

Finally A. J. Bhattacharyya and Maier established the concept of Soggy-sand composite electrolytes for lithium batteries [29, 33, 34] advancing the search for new electrolyte compositions which combine their favorable mechanical properties, the chemical compatibility with the electrodes at the interface [32, 33, 35, 36], their ability to easily incorporate into the electrodes, promising ionic conductivities, and enhanced lithium transference numbers. The results are rather surprising at first glance as one would expect a loss of conductivity due to the fact that the inserted particles should simply increase the viscosity of the electrolyte, and hinder the ionic movements by blocking the pathways. However as described in the following sections the concept to describe the observed phenomena is by far more complex. It has been observed and will also be shown in this thesis that the properties of the composite electrolytes can be varied by the types and morphologies of applied materials (solvent, salt, filler) and their volume fraction.[36] To understand the investigated effects it is indispensable to consider and further develop fundamental concepts on the local and macroscopic scale as these can give a guideline to find the suitable composite electrolyte for certain requirements.

1.4 Concept of Heterogeneous Doping Serving as a Basis for the Soggy-Sand Model

The Soggy-sand model has been one of the rare cases in science in which the experimental findings could at least partly be predicted by a fundamental theoretical approach. This concept of heterogeneous doping [37] was established by J. Maier and served as the explanation for the unexpected strong synergistic conductivity effects in multiphase composites originating in solid-solid systems. It was found in early research attempts that the admixture of insulating oxides such as Al_2O_3 and SiO_2 to weak cation conductors such as Li-, Ag-, Tl- halides could strongly enhance their ionic conductivity.[37-39] When γ- Al_2O_3 was used the conductivity increased by several orders of magnitude at room temperature, in particular for mesoporous starting materials. Similar phenomena were observed for CaF_2 and PbF_2 when doped with SiO_2.[37-39] The concept to explain these findings focuses on the influence of the ionic space charge regions. They arise as a result of the different local free energies of a defect between the bulk (the interior of the starting material) and the grain boundary – i.e. the contact area – between particles of the main material and the oxide filler particle. As a consequence one ionic species (Li^+, Ag^+, Tl^+ for cationic conductors and F^- for anionic conductors) of the main material is preferentially adsorbed at the surface of the oxide filler causing an enhancement of the dissociation of ion pairs leading to a local increase of the ionic conductivity. Thereby the ions are removed from their energetic ground state represented by the ion pair. The mobile charge carriers at the interface determine its potential by their number and count as the majority charge carriers. In the solid-solid mixture it is furthermore known from literature that the oxide particles preferably arrange themselves at the grain boundary of the ionic conductors and in such a way that they create continuous pathways. From certain filler volume fractions (φ) on, often of surprisingly low value,[37, 40] ionic transport is possible from one electrode to the other via stable particle networks (Fig. 4).
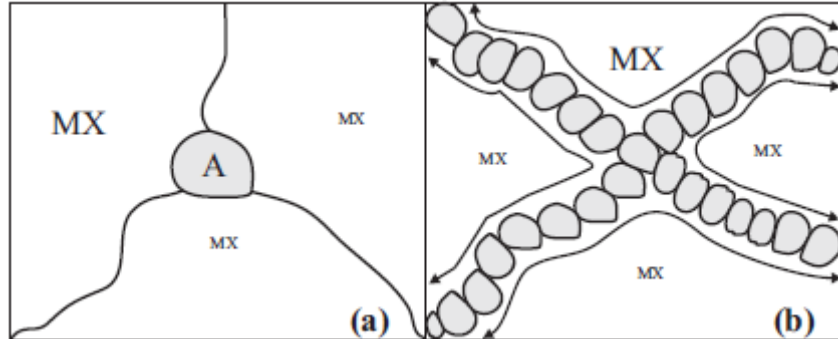
Fig. 4: Induction of highly conductive boundary layers on insulating filler particles by cation adsorption in the ionic conductor MX. a) Isolated A-grain. b) Formation of coherent paths between the MX grains.[40]

In such a case the overall conductivity σ_m can be approximated by

$$\sigma_m = (1-\varphi)\,\beta_\infty \sigma_\infty + \varphi \beta_L \sigma_L \tag{2}$$

Equation (2) arises from the assumption of ideal parallel switching between percolating pathways in the bulk with ionic conductivity σ_∞ and in the grain boundary with ionic conductivity σ_L. The factors β_∞ and β_L represent the portion of pathways that actually contribute to the ionic conduction out of all formed pathways in the bulk and at the interface respectively. Only with the fulfilled condition of continuous conducting pathways the ionic transport can – in an effective way – be extended from the local to the macroscopic scale.

Analogous effects have been observed or are assumed for composite electrolytes containing polymers (e.g. PEO) and lithium salt LiX.[16, 41-43] However, in these systems the picture is even more complex due to the fact that the ions in filler-free polymers are transported via the mechanisms of intrachain hopping in the course of which the polymer chain segments arrange themselves around the ion for reversibly coordinating it with suitable functional groups (e.g. electrostatic interaction of ether groups with the cation, entropy driven) and via the interchain hopping mechanism during which the ion is transferred between two individual polymer chains (Fig. 5).[18]
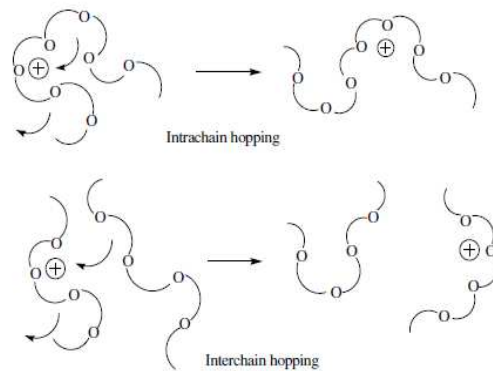
Fig. 5: Ionic conduction mechanisms in filler-free polyether electrolytes.[18]

As far as monomeric organic solvents are concerned the ionic transport is ensured by the motion of an ion together with its solvation cloud which consists of several solvent molecules. If the solvent features a rather low dielectric constant ε, a high amount of ion pairs in the bulk electrolyte is the consequence. Then, starting from the energetic ground state of the ion pair (Fig. 6, bottom) the dissociation of the salt is enhanced by the partial adsorption and trapping of one ionic species to the particle surface and the resulting release of lithium ions into a diffusive cloud around the particles (Fig. 6, top).

Fig. 6: Mechanistic (top) and thermodynamic (bottom) picture of Soggy-sand electrolytes.

The type of species that is adsorbed on the surface is strongly dependent on the chemical nature of the oxide filler. SiO_2 which has so far turned out to be the most effective heterogeneous dopant as it features hydroxyl (-OH) groups at the surface which are able to

preferentially adsorb salt anions.[33, 34] An indication for this is given in aqueous solution in which SiO_2 typically shows an acidic pH of zero charge ($\approx$ 3).[33]
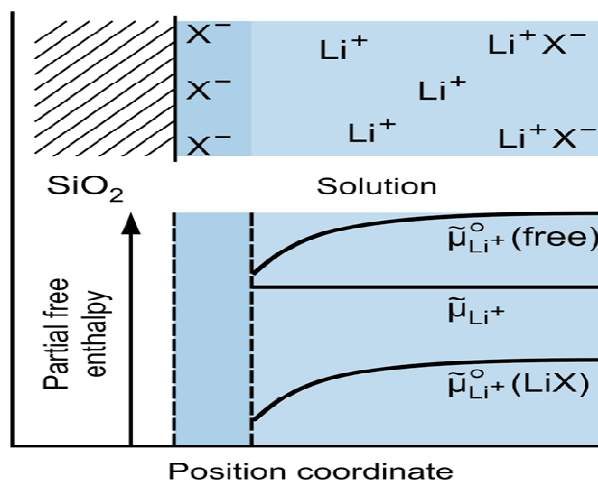
Local adsorption effects have been reported in $LiBF_4$ + EC/PC electrolyte systems doped with $BaTiO_3$ and Al_2O_3 with, however, very weak conductivity effects.[35] Interestingly, the same mechanism has also been confirmed by investigations of Beyazyildirim et. al. in the context of fuel cell electrolytes using imidazole doped with TiO_2 nanoparticles.[44] Thereby the anion was – in accordance with the results from the lithium electrolytes – adsorbed at the acidic filler particle surface (TiO_2, ZrO_2) resulting in an enhanced proton conductivity. The starting point in this context is the undissociated liquid (imidazole) being partly dissociated into H^+ and imidazolate.

In good accordance with the predictions on the effects on ionic conductivity from the concept of Heterogeneous Doping the first Soggy-sand electrolyte was developed by A. J. Bhattacharyya and J. Maier.[34] Even though earlier work on polyethylene oxide by other groups indicated that the addition of oxide fillers at least does not reduce the ionic conductivity or may even increase it very slightly.[45, 46] In the following years systems with various compositions have been explored that showed good agreements with the Soggy-sand model. Yet they also displayed the inherent complexity making the characterization non-trivial, especially with optical methods.[47] Even though this class of materials has not reached a status of technical applicability it is still promising for the Li-battery and solar-cell applications.[36, 48]

1.5 Colloid Chemistry in the Context of Composite Electrolytes

It is important to notice that the transfer of the Heterogeneous Doping concept from solid state to Soggy-sand systems is not without difficulties as the energetic ground state in the first case is represented by the regular ion whereas the ion pair takes over this role in liquid systems. It has been observed previously [30] that the practically achievable σ_m is significantly below the value that may be expected from Equation (2). This has been ascribed partly to the fact [31] that the particle networks in semi-solid Soggy-sand systems – in contrast to the networks in the pure solid state – are complex which strongly influence the ionic transport. To understand this phenomenon the principles of colloid chemistry that are taking effect in this context have to be considered.

In general terms, colloid chemistry is the scientific domain concerned with the synthesis and characterization of a dispersed phase within a continuous medium. Here the focus is restricted to solid particles with a size between 1 nm and few micrometers in a liquid phase. Under this condition dispersions can be created that appear to be homogeneous and are at least kinetically stable for long time periods. The typical adjustable screws for making new materials when focusing on one specific solvent are particle size, morphology and the chemically functional groups on the filler's surface. These properties determine the interactions between particles and the interaction between particle and solvent. The situation becomes significantly more complex if a salt is introduced as well.

A key feature of a particle for a promising applicability in colloid science is its surface-to-volume ratio. One should note that the gravitational force leading to sedimentation is given by

$$F_g = m_p g = (\rho_p - \rho_s) V_p g = (\rho_p - \rho_s) \frac{4}{3} \pi r^3 g \tag{3}$$

for spherical particles revealing that the gravitational force strongly depends on the particle size (ρ_p: particle density, ρ_s: solvent density). Equating Equation (3) with Stokes' law and solving to the sedimentation velocity v leads to

$$v = \frac{2 \Delta \rho g r^2}{9 \eta} \tag{4}$$

which includes a quadratic dependence on the particle radius but also an inverse proportionality to the overall viscosity. The increase of the latter in the course of particle admixture is more strongly pronounced for systems in which particles attractively interact with each other than for systems in which they are completely separated. Hereby the surface of the particle plays a major role.

When it features suitable functional groups such as hydroxyl or amine, ion adsorption and double layer creation are the consequence of the particle-solvent and particle-salt interaction. This influences the particle-particle interaction as the particles then carry an equal electrical charge and repel each to a greater extent and distance. As pointed out in literature, however the double-layer repulsion is not an energetic effect in the first place, rather an entropic effect owing to loss of diffusive zones.[49] The main attractive forces on the other hand are the Van-der-Waals and dipole-dipole interactions being dominant at short distance. The first arises from induced dipoles whereas the latter originates from polar functional groups at the surface. In the extreme case the particles can even form chemical bonds between each other (e.g. ether

bridges). Whereas the Van-der-Waals interaction for two point centers is characterized by a decay with a distance law characterized by high exponents it has been shown that for two extended spheres it decays according to $\propto \Delta^{-1}$ with Δ being the surface-to-surface distance.[49]

In any case, the underlying concept to describe the observed effects is the Derjaguin-Landau-Verwey-Overbeek (DLVO) theory.[50] It describes the particle interaction energy as a function of the interparticle distance when two particles approach each other owing to Brownian motion. The situation when such particles attract weakly is shown below (Fig. 7). The second minimum is usually less important and not considered here.
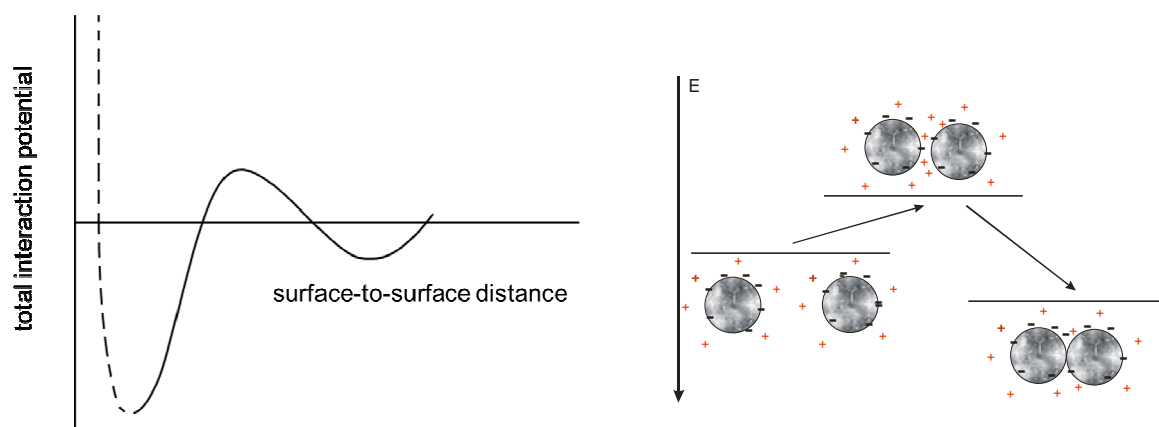

Fig. 7: Left: Typical interaction potential between two particles in a liquid medium in the case when particles attract weakly. This diagram represents the situation in Soggy-sand electrolytes. The dashed steep increase occurs on atomic interpenetration. **Right:** Model for two particles passing through an energetic maximum for aggregation.

Thereby the maximum arises from the repulsive Coulomb interaction which together with the arising loss of configurational entropy upon aggregation creates a maximum in the course of the particle approach.

It depends on the surface groups and particle morphology if particles can aggregate in a way that leads to coagulation by formation of large spherical clusters or in a way that the particles are able to form networks whose structure is significantly different from a spherical shape. If this condition is fulfilled fractal networks which are often very stable can be formed. This aspect is discussed in more detail in the next chapter. Here it suffices to state that the particle networks lead to a variety of rheological effects (e.g. shear-thinning, shear-thickening) that are beyond the Newtonian behavior and mechanically stiffen the system.

1.6 Network Structure and its Influence on the Ionic Conduction Mechanism

For the overall ionic conductivity enhancement it is, as mentioned before, not sufficient for a composite system to contain particles that can enhance the ionic dissociation. A long-range transport along the space charge layers of the particles is only possible if they are connected continuously (More precisely it suffices that they are almost continuously connected owing to the finite conductivity of the bulk phase (see chapter 3.1). A similar situation for the solid state was shown in Figure 4. Here it is expected and shown experimentally that one maximum of the curve showing the ionic conductivity as a function of the volume fraction φ is expected which is very sharp and steep. Below the critical volume fraction the conductivity is regarded to be negligible. This critical volume fraction is well-known as the percolation threshold for which the first continuous particle network is formed. σ_m can then be expressed by Equation (2). Yet if the depleted counter carrier can be neglected, σ_l, the conductivity in the space charge zone, can also be given as[37]

$$\sigma_l = u\Omega\Sigma \tag{5}$$

where u denotes the ionic mobility, Ω stands for the surface to volume ratio ($\Omega \approx 6/r$ for spherical particles) and Σ represents the charge density that can be adsorbed at the particle surface.

In the context of soggy-sand electrolytes the situation is more complex owing to the fact that β_L is a complex function of φ [36] as the character of the network structure can be more or less fractal in dependence of the type, but also of the total amount of particles. This leads to a varying number of pathways that can effectively contribute to the ionic transport. Even for two systems with the same composition it can by no means be expected to arrive at exactly the same ionic conductivity due to the mainly statistical network formation caused by the underlying hit-and-stick mechanism that is addressed again below. It has been observed that the percolation threshold for the soggy-sand electrolytes is reached for much lower φ in comparison with the solid state case (here, for both grain sizes being similar and the composite morphology being determined by a random mixture, $\varphi \approx 0.3$ is usually determined). Additionally the difference of the ionic conductivity at the space charge layer

and in the bulk electrolyte which is estimated for one example later on is rather small compared with the solid state as the ionic conductivity of the filler-free electrolyte is already high. Therefore ionic conductivities in the composite systems are usually measured that are typically not more than to five times higher in maximum compared to the filler-free solution. Regarding the principles of percolation in dispersions it is appropriate to reconsider the main physical influences on particle aggregation. The particles are moving due to their own Brownian motion and the fluidity of the surrounding solvent. Its velocity depends on temperature. The attractive forces between particles cause formation of clusters via aggregation. Over time these clusters aggregate with each other forming large networks. According to Smoluchowski's kinetic theory [51] and work by Witten and Sander,[52, 53] two basic mechanisms for aggregation can be distinguished that determine the final structure of a network at a given particle volume fraction. They represent the borderline situations whereby the aggregation mechanism within an experimentally investigated system usually exhibits both contributions. The first is the diffusion limited aggregation (DLA) in whose case the particle interaction is strongly attractive leading to an exclusive limiting of the aggregation process by the mutual particle/cluster diffusion. This mechanism then leads to fractal clusters. If the interaction potential shows an intermediate maximum and the potential minimum is not very deep the aggregation process is limited by the reaction rate (RLA). Here the aggregation rate is slow whereby the process can be reversible. As a basis of both mechanisms the already described DLVO theory which takes into account attractive van-der-Waals and repulsive Coulomb forces proves to be successful. Their strengths are dependent on the salt concentration, the type of particles and the solvent nature. It is worthwhile to mention that there is a thin line between aggregation and coagulation which is only dependent of the particle distance at which the potential minimum is present.

1.7 Motivation

For improvements of the conductivity and / or the mechanical properties of an electrolyte in a certain application field it is indispensable to investigate the fundamentals of the ionic interaction among dissolved ionic species but also with the solvent as it has often been observed that the electrolyte performance is poorer for a given electrolyte composition than expected by merely considering the dielectric constant. This leads to the conclusion that

gaining an insight into atomistic interactions in electrolytes using both experimental and theoretical approaches is required as a basis for the applied research.

This work is aimed at covering both fundamental problems as well as investigations on new composite materials classes for application in lithium-ion batteries.

As far as the fundamental questions are concerned the time-dependent conductivity increase in certain systems that has initially been found by accident is investigated in more detail with respect to network kinetics phenomena. Furthermore from the literature point of view an effort has been made to predict physicochemical properties of a Soggy-sand electrolyte which – when this approach can be generalized to a greater extent – could serve as a support for finding suitable composite electrolytes for a certain purpose. With the same objective also theoretical investigations on the interplay between network structure and physical properties on the basis of Monte Carlo simulations combined with Finite Element calculations are made. Concerning lithium-battery electrolytes in general, this work pursues the question that arose in recent years if ion pairs are really just an inactive species within an electrolyte with respect to ionic conductivity. Additionally efforts are made to elucidate the typical σ vs. φ as well as the t_{Li+} vs. φ-plots of Soggy-sand electrolytes in more detail especially for high particle volume fractions.

In terms of applied materials research two components that have previously not been used in the context of composite electrolytes are peered. On the one hand mesoporous filler particles appear to be suitable due to their high specific surface areas. Replacing the conventional solvents with the recently well noticed ionic liquids taking advantage of their fascinating electrochemical properties on the other hand appears to be a gainful approach as well.

2 Experimental Section

2.1 Electrolyte Materials

2.1.1 Solvents

In order to be applied as components in lithium battery electrolytes, solvents have to fulfill several conditions. Apart from the safety criteria such as high flash point and low toxicity it is essential that they provide sufficiently fast ionic transport. For that purpose, solvents were chosen that are characterized by a good solubility for the dissolved lithium salts leading to a satisfactory conductivity of the pure salt containing electrolyte are typically chosen. Even though protic solvents seem to be suitable at a first glance, their applicability is limited due to their high reactivity in contact with typical anode materials (RH + Li → Li$^+$ + R$^-$ + ½ H$_2$) such as lithium containing carbon leading to hydrogen formation. In addition to that, such solvents could lead to proton conductivity in addition to the salt conductivity which would not simply be an additional contribution to the overall conductivity but strongly influence the conduction mechanisms of fundamental interest, especially in the case of filler-containing materials. In recent studies,[30] poly(ethylene glycol)dimethyl ether, PEG-150 (M$_w$ = 150 g·mol^{-1}, CH$_3$O[C$_2$H$_4$O]$_n$CH$_3$, n~3, Fluka) as well as dimethylsulfoxide, DMSO (M$_w$ = 78.13 g·mol^{-1}, C$_2$H$_6$SO) proved to be suitable solvent components for Soggy-sand electrolytes. This is due to the fact that both solvents feature polar groups such as ether-linkage (−O−) in the case of PEG-150 or a sulfonyl group (−S(=O) −) as far as Dimethylsulfoxide is concerned. Additionally these solvents ensure a high electrochemical stability as they hardly undergo redox reactions.

An important part of the presented research is concerned with in situ recording of Soggy-sand effects that – as will be described later – are only recordable within solvents that have a very low dielectric constant. The perfect model systems for that purpose make use of THF as solvent as it fulfills the above condition, but, even more important, precise values for ion pair concentration for the system LiClO$_4$ + THF are available from the literature.[54]

Prior to the use, all solvents were distilled and kept in a glove box over molecular sieve (4 Å pore width) under argon atmosphere to prevent incorporation of water. The properties of used solvents (water content always <0.1% according to Karl-Fischer titration) are listed in Table 1.
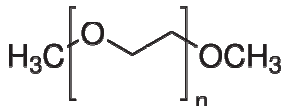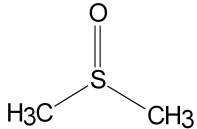
Solvent	Molecular Structure	Melting point T_m [°C]	Boiling point T_b [°C]	Viscosity η [cP]	Dielectric constant ε	Density ρ [g·cm^{-3}]
PEG-150	H$_3$C$[$O$-$CH$_2$CH$_2]_n$OCH$_3$	<-2	150	6.9	23.9	1.016
DMSO	H$_3$C$-$S($=$O)$-$CH$_3$	18.6	189	1.99[55]	46.5[55]	1.096
THF	(tetrahydrofuran ring)	-108.4	65.8	0.46[55]	7.43[55]	0.889

Table 1: Properties of solvents used in electrolytes at T = 25°C.

2.1.2 Lithium Salts

For the applicability of lithium salts in lithium battery electrolytes – apart from their chemical, electrochemical and thermal stability – it is crucial to ensure that they have good solubility in appropriate solvents. This property is highly influenced by the structure of the anion in such a way that it is beneficial if the negative charge is shared between several anion atoms. In that case, the attractive Coulomb force towards the lithium ion is lowered and the salt is more easily dissociated.

In addition to this aspect, it also has to be assured that the present dissociated ions show a sufficient mobility to reach a satisfactory conductivity of salt solutions.

In this study two lithium salts are used: lithium perchlorate (LiClO$_4$) and lithium trifluoromethane sulfonate (lithium triflate, LiF$_3$CSO$_3$).

2.1.2.1 Lithium Perchlorate

Lithium perchlorate (LiClO$_4$, Fig. 8) is a lithium salt commonly used for lithium ion battery electrolytes owing to its good solubility and high ionic conductivity in commonly used solvents (σ(1 M LiClO$_4$ + propylene carbonate (PC)) = 5.6 · 10^{-3} S·cm^{-1}, σ(1 M LiClO$_4$ + ethylene carbonate/dimethyl carbonate (EC/DMC)) = 8.4 · 10^{-3} S·cm^{-1}, σ(1 M LiClO$_4$ + DMSO) = 6.2 · 10^{-3} S·cm^{-1})[56, 57] combined with a high

Fig. 8: Molecular structure of lithium perchlorate.

electrochemical stability towards the anode.[56] Nevertheless, under harsh conditions such as high temperatures and high current charge, lithium perchlorate can act as an oxidant due to the high oxidation state of the chloride atom (VII). However, the salt is often employed under mild conditions where it is kinetically stable and not hygroscopic. The ionic radii are 0.060 nm for Li$^+$ and 0.236 nm for ClO$_4^-$.[18]

Lithium perchlorate (Sigma-Aldrich, purity: 99.99%) is kept in a glove box and used as received.
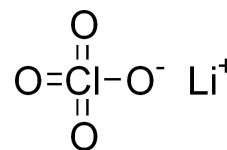

2.1.2.2 Lithium Trifluoromethane Sulfonate

Similarly to lithium perchlorate, within the anion of lithium triflate (LiF$_3$CSO$_3$, Fig. 9) the negative charge is shared between three oxygen atoms via mesomeric stabilization effects assisted by the strong inductive effect originating from the three fluorine atoms. Lithium

Fig. 9: Molecular structure of lithium triflate.

triflate is a convenient solute for fundamental investigations with respect to ion conduction mechanisms even though its conductivity in typically used solvents is lower than LiClO$_4$ (see Fig. 21 in chapter 3.1). This is due to the fact that the lithium atoms as well as the fluorine atoms can be used as tracers Pulsed Field Gradient Nuclear Magnetic Resonance (PFG-NMR) whose principles will be described below (see section 2.2.4).

Lithium triflate (Sigma-Aldrich, purity: 99.995%, trace metals basis) is kept in a glove box and used as received.
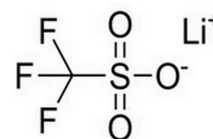
2.1.3 1-Ethyl-3-methylimidazolium trifluoromethanesulfonate (EMIM OTf) as a Model Ionic Liquid

Ionic liquids come into focus for battery applications in the last decade, 1-Ethyl-3-methylimidazolium trifluoromethanesulfonate (EMIM OTf, Fig. 10) is chosen as it not only shows one of the highest ionic conductivities [58] but is also well compatible with lithium triflate as it has the same anion which is detectable by ^{19}F-NMR while hydrogen atoms are contained solely by the cation allowing the cationic diffusion coefficient to be measured with ^{1}H-PFG-NMR.
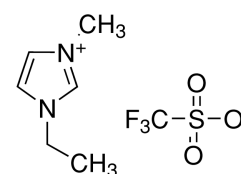
Fig. 10: Molecular structure of EMIM OTf.

1-Ethyl-3-methylimidazolium trifluoromethanesulfonate (Sigma-Aldrich, purity: ≥99.0%) is kept in a glove box and used as received.

2.1.4 Silicon Oxide Fillers

As shown in the introduction of this thesis, mechanical and electrical properties of the composite electrolytes are highly dependent on the choice of the filler material. Here silicon oxide is chosen with different morphologies and particle sizes due its high number of acidic surface groups (hydroxyl groups). The surface is schematically sketched in Figure 11. Some structural characteristics (particle size and density) of used silica fillers are shown in Table 2 while further structural details will be described in the result section.
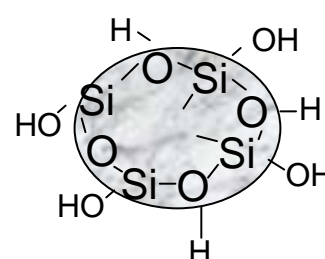
Fig. 11: Schematic presentation of a silicon oxide particle surface.

The density is measured with the help of a pycnometer (indicated by *) when it is not given by the manufacturer. The particles were dried at 300°C under vacuum for 24 hours (with exception of benzene bridged periodic mesoporous silica) before being kept in the argon filled glove box. After heat treatment the water content for all samples was around 100 ppm/g, as determined by Karl Fischer titration.

Type of silica filler	Particle size [nm]	Density [g·cm^{-3}]
SiO$_2$-fumed (Sigma-Aldrich)	7	2.44*
SiO$_2$ (Sigma-Aldrich)	100	2.46*
Benzene bridged periodic mesoporous silica (B-PMO) (synthesized by F. Hoffmann et. al.) [59]	~12000	2.54*
Mesoporous silica (MCM-41) (Sigma-Aldrich)	~200	2.6
Mesoporous silica (MSU-H) (Sigma-Aldrich)	~150	2.6

Table 2: Basic structural properties of investigated silica oxide fillers.

2.2 Experimental Techniques

2.2.1 Microscopic Techniques (SEM, TEM, CFM)

Scanning electron microscopy (SEM) and transmission electron microscopy (TEM) are used to gather information on size and morphological characteristics of the silica filler particles. Both techniques are based on the interaction of an electron beam with atoms and electrons of the sample. Field emission scanning electron microscope JEOL 6300F (Tokyo, Japan) was applied for SEM imaging.

For particles having sizes in the low nanometer range or containing mesopores TEM images have been recorded using a JEOL 4000EX (acceleration energy: 400 keV) and a Zeiss SESAM (Carl Zeiss) microscope (acceleration energy: 200 keV). Sample preparation was performed by dispersing particles in ethanol using an ultrasonic bath. The dispersion was then deposited on a conductive silicon wafer (SEM) or on a carbon grid (TEM) and dried before being investigated in a microscope under high vacuum.

Even though electron microscopy is suitable for particle characterization it is not possible to infer from the obtained results on their ability to form aggregates[36, 54] in the composite electrolyte. Finding a way to visualize the formed networks and the positions of particles in the liquid electrolyte is not a simple task as most of microscopy techniques are based on measurements under vacuum which do not allow for any liquid components.

An elegant way to characterize the structure of aggregates and particle networks in a composite electrolyte is the use of confocal fluorescence microscopy (CFM)[60] (Fig. 12)[61], a technique which is mostly used in the field of biochemistry. The advantage of such a technique lies in the principle of recording images with depth selectivity, the so-called optical sectioning. The quality of the obtained image is higher compared to conventional electron microscopy as the superimposition from multiple depths is prevented.

Fig. 12: Experimental setup of a confocal microscope.

In the confocal microscope, a laser beam is focused with help of an objective lens into a small volume within the sample. The beam stimulates an emission of fluorescent light from molecules incorporated into the bulk of the particles
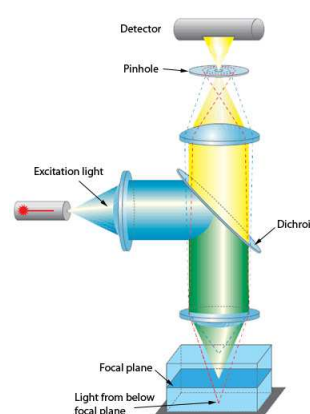
(described in more detail in section 3.1). Both reflected/scattered and the fluorescent rays are then re-collected by the lens and partly directed to a detector equipped with a selective filter for fluorescent wavelengths and finally to a photomultiplier tube which transforms the optical signal into a recordable image.

The images were recorded with an inverted AxioVert 200 M microscope (Zeiss). The fluorescence of the particles was stimulated with a Xe lamp and a no. 38 eGFP filter (Zeiss) with an excitation wavelength of 470 ± 40 nm, an emission wavelength of 52550 nm, and a beam splitter at 495 nm. The signals were detected with a 63x C-Apochromat 63x/1.20 W Korr UV-vis-IR object lens (Zeiss) and an ORCA-ER CCD camera (Hamamatsu).

2.2.2 Nitrogen Sorption Surface Analysis

To determine the specific surface area of the utilized nanoparticles, N_2 adsorption and desorption isotherms were recorded by an Autosorb-1 Quantachrome Analyzer. The analysis used in the thesis was based on the model of Brunauer, Emmett and Teller which describes the physical adsorption of gas molecules in form of a single layer on a solid surface.[62]

2.2.3 Differential Scanning Calorimetry (DSC)

For characterizing the thermal properties of pure and doped EMIM OTf the Differential Scanning Calorimetry (DSC) technique was applied. Data were obtained between -20°C and 60°C at a heating/cooling rate of 10 K/min by using a Pyris 1 scanning calorimeter (Perkin Elmer Life And Analytical Sciences, Inc.). For that purpose the samples were loaded into aluminum pans under argon atmosphere. After calibration with an empty aluminum pan, the thermograms could be recorded.

2.2.4 Pulsed Field Gradient Nuclear Magnetic Resonance (PFG-NMR)

The PFG-NMR represents an indispensable tool in the context of modern studies of dynamics in liquids and solids. This is due to the fact that the measured signal gives information on the translational motion of species containing the investigated isotope without being disturbed by

vibrational or rotational modes as those are taking place on time scales that are three to six orders of magnitude faster.

Another main advantage of this technique is the directly measurable self diffusion coefficient D (Tracer diffusion) not implying any atomistic models required for data analysis in contrast to other measurement techniques the interpretation of which requires additional information.

The random walk of a species without external influence due to diffusion is described by Fick's laws of diffusion [63]

$$\frac{\partial c(r,t)}{\partial t} = -\nabla \cdot J(r,t) \tag{6}$$

And for a constant D

$$\frac{\partial c(r,t)}{\partial t} = D\nabla^2 c(r,t) \tag{7}$$

(c denoting the of the isotope, J being the diffusion flux (amount of substance per unit area per unit time) and r indicating the position of the isotope) according to the Einstein-Smoluchowski Equation. The diffusion coefficient can be connected with the average square displacement to

$$\left\langle \left(r^2 - r_0^2\right)\right\rangle = 6Dt \tag{8}$$

To detect this motion two conditions have to met: (i) a detectable isotope (with gyromagnetic ratio γ) located at position r precesses with the Larmor frequency

$$\omega(r) = \gamma B(r) \tag{9}$$

with B indicating the magnetic field strength at r and (ii) the possibility of locally changing the magnetic field gradients to enable a detection of the spatial positions of the specific nuclei. The resulting Larmor frequency is then the sum of a frequency that is spatially independent and resulting from the homogeneous magnetic field B_0 and a spatially dependent term resulting from a magnetic field gradient G:

$$\omega_{eff}(r) = \omega_0 + \gamma(G \cdot r) \tag{10}$$

In this context great attention is to be paid to the spin echo technique as it ensures the refocusing of the magnetization in the created inhomogeneous magnetic field by the motion of spins. To measure the diffusion coefficients the most common Stejskal-Tanner spin echo diffusion technique is applied whose principle is shown in Fig. 13. Initially an ensemble of spins that diffuse within the sample is present. With application of a 90° radio frequency pulse

the macroscopic magnetization is flipped from the z-axis into the x-y plane. Afterwards a gradient pulse of duration δ is applied causing a phase shift for the spins before a 180° radio frequency pulse reverses the sign of the phase angle. With a further gradient pulse of equal strength and duration after a time interval of Δ from the first gradient pulse, an effective field gradient has been applied in total.
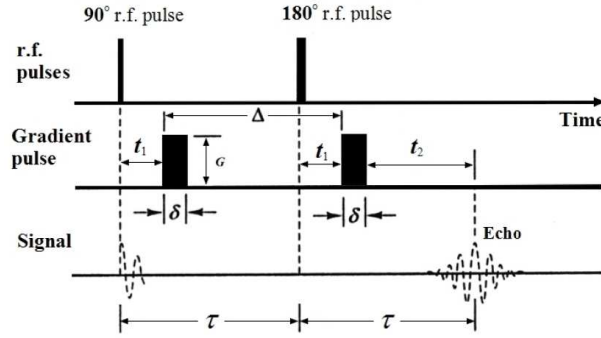

Fig. 13: The Stejskal-Tanner pulsed field gradient spin echo diffusion experiment[64]

As a result of the movement of the spins and of the attenuation due to spin-spin relaxation the intensity of the detection signal after $t = 2\tau$ is given by

$$S(2\tau) = S(0)\exp\left(-\frac{2\tau}{T_2}\right)\exp\left[-D(\gamma G\delta)^2\left(\Delta - \frac{\delta}{3}\right)\right] \tag{11}$$

in which the third factor contains the diffusion coefficient D whereby G, Δ and δ can be altered independently during the experiment. By plotting $S(2\tau)/S(0)$ as a function of G while keeping the other parameters constant, D can be determined.

2.2.5 Electrochemical Impedance Spectroscopy

Impedance spectroscopy is probably the most prevalent method for the characterization of electrical characteristics of samples.

If alternating voltage of small amplitude is applied to materials placed between two electrodes alternating current of the same frequency is created. It can be deconvoluted formally into one component that oscillates in phase and into another that is shifted in phase by $\pi/2$ with respect to the voltage. Thereby the relationship between the amplitude of the component of the current $\hat{I}_{0,real}$ being in phase with the voltage and the voltage amplitude $\hat{U}_0$ is proportional

to the real part $\sigma'(\omega)$ of the complex conductivity $\hat{\sigma}(\omega)$. This part can be calculated with help of

$$\sigma'(\omega) = \frac{\hat{I}_{0,real}}{\hat{U}_0} \underbrace{\frac{d}{A}}_{k} \tag{12}$$

The second quotient denotes the cell constant k that can be determined by calibration measurements. The real part describes the part of the dissipated energy. With an analogous definition of the imaginary conductivity ($\hat{I}_{0,imaginary}$ being the amplitude of the current's component which is shifted in phase by $\pi/2$)

$$\sigma''(\omega) = \frac{\hat{I}_{0,imaginary}}{\hat{U}_0} \frac{d}{A} \tag{13}$$

describing formally the energy stored within the system the total complex conductivity can be written as

$$\sigma(\omega) = \sigma'(\omega) + i\sigma''(\omega) \tag{14}$$

The specific impedance i.e. the impedance $\hat{Z}$ related to the geometric electrode parameters is given by

$$Z_s(\omega) = Z_s^{'}(\omega) - iZ_s^{''}(\omega) = 1/\hat{\sigma}(\omega) \tag{15}$$
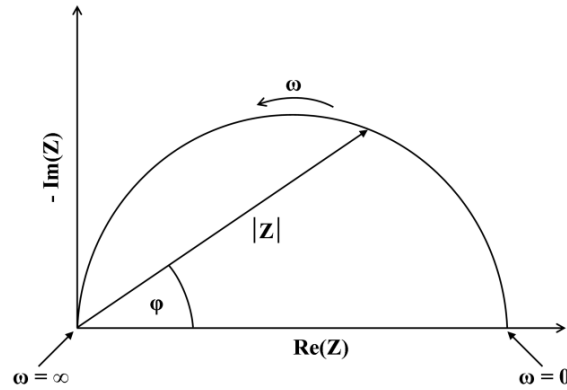
Fig. 14: Nyquist diagram of a circuit which consists of a resistor in parallel to a capacitor.

In the investigated electrochemical systems the main effects occurring can be described by capacitors and resistors. Therefore for variable frequencies the negative imaginary part of the impedance (ordinate) is plotted versus the real part of the impedance resulting in the so-called Nyquist diagram (also known as Cole-Cole plot, Fig. 14). It consists in the simplest case – a

pure charge transfer reaction (equivalent circuit: oscillating circuit containing a parallel connection of an ohmic resistor with a capacitor) – of a single semicircle.

The impedances of low frequencies are located at the right hand side of the plot and those for high frequencies at the left hand side. They can be presented by a vector pointing from the origin to the particular point on the semicircle and whose length gives the absolute value of the impedance. The phase shift is shown by the angle between the real axis and the vector. In such plots the frequency is an implicit parameter unlike in Bode plots which are characterized by plots of $\lg\left\|\vec{Z}\right\|$ and φ versus $\lg\omega$.

The impedance spectra of the investigated electrolytes usually do not show a complete semicircle as far as the bulk resistance is concerned due to the technically conditioned upper frequency limit. Similarly from the semicircle representing the electrolyte/electrode interface only the arising arc is observed as the ion blocking character of the electrodes causes a very large resistance.

Fig. 15: top: Equivalent circuit for investigated electrolytes. Bottom: typical impedance spectrum (0.1 M LiOTf + PEG-150, room temperature). Inset: impedance spectrum at high frequencies.

For data analysis the program Zview 2 is used. The equivalent circuit being the most suitable for the investigated electrolytes is shown in Fig. 15 (top) together with a typical impedance spectrum (Fig. 15, bottom) and described in the following. It consists of a frequency independent ohmic resistor R_0 which is very small and takes into account the resistance of cables etc. In series to this resistance a parallel circuit is contained that takes account of the real frequency dependent electrolyte resistance R_1 and the constant phase element CPE-1. For analyzing the interface situation a further parallel circuit follows with the elements featuring a real charge transfer resistance of the electrolyte into the electrode R_2 as well as a further CPE-2. In special cases the phase element can be substituted by a capacitor. Yet with this assumption the fitting of the data is inaccurate. The phase element has an impedance according to
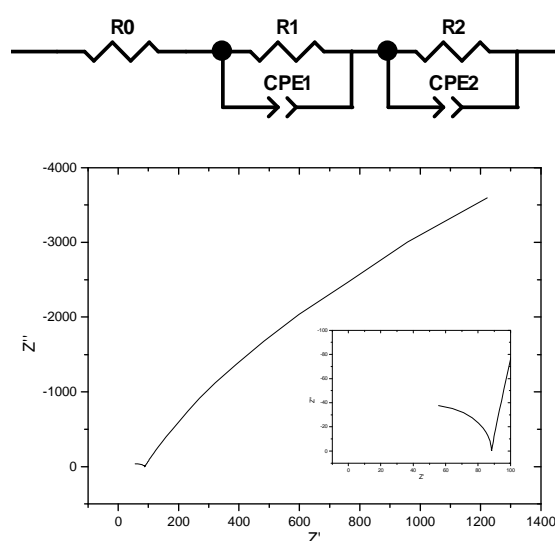
$$Z(\omega) = \frac{1}{Q(i\omega)^n} = \frac{1}{Q_0 \omega^n} e^{-\frac{\pi}{2}ni} \qquad (16)$$

(n: order) and the constant phase $(-90 \cdot n)°$. For $n=1$ the factor Q corresponds to the capacitance of a capacitor.

To interpret the elements of the equivalent circuit in the sense of material properties of the system physical and geometrical models have to be taken as a basis. In the case of the lithium conductors concerned here, space charge layers (rigid part) have to be considered in immediate surroundings of the nanoparticles. With that knowledge the total capacitance of this double layer system can be written as a series connection of two capacitors according to

$$\frac{1}{C_D} = \frac{1}{C_{rigid}} + \frac{1}{C_{diffus}} \qquad (17)$$

with C_D being the capacitance of the electrolytic double layer deriving from CPE-1, C_{rigid} being the capacitance of the rigid space charge layer and C_{diffus} denoting the capacitance of the diffusive layer. Generally, constant phase elements have to be taken, one reason is that the electrolytic structure varies in the surroundings of the particles or the vicinity of the electrodes.

The sample cells used for EIS consist of a gold plated vessel that can be sealed to avoid the penetration of air and moisture. It further contains two disc shaped gold-plate steel electrodes of which one is installed whereas the other is clamped from the top (see Fig. 16) whereby the electrolyte is located in between. After the preparation in the Glove Box the cell is installed into a sealed chamber through which Argon is led. The temperature of

Fig. 16: Sample cell with teflon ring for adjustment of a fixed electrode distance and electrode diameter.

the sample is measured by a thermocouple (PT100, resistance thermometer) placed in the proximity of the cell and balanced with the thermostat Lauda RC6CP enabling the realization of temperature differences less than 0.1 °C.

The recording of the impedance spectra was carried out with a Solartron SI 1260 Impedance/Gain Phase Analyzer and a Novocontrol High Resolution Dielectric Analyzer in the frequency range from 10 MHz to 100 mHz and at a load voltage of 0.1 V. Measurements could be run in software-controlled heating and cooling cycles or as a function of time in an automated way.

31

2.2.6 DC Polarization

A very important physical parameter for battery electrolytes in both applied and fundamental regards is the lithium transference number. Looking at the ionic radius of lithium in comparison with the typical salt anions, the cation is much smaller and should move faster through the electrolyte at first glance if the charges of both ions are equal. In reality this is not observed for most of the electrolytes. Rather normally the mobility of the anion exceeds that of the cation. This is due to solvation effects that are more severe if small and polarizing ions are considered. To identify the contributions of the individual species several experimental techniques are known of which some can only be applied for certain systems. These contributions are quantitified by the transference number, which is defined by

$$t_+ = \frac{i_+}{i_+ + i_-} = \frac{i_+}{i_{total}} = 1 - t_- \tag{18}$$

According to this Equation the lithium transference number is the amount of current transported by lithium i_+ in relation to the total current.

In this work composite electrolytes are investigated which are not appropriate for measurement techniques as the method of moving interfaces [65] or the Hittorf method [65, 66] due to the higher effective viscosity. Therefore the better suited DC polarization method described by Bruce and Evans is applied.[67-71]

In this situation lithium electrodes are used which are able to reversibly exchange lithium ions but are blocking the anions. The symmetrical configuration of this cell is

Li (metal) | Li$^+$X$^-$ containing electrolyte | Li (metal)
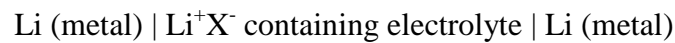
The applied electric field difference in this two electrode setup affects both ions in the same way. Therefore the transference number according to Equation (18) can also be written in terms of ionic conductivities, as for a parallel switching $R = R_+ R_- / (R_+ + R_-)$:

$$t_+ = \frac{\sigma_+}{\sigma_+ + \sigma_-} = \frac{\sigma_+}{\sigma} = \frac{R}{R_+} \tag{19}$$

If such a setup is polarized with a DC voltage ΔV the total conductivity of the electrolyte can be determined at the time t = 0.

Over time the initial current drops until a constant equilibrium current is reached which only originates from the non-blocking ionic species. The applied voltage causes the migration of ions in the electric field. As the lithium electrodes are only reversible for Li ions the anions accumulate at the anode lowering their concentration at the cathode. Due to this effect a concentration gradient is established.[71, 72] Therefore the motion of the anions is reduced and eventually comes to a complete stop. As a result the lithium ions are the only conducting species whereby the electric current is reduced.

For the analysis of the DC polarization an assumption is made, namely the influence of ionic interaction is neglected, but will be later addressed in detail (chapter 3.3). In that case and for a potentiostatic situation the initial overall resistance is given as

$$\frac{\Delta V}{I_0} = R_{SEI,0} + R \tag{20}$$

with ΔV indicating the applied potential difference between the electrodes, I_0 denoting the initial current. Eq. (20) also takes account of serial (initial) interface resistance due to passivation layers (solid electrolyte interphase, SEI) at the electrodes ($R_{SEI,0}$). R is the total electrolyte resistance characterized by a parallel connection of anionic resistance R_- and cationic resistance R_+. In the steady state the overall resistance is

$$\frac{\Delta V}{I_\infty} = R_{SEI,\infty} + R_+ \tag{21}$$

whereby $R_{SEI,\infty}$ refers to the SEI-resistance in the steady state. Combining the Equations (19), (20) and (21), t_+ can be deduced from

$$t_+ = \frac{I_\infty \left(\Delta V - I_0 R_{SEI,0} \right)}{I_0 \left(\Delta V - I_\infty R_{SEI,\infty} \right)}. \tag{22}$$

Equation (22) is valid for real cells in which processes taking place at the electrode surface can be mainly ascribed to the charge transfer and the ionic conduction through the dynamic passivation layer, i.e. an intrinsic electrical resistance of the passive film.

$R_{SEI,0}$ is determined experimentally first from initial AC conductivity measurement by analyzing the real resistance of the second semicircle which corresponds to the interface resistance. Afterwards the DC experiment is carried out to obtain the initial I_0 and I_∞ values. For that purpose a Keithley 6487 Picoammeter is used to record the current during a time

period of 10 hours at a potential of 10 mV. Finally $R_{SEI,\infty}$ is determined by a further impedance measurement in the steady state.

2.2.7 Electroacoustic Spectroscopy as a Measurement Tool for the ζ-Potential

A condition for the mechanical stability of dispersed particles in the liquid is the formation of an electrolytic double layer such as diffusive charge clouds consisting of cations which have been created due to the adsorption of anions on acidic particle surfaces. The cations are not all arranged within the outer Helmholtz layer but arranged within the diffusive double layer extending from there to the bulk. The potential difference between the outer Helmholtz layer and the bulk electrolyte is the so-called ζ-potential. It can be measured by exerting external electric or acoustic fields. Acoustic stimulations cause particles to carry out movements relative to the liquid whereby they are momentarily shifted away from their diffusive double layer. This causes the creation of reversible dipoles (Fig. 16, bottom). As the ζ-potential increases with the surface charge, with its help the kinetic stability of dispersions may be estimated. It is known [73] that from high absolute values of the ζ-potential (|ζ| > 30 mV) particle aggregations are relatively improbable due to strong double-layer repulsion. In non-polar systems the diffusive layer is rather extended due to the low ionic concentration in the dispersion and resulting low screening.

To determine the ζ-potential a method is applied that is based upon the electroacoustic phenomena and does not rely on a high sample dilution (Fig. 17). For that purpose an ultrasonic wave (frequency 3 MHz) created by a piezoelectric transformer out of an AC voltage spreads through the electrolyte. If it thereby hits a particle it causes it to move. This translation induces electric potentials at the particles according to the Debye-Hückel theory.[74] Due to this effect a measurable alternating current, the colloidal vibration current (CVI), is induced. The latter is measured as a

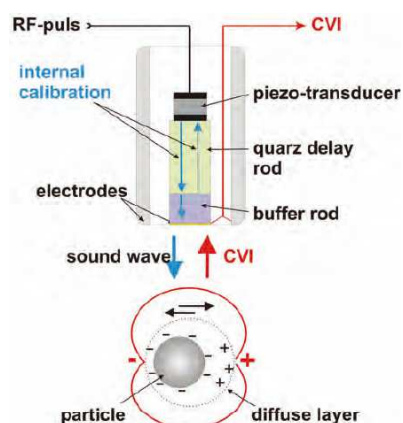**Fig. 17:** Top: experimental setup for ζ-potential measurements. Bottom: charge redistribution around a particle due to irradiation of sound waves.

colloid vibration potential (CVP) between a stainless steel electrode and a gold electrode.[75-77]

The theoretical basis has been given by Enderby and Booth [78] and later by O'Brien.[79] In this approach the dynamic electrophoretic mobility μ_D is introduced and connected to the CVI (k: cell constant, $\rho = (\rho_p - \rho_m)\rho_m^{-1}$, ρ_p: particle density, ρ_m: liquid density, $|\nabla P|$: pressure gradient of the sound waves):

$$CVI = k\rho\varphi\mu_d |\nabla P| \tag{23}$$

For $\kappa r \square 1$ (κ: reciprocal Debye length, r: particle radius), i.e. for thin double layers, it was shown [76, 77] that μ_d is connected with ζ via

$$\mu_d = \frac{2\varepsilon\zeta}{3\eta}\left(1 + f(\lambda, \omega')\right) \tag{24}$$

with η denoting the dynamic viscosity and f being a complex function of the surface and bulk conductivity. The ζ-potential is measured by using the DT-1200 (Dispersion Technology, Inc., Quantachrome) experimental setup.

2.2.8 Rheological Measurements

Important aspects of appropriate battery electrolytes are – apart from the electrochemical properties and safety issues – the mechanical characteristics. A common experimental procedure in this context is the analysis of the rheological properties.

In such measurements the viscosity η is obtained by measuring the shear stress τ as a function of the shear strain rate $\dot{\gamma}$ (varied from 2-1000 s^{-1}) using a cone-plate configuration (Haake RheoStress 1, Fig. 18[80]). Here the flat cone rotates while the lower plate is fixed. With help of a force sensor the stress in the normal direction can be derived. The main advantage of the cone-plate configuration is the locally homogeneous distribution of the shear strain rate.

Fig. 18: Geometrical setting of a cone plate viscosimeter.

In the setup τ is obtained by measuring the torque M_d required for rotating the cone (radius R) at a

certain strain rate according to:

$$\tau = \frac{3M_d}{2\pi R^3}$$

(25)

The viscosity as a function of the shear strain rate $\dot{\gamma}$ can then be derived as

$$\eta = \frac{\tau}{\frac{dv}{dy}} = \frac{\tau}{\dot{\gamma}} = \frac{3M_d}{2\pi R^3} \frac{\tan \Psi_0}{\Omega}$$

(26)

(Ψ_0: angle between cone and plate, Ω: angular velocity of the cone)

2.3 Simulation Approach for Investigations of Properties of Soggy-Sand Electrolytes Based on Monte Carlo Algorithm and Finite Element Analysis

2.3.1 Monte Carlo Method and Aggregation Models

In this thesis the "Monte Carlo" technique was used to model the formation of the percolating oxide clusters due to the "random walk" of oxide particles. The "Monte Carlo Method" term was used at first by the physicists N. Metropolis, S. Ulam and von Neumann [81] to model stochastic processes. Their calculations predicted the flux of neutrons in an atomic bomb. The flow of neutrons following random paths through a mass of uranium molecules could only be modeled on a computer and not predicted from theory.[82] Despite having most of the necessary data, the problem could not be solved with theoretical calculations. However, with the computer technology a solution was found by means of the Monte Carlo computer simulation.[83] Monte Carlo simulation methods are useful for modeling phenomena with significant uncertainty in inputs and/or systems with a large number of coupled degrees of freedom. Those techniques are often the only practical way to sample random variables governed by complicated probability density functions.

A key idea in colloidal science that launched the study of particle aggregation and gelation is that of fractal formation.[52, 53, 84] Witten and Sander[52] made a breakthrough by proposing the Diffusion-Limited Aggregation (DLA) model. In this model a particle is released from the rim

of a simulation box and allowed to diffuse (via random walk). When two diffusing particles hit one another, aggregation occurs. One of the famous Witten and Sander fractals, obtained by "Monte Carlo" technique is shown in Fig. 19.[52]

Fig. 19: Fractal cluster from Witten and Sander created by the random aggregation of 3600 particles on a square lattice.

The shown cluster has a fractal dimension of 1.7. In the end of a simulation based on the pure DLA model, particles either stick to an initial "seed" particle or disappear. Due to iteration, a fractal cluster is formed. It was shown by Weitz et. al.[85] that this model is able to analyze the structure of real particle aggregates.

In this simple DLA model, two colloidal particles always bind irreversibly upon meeting. In more advanced approaches, the binding probability is less than unity allowing for subsequent debonding.[86] Even though this phenomenon is often denoted as Reaction-Limited Aggregation (RLA), this term is only appropriate if the binding/unbinding process is sluggish compared with diffusion.

Furthermore in the process of cluster-cluster aggregation (CCA) model also clusters are able to diffuse and bind. In the case of diffusion being the rate determining process, the situation is termed diffusion-limited cluster aggregation (DLCA). This computational model was independently developed by Meakin et. al. [87] and Kolb et. al. [88] to describe fractal growth.

In the last years modeling of the formation of fractal [84, 85, 89] networks and their stability has been performed in solid [90, 91] as well as in liquid [92] composite electrolytes. However the latter simulation is restricted to cases in which the aggregation process can be separated temporally from the coarsening steps. Additionally the hit-and-stick mechanism is irreversible

and is based on a purely statistical approach which does not account for material specific properties in experimentally investigated composite electrolytes.

A further study of the local space charge zone overlap in these and similar nanocomposite systems [93] has been published by Goodyer et. al.[94] The understanding of how the external parameters (such as type and amount of particles, solvent, salt concentration) have to be adjusted to achieve a certain conductivity enhancement in a composite electrolyte compared to the particle-free electrolyte is of great importance, especially in the case of Soggy-sand electrolytes. Additionally it is not only the sheer conductivity enhancement which is of interest for basic research but also other features, such as the fractal dimension of the cluster, its percolation probability, the average amount of neighbors of one particle within the cluster etc.

However, so far the knowledge of the above relationships is only limited, mostly due to the restricted experimental possibilities to time-dependently observe the particle aggregation.[95] Here a Monte Carlo [81] approach is presented to simulate the aggregation and coarsening process in dependence of time, particle volume fraction and type of particles. In a second step conductivity of the so obtained network structures are analyzed by further numerical calculations. The simulation gives an insight how to choose materials in the experiment in the context of Soggy-sand electrolytes to achieve certain physical properties.

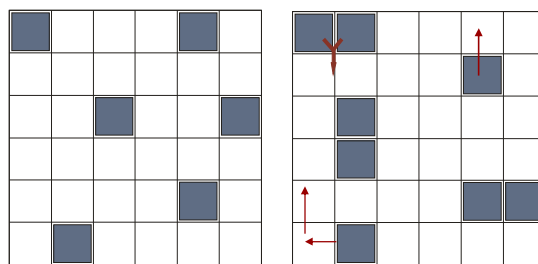## 2.3.2 Monte Carlo Simulation and Finite Element Calculation Methods

Fig. 20: Left: initial occupation of 2-dimensional lattice sites by particles. **Right:** Aggregation of particles to clusters and movements on the lattice.

sites are randomly (runtime controlled) placed in the system with a predetermined particle concentration c. [87, 96, 97] In this simulation the concentrations vary from 0.056 to 0.25. Due to the two-dimensional approach and other assumptions arising from the nature of Monte Carlo simulation these values do not quantitatively correlate with an experimental particle volume

fraction. It has been observed experimentally in many composite electrolytes that for larger volume fractions than 0.08, the particles are not wetted homogeneously and the electrolyte appears to be solid rather than gel-like which results in very low conductivities.[30] However, the concentration values investigated by the simulation cover the range from very low to high volume fractions and allow for qualitative conclusions in these regimes.

The particles and the formed clusters (aggregations of several particles) are allowed to move in all possible directions, also diagonally. The probability for a movement in a certain direction is equal unless gravity force plays a role which would lead to the influence of sedimentation (not considered in the simulations discussed in this contribution). The second and exclusively investigated influence on a particle in terms of mechanistic studies is the interaction with other particles with respect to DLVO (Derjaguin-Landau-Verley-Overbeek) theory.[98] The total interaction potential acting on a particle is hereby a summation over the specific potentials. These are

> (1) the interaction potential of hard spheres which allows a lattice site to be occupied by only one particle
>
> (2) the attractive potential $V_{attractive}$ implying Van-der-Waals interaction and attractive Coulomb interaction (mainly based on entropic effects)
>
> (3) the double layer repulsion between particles of equal surface charge

The points mentioned lead to the potential minimum that results from the contribution of two short-range interactions: the weak particle-particle interaction (Van-der-Waals interaction) and the strong particle-particle interaction due to their surface groups, e.g. dipole-dipole interaction. It can be of physical and/or chemical nature.

In reality the particles such as SiO_2 have end groups on their surface, e.g. hydroxyl groups, that partially adsorb the ions of the conducting salt. Hence not only long-range Coulomb repulsion becomes important, but also the entropic contribution by the space charge zones. The resulting energy maximum is kept constant for all simulation results shown below (chapters 3.1 and 3.2.6). In the simulation the described minima and maxima in energy are discretely taken into account whereby no continuous energy curve is passed through. The secondary minimum for high particle distance representing a loose interparticle attraction is usually very flat and therefore neglected.

With this technique in principal many different composite systems can be simulated notwithstanding the parametric treatment of solvent and ionic influence. To simulate a specific combination of solvent, salt and nanoparticles the strengths of the particular interactions have to be considered and should at least be qualitatively known.

For these investigations the particle interaction potential $V_{attractive}$ is varied from 50 meV (low interaction energy) to 150 meV (high interaction energy). On the one hand in the described simulation the used parameter values are in the range (order of magnitude) of Van-der-Waals interactions between nanoparticles. On the other hand it should be stressed again that the used assumptions, such as a 2-dimensional box, do not allow for a quantitative but only a qualitative interpretation.

When a particle is selected to move to a new lattice site ($x_{n+1} = x_n \pm 1$ and/or $y_{n+1} = y_n \pm 1$) the energy is calculated for the previous site, the new site and for the transition state. For a specific site the energy is defined as a sum of the interaction energies:

$$E = N_{Neighbors} \cdot E_{attractive} \tag{27}$$

Now the energy difference ΔE between the initial and the transition state[1] is calculated. According to the Metropolis algorithm the probability p of moving the particle is given as follows [99-101]:

$$p = \exp\left(-\frac{\Delta E}{k_B T}\right) \tag{28}$$

Here the movement is only successful if p is larger than a generated random number. In this way a kinetic aggregation mechanism is simulated. When particles have agglomerated and formed a cluster they are still considered as individual particles. Additionally also the whole cluster is treated as an object that can move according to the laws described before. Its diffusion coefficient is inversely proportional to the square root of the number of particles it contains. This is an approximation of the Einstein-Smoluchowski Equation. The possibility to address both bound particles in clusters and clusters themselves allows not only a movement of agglomerates but also the "coarsening" (described later) of them as the single particles of these clusters can still move. Additionally single particles are allowed to leave clusters if they

---

[1] The energy maximum between initial and final state.

are able to overcome $V_{attractive}$. However in reality not only small particles are able to leave the clusters but also bigger parts of the cluster can break off. Therefore objects of a third type, sub-clusters, are included in the simulation. Hereby the clusters are analyzed in order to find connection points of sub-clusters to the main cluster which feature only few particles. There, the sub-clusters can possibly break off from the main cluster. The choice of the considered weak connection sites is carried out randomly. The sub-clusters are then able to move within the cluster (coarsening) or to break off completely and form new clusters.

In total, four possibilities of movement exist for the species: movement into free space, sticking, debonding [86] and coarsening.

The probabilities of these movements depend on the respective energies along the reaction coordinate. The coarsening of a cluster means the rearrangement of particles and sub-clusters within the cluster in order to occupy more favorable sites where they are surrounded by a larger amount of neighbors. For the coarsening an additional factor, the surface diffusion coefficient, is introduced. It depends on the energy difference between the bonded initial and final states and the transition state diagonally between two adjacent particles (Fig. 21). The extreme situations are sliding without energy barrier and a required complete debonding before the creation of a new bond to an adjacent surface particle.
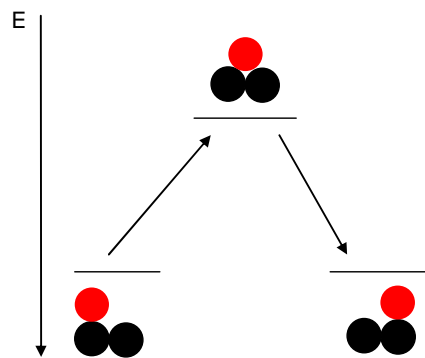

Fig. 21: Transition between two particle-particle bonding situations on the cluster surface.

The coarsening rate (cf. the activation barrier) exponentially depends on the binding energy difference between the initial and the transition state. This energy difference is determined by the number of direct neighbors.[36, 92]

As a result the coarsening of a particle which has to debond from only one bonding partner is quick whereas this event is greatly decelerated if the decisive number of contacts is doubled. In the model of Fig. 20, it is the energy difference between the middle state and the initial state situation. The phenomenon of doubling the activation energy is shown by means of the following estimate.[36]

If the forward rate constant can be expressed to

$$\bar{k}_1 / k_0 = \exp- \frac{\bar{E}_1}{RT} \tag{29}$$

with $\bar{E}_1$ being the activation energy of the forward process and k_0 being inversely proportional to an attempt frequency, then doubling of $\bar{E}_1$ results in

$$\bar{k}_2 = \bar{k}_1^2 / k_0 \quad \text{or} \quad \bar{\tau}_2 = \bar{\tau}_1^2 k_0, \tag{30}$$

($\bar{\tau}$: exponential relaxation time with $\bar{\tau} = 1/\bar{k}$). If $\bar{E}_1$ is varied from 0.2eV to 0.001eV, then, for $\bar{\tau}_1 = 1\text{h}$, $\bar{\tau}_2$ is reduced from 1000h to 1h.

Hence in the case of large activation energies, coarsening finally leads to a self-stabilization of partly compacted clusters.[36]

As all the parameters that control the movement of the particles can be adjusted, many different composite electrolyte systems can be simulated. Additionally the distinct types of moving that are explained above do not have to be treated separately but follow simultaneously from the used energy barriers. Hence also the coupling between these types of movements is included.

During the simulation the clusters are analyzed concerning possibly formed percolation pathways through the lattice. Additionally analyses are made concerning e.g. average particle energy, average amount of particle neighbors, radii and fractal dimensions of the largest clusters.

The radius of a cluster is defined as

$$r = \frac{1}{n} \sum_{i=1}^{n} \sqrt{(x_i - x_0)^2 + (y_i - y_0)^2} \tag{31}$$

where n is the number of particles and x, y are coordinates of each occupied place (x_0, y_0: coordinates of the center of mass). The fractal dimension d_f can then be determined from

$$n \propto r^{d_f} \tag{32}$$

An important aim is the analysis of the network structure / total conductivity relationship. As the bulk electrolyte conductivity (corresponding to the filler-free electrolyte) is not negligible, the overall conductivity of a soggy-sand electrolyte is a complex function of time and can be only numerically treated. It can be calculated in relationship to the initial state of the simulation or the particle-free electrolyte. This is done by an analysis using the finite element program COMSOL Multiphysics (COMSOLAB, version 4.0a). It is able to numerically calculate the total current in the lattice under consideration of the boundary conditions.

For that purpose the coordinates of the particles in the created clusters are transferred to the Finite Element Methods (FEM) program. In that context an analysis is made to verify if the position of a particle is at the surface or in the bulk of a cluster. In total three parametric values of the conductivities in composite electrolyte systems have to be set, namely the conductivity in the particle-free areas (indicated as "solvent bulk"), the conductivity at the surface of the particles at the edge of a cluster and the conductivity in the cluster bulk.

As to the first value the assumption is made that the conductivity in the solvent bulk is not influenced by the effect that the particles decrease the amount of ions and ion pairs in the unaffected bulk solvent and therefore also slightly reduce the conductivity in the solvent bulk. The effect of enhanced ion pair dissociation occurs at the interface between the particles and the electrolyte.[29] Hence the region of improved ionic transport is located in the diffusive layer in the vicinity of the particles.

An estimation of the surface to solvent bulk conductivity can be made if one considers the total conductivity σ_m in a composite electrolyte similarly to Equation (2). It is approximately given [37] as

$$\sigma_m = (1-\varphi)\sigma_\infty + \varphi \cdot \beta_L \Omega \Sigma u_v F \tag{33}$$

Here β_L stands for the degree of percolation (usually in the range of 0.2 to 0.5), σ_∞ is the bulk solvent conductivity, Ω stands for the specific particle surface, Σ is the integrated charge density at the interface, u_v represents the ionic mobility at the interface which can be directly calculated from the molar conductivity and F is the Faraday constant. According to Equation (5) the ratio of the particle surface conductivity and the bulk conductivity results to

$$\frac{\sigma_\lambda}{\sigma_\infty} = \frac{\Omega \Sigma u_v F}{\sigma_\infty} \tag{34}$$

With the assumption of an unaffected bulk solvent conductivity in composite electrolytes σ_∞ is experimentally accessible by measuring the AC conductivity with ion-blocking electrodes. Accordingly also Ω, Σ and u_v are experimentally determinable so that the quotient $\dfrac{\sigma_\lambda}{\sigma_\infty}$ can be estimated.

With the input parameters current density streamlines can be calculated. They represent current pathways which are influenced by the higher conductivity in the vicinity of the particles. Here the (electrical) flow line density is proportional to the current density. The thickness of the space charge layer chosen is just identified with the pixel size. This is a strong simplification compared to the approach of Goodyer et. al. [94] in which the concentration of ions is analyzed in dependence of space charge layer thickness. However, for the investigation of overall conductivity evolution this treatment leads to reliable results if the particle surface to bulk solvent conductivity ratio, in principle the integrated ionic strength of the space charge layer, is chosen accordingly to experimentally determined parameters.

It may lead to misinterpretations if one tries to directly correlate the time scale of an *in situ* experiment with the simulation steps leading to network structures that allow conclusions about the processes in the experiment. For improving this key point while following the general rules of kinetic Monte Carlo simulation an additional approach is made that deals with the energy fluctuation. Equation (28), the determining expression for a movement of a cluster with p being the movement probability in this case, can be transformed to

$$\Delta E = -k_B T \ln p \qquad (35)$$

The time variable for the movement in a certain direction (here $\Delta \vec{x}$ without limitation of generality) is introduced by the use of the Stokes Equation ($\vec{v}$: movement velocity)

$$\left| \vec{F}_R \right| = 6\pi\eta r \left| \vec{v} \right| \qquad (36)$$

which can be rewritten as

$$\frac{\Delta E}{\left| \Delta \vec{x} \right|} = 6\pi\eta r \frac{\left| \Delta \vec{x} \right|}{\Delta t} \qquad (37)$$

with $\left| \Delta \vec{x} \right|$ being the distance of movement for the particle. As the simulation is based on a two-dimensional lattice with discrete movement steps of one lattice point, $\left| \Delta \vec{x} \right|$ is assumed to be constant. A simplification is the independence of the local viscosity η of the cluster

structure. It is assumed to be constant over the whole electrolyte and is also experimentally accessible. With Equation (35) the expression can be transformed to

$$\ln p = -\frac{6\pi\eta r |\Delta\vec{x}|^2}{k_B T \Delta t}$$

(38)

Hence for constant temperature the relationship

$$\Delta t \propto -\frac{r}{\ln p}$$

(39)

is found which is similarly used in other kinetic Monte Carlo simulation approaches.[102]

3 Results and Discussion

3.1 Network Formation Kinetics

In the context of Soggy-sand electrolytes the properties of the network structure and its stability are important not only for the mechanical properties but also for the electrical properties. Only in the vicinity of an expanded fractal network throughout the electrolyte cations can be transported in a quick and efficient manner along the percolation pathways. Interruption of space charge layers becomes more unfavorable for the overall conductivity the higher the ratio of space charge to bulk conductivity. As this ratio is not particularly large for low volume fraction of filler particles, a substantial fraction of the overall conductivity will involve bulk conduction only. This more complicated behavior is not taken account of by Eq. (33). Under unfavorable conditions, spherical clusters are formed due to the particle-particle aggregation. As a consequence the liquid can hardly interpenetrate the aggregate favoring its sedimentation. The formed network can be regarded as a "macro-particle" whose mass is more or less concentrated in a small area resulting in a gravitational force on the network which exceeds the frictional force of the liquid by far.

First studies on the time dependent ionic conductivity of freshly-prepared Soggy-sand electrolytes ((LiClO$_4$ + PEG-150):SiO$_2$ systems) have shown that the initial conductivity is steeply lowered within a short time span before flattening towards the steady state (A. Jarosik, PhD thesis)[92] which is usually still higher than the ionic conductivity of the filler-free electrolyte. During this process which is often significantly slower than the initial network formation the cluster tends to minimize its surface energy by surface diffusion of the particles by transferring constituents of the filler particle from a lowly connected site to a position with more neighbors (coarsening effect). As a consequence the mechanical properties deteriorate and the ionic conductivity drops due to the fact that the favorable ionic transportation pathways become shorter or even get interrupted. Furthermore, filler sedimentation becomes more likely. As a conclusion it can be stated that the prevention of such massive network coarsening is one of the key factors for obtaining applicable composite electrolytes. It is naturally dependent on the choice of the components, in particular the filler type. Particles characterized by a high surface-to-volume ratio and covered with suitable functional groups are more likely to be fixed at an outer branch of the network in accordance with the principles

of the theory of diffusion limited aggregation (DLA). Fortunately, the coarsening process is self-slowing down as the number of contacts exponentially decelerates to further rearrangement (cf. section 2.3.2).[92]

The (LiClO$_4$ + THF) system has been chosen for more detailed network kinetics studies due to the special characteristics of the solvent (low dielectric constant leading to pronounced second phase effects). Previously, Bhattacharyya et. al. reported more pronounced conductivity maxima for THF containing samples at higher φ values.[33] Network formation occurs almost instantaneously in the case of higher volume fractions ($\varphi \geq 1\%$) and small particle sizes. Thus, spherical particles of larger sizes (50 nm) have been chosen as fillers while fractions were kept at low values ($\varphi \leq 0.3\%$).

LiClO$_4$ and LiOTf are used as lithium salts with a fixed concentration of 0.1 M. The ionic conductivity as function of time for the different samples is shown in Figure 22.[95] The major "trick" enabling in-situ recording network formation was the use of extremely small filler volume fractions such that collision events leading to aggregation are of very low probability as pointed out below.
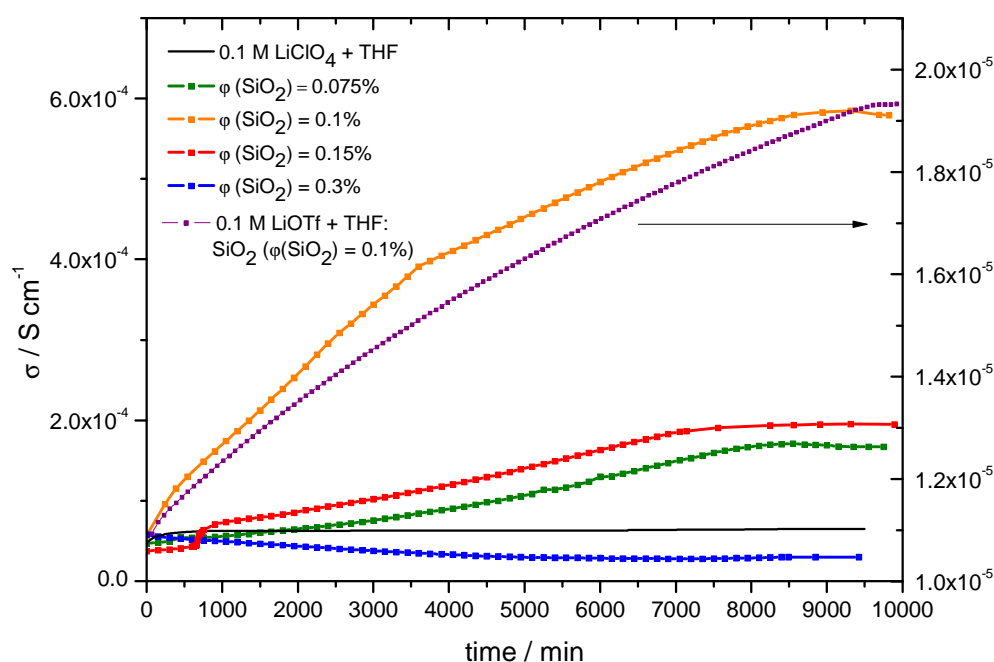

Fig. 22: Time dependent ion conductivity of 0.1 M LiClO$_4$ + THF as a function of SiO$_2$ volume fraction.

In Figure 21 it can be seen that the conductivities show a strong increase at the beginning of the measurement decelerating in the further course until a maximum is reached. After that

point a small decrease is observed for φ=0.075% containing electrolyte, possibly due to coarsening. Due to the fact that the bulk conductivity is not negligible the overall resistance has to be regarded as a series of individual resistances in which the bulk contributions are higher in comparison to the space charge contributions. This means that in these systems conductivity enhancements are possible to be observed even when the percolation threshold is not reached due to the fact that the lithium ions can be transported between clusters in a satisfactory way. As a result the shape of the conductivity curves can be interpreted according to the following scenario: just after the sample preparation the particles are rather homogeneously dispersed throughout the electrolyte. During the measurement the particle diffusion driven by the Brownian motion leads to the formation of small clusters which increases the ionic transport along their space charge zones. As the clusters continuously gain in size their diffusion velocity decreases resulting in an alleviated enhancement of the conductivity up to a maximum which represents either the presence of very few large clusters or a single expanded particle network. Again it should be stated that in this case a full percolation is not necessarily required due to the complex interplay between space charge layer and bulk contributions to the ionic conductivity. The conductivity is slightly lowered subsequent to the maximum probably due to the influence of the coarsening effect which naturally also occurs for very low particle volume fractions. Obviously for the sample containing 0.3% the network formation kinetics are so fast that only coarsening kinetics can be observed. For higher volume fraction, the magnitude of the enhancement agrees with the typical dome-shaped $\sigma(\varphi)$ functionality (increase due to the increased proportion of surface conduction at low φ and decrease due to formation of blocking morphologies at high φ). For LiOTf as an alternative salt, very similar effects are observed even though the total conductivity is about an order of magnitude lower than with $LiClO_4$ due to the fact that the attractive interactions between the anion and the cation are stronger favoring the ion pair than for $LiClO_4$. The linear segments in the time evolution (Fig. 22) can be attributed to the presence of different size classes of clusters in agreement with very different respective velocities.

To understand the observed effects it is important to keep in mind that the starting point is a sample in which the admixed particles are rather homogeneously dispersed. In the case of samples with $\varphi > 0.01$, measured electrical properties are affected by the presence of a particle network that self-rearranges slowly. When the particle volume fractions are much

lower, a new situation needs to be considered.[36] In general the aggregation process is based on the diffusion of particles towards each other. Thereby the particle collision frequency is $\propto \varphi^2$. As a result of this dependency it is not possible to observe network formation phenomena in the case of $\varphi > 0.01$ due to the almost instantaneous network formation already in the course of the sample preparation. However with the proper measurement technique these effects can be recorded if $\varphi < 0.01$. As seen in Figure 21, the ionic conductivity is changed over time raises the question if the increase of the ionic conductivity over time can be really attributed to the network formation revealing conductivity measurements as a suitable tool for in-situ recording of such processes in composite electrolytes. As already described before, large networks are required to enhance the ionic conductivity in these systems. In the following a chain of thoughts based on simplified mean field scenarios is made to verify the plausibility of the ascription of the observed conductivity enhancements to network formation phenomena.[36]

The mean distance (δ) between cubic particles with a diameter R is $\delta = R/\varphi^{1/d}$ (d-dimensional). The assumption of cubic shape of the particles is a simplification whereby the mistake made is very small as results for spherical shapes only slightly deviate.[103] From the given Equation it should be noted that δ only weakly depends on φ in comparison with R. This means that the particle density is still quite high even at low particle volume fractions for a homogeneous distribution of nano-sized particles in the composite electrolyte. For example if R = 1 nm whereas φ is chosen to $\varphi = 10^{-3}$, δ is only 10 nm. Hence the particle collision kinetics leading to measurable effect are still taking place at a reasonably recordable time scale. In a further consideration a highly artificial 3D morphology is assumed in which all particles are arranged in the form of parallel chains of diameter R. As can be easily shown the average distance δ' between obeys the relationship $\delta' \propto R/\varphi^{1/2}$. Furthermore the average number of chains per (electrode) area is proportional to φ / R^2. When R and φ are chosen to be $R = 1\,\mathrm{nm}$ and $\varphi = 10^{-3}$, still 1000 percolating chains would be present per square micrometer.[36] However, when it comes to the hit-and-stick mechanism which is predominant here, fractal networks are formed. The percolation threshold with the critical volume fraction $\varphi = \varphi_c$ in which case ($d = 3$) is $\propto (L/R)^{-(3-d_f)}$ [89] with L being the length of the considered

space. Typical values of d_f are smaller than 3 (from 1.4 to 1.8 as reported by A. Jarosik et. al.)[31]. Hence the percolation threshold tends to zero if $R \rightarrow 0$.[36] Enhancement effects on the ionic conductivity can then indeed be expected even if φ is small. Here the relationship between the bulk conductivity and the conductivity at the space charge layer of the particles plays a major role which will be discussed in more detail later.

To support the conclusions made from the conductivity measurements and to visualize the particle networks, further experimental techniques need to be applied to the investigated systems. A technique with which one is able to investigate whole network structures in the final system and not just non-dispersed particles is however difficult to find as regular microscopy techniques (SEM, TEM) usually generate images in which particles are optically covered by other higher laying particles. A technique of choice that is used in this thesis is Confocal Fluorescence Microscopy which is commonly used in cell biology allowing images of the composite sample to be recorded within one plane. It therefore represents a formidable tool for network structure investigations in liquid systems not only of a given structure but also of its formation and rearrangement over time. One key condition for the applicability of this method is the use of nanoparticles that contain dye molecules in their interior which can be excited by laser light and show fluorescence as a consequence. Given a range for excitation of 470 ± 40 nm, Rhodamine 6G was chosen a suitable dye. Owing to an elaborate sol-gel synthesis procedure developed by Marjan Bele [104] the dye molecules were embedded into a layer below the surface of the SiO_2 nanoparticles (80 nm particle size) leaving the SiO_2 surface chemistry unchanged. The particles and the salt are admixed to 2,2,3,3-tetramethyltetrahydrofuran featuring a slightly higher boiling point compared to previously used THF (T_b = 121°C) as solvent evaporation in the sample holder had to be avoided. However, the physical properties of the two solvents are very similar due to a well comparable molecular structure and a similar dielectric constant ($\varepsilon \approx 5$).[105] This is also reflected in further conductivity measurements on these systems that are highly comparable to the data obtained with the conventional particles and solvent. A typical measurement of the composite electrolyte with $\varphi = 0.15\%$ over several days is shown in the Figures 23a-c.
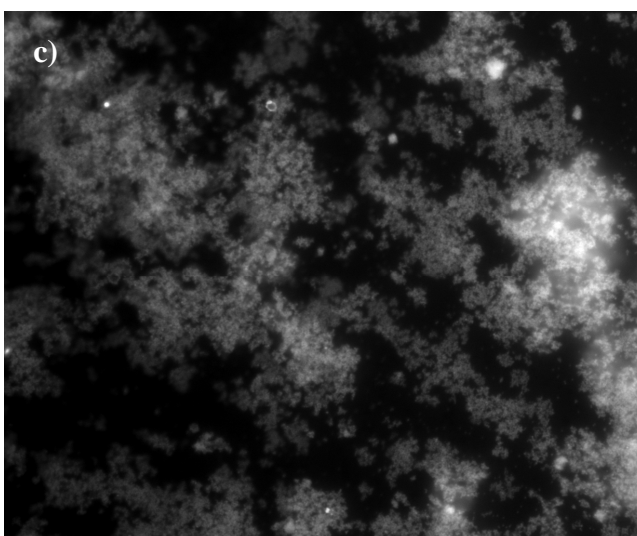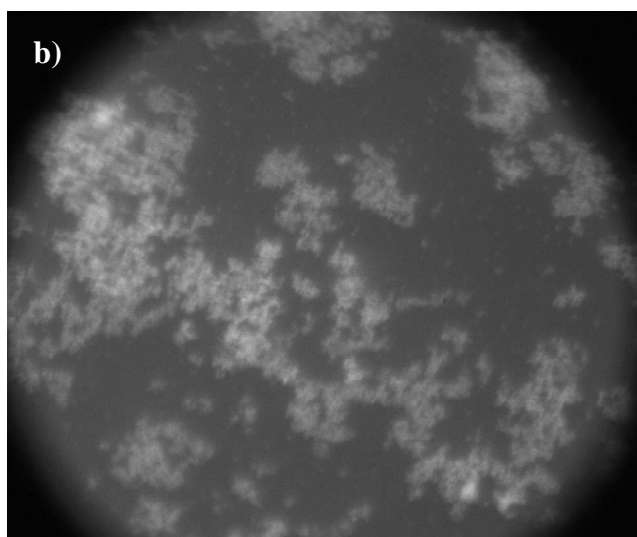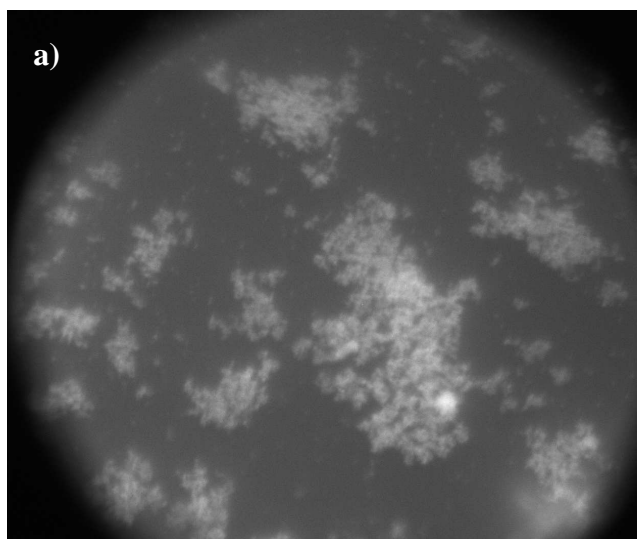
Fig. 23: CFM image of 0.1M LiClO₄+ 2,2,3,3-tetramethyl-THF: dye-sensitized SiO₂ (particle size 100 nm) with φ(SiO₂) = 0.15% after a) 5 hours, b) 3 days and c) 5 days. The total image width is 142 μm.

According to Figure 23a, individual clusters of different sizes are present even few hours after the sample preparation. From that point on typically coherent fractal network formation is observed (Fig. 23b). Such particle networks are not equally distributed throughout the electrolyte due to low volume fraction but otherwise the shown network is rather representative. Subsequently, larger fractal clusters containing denser agglomerates of particles are formed after 5 days due to coarsening (Fig. 23c).

It is known that under the impact of ultrasound, aggregated particles can be again separated. However, it needs to be ensured that the ultrasonic treatment is not invasive enough to prevent any changes of the chemical or physical nature of the nanoparticles. The result of such sample treatment in terms of the electrolyte's ionic conductivity is shown in Figure 24.
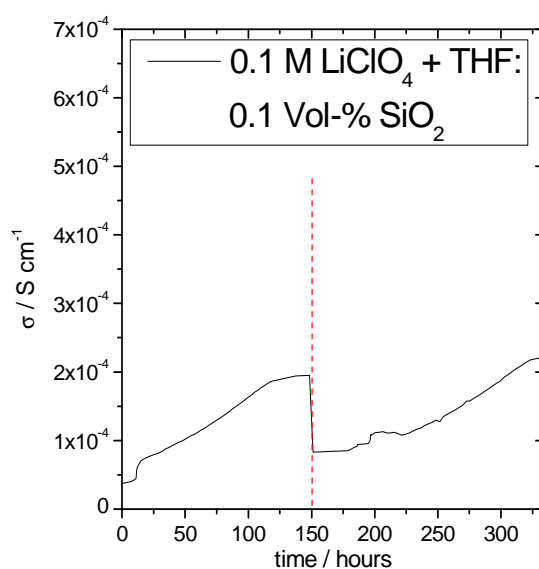

Fig. 24: Time dependent conductivity in 0.1 M $LiClO_4$+THF ($\varphi(SiO_2)$ = 0.1%) in combination with ultrasonic treatment (pulses of low intensity with frequency of 0.2 Hz for 1 min) in between (dashed line).

The ionic conductivity of the 0.1 M $LiClO_4$ + THF: 0.1 Vol-% SiO_2 electrolyte is measured as a function of time. As shown before, a time-dependent conductivity increase is observed. When the steady state is reached and just before the noticeable conductivity decrease due to coarsening (150 hours), the sample is treated with an ultrasound finger under argon atmosphere (marked with a red dashed line). As a result, the initial conductivity drops to a value that is almost identical to the conductivity just after the initial sample preparation with a small deviation probably due to partial solvent evaporation in the course of ultrasonic treatment. This shows that the formed network is broken up resulting in a situation in which

the particles within the sample are again rather homogeneously dispersed. Yet, more interesting than this phenomenon is the fact that over time the conductivity rises again in a very similar manner as before the ultrasonic treatment. This simple experiment therefore shows that the network formation process is reversible and at the same time it is a reliable confirmation of the network formation theory as previously seen in CFM. Furthermore, these results exclude the possible influence of impurities (e.g. water) brought into the solution through the particles as alternative explanation of the conductivity effects.

Zeta potential measurements have proved to be a versatile tool in the context of Soggy-sand electrolytes as they allow observation of local scale (ionic adsorption at the interface) as well as macroscopic scale phenomena. This is due to the fact that the measured effective Zeta potential is also strongly dependent on the degree and structural character of particle aggregation. Even though the quantitative analysis is difficult due to the fractal form of the aggregates, the qualitative interpretation is straightforward. The result of the time-dependent Zeta-potential measurement is shown in Figure 25.
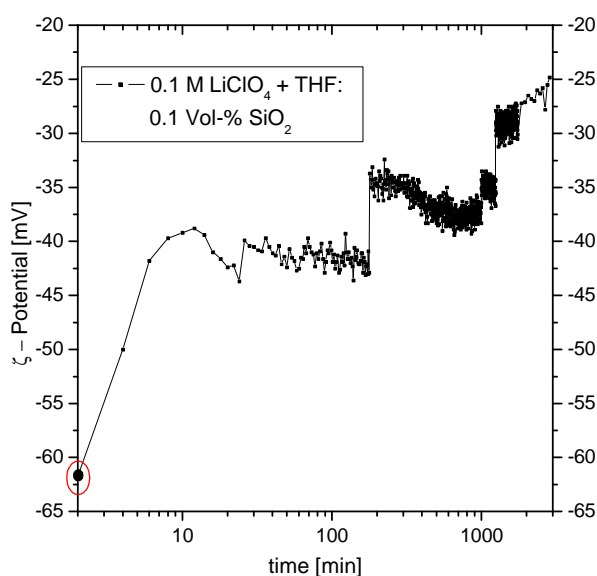

Fig. 25: Time dependent effective ζ-potential of (0.1 M $LiClO_4$ + THF):SiO_2 ($\varphi(SiO_2) = 0.1\%$)

Freshly prepared 0.1 M $LiClO_4$+THF: SiO_2 yielded an effective (i.e., semiquantitative) ζ-potential of -62 mV (Figure 25). The high value is typical for stable colloidal dispersions [75] and high enough to prevent flocculation and sedimentation. The negative sign indicates a

negative surface charge of the SiO$_2$ particles which corresponds to anion adsorption. With time, the absolute value of the ζ-potential decreased significantly (-25 mV after 3000 min), pointing towards particle agglomeration [106] which is connected with a lower surface charge/density ratio. The simplest and most obvious reason for the lowered ζ potential is the decrease in local surface charge due to newly formed particle-particle contacts. However, as already mentioned, calculation of the ζ-potential is based on a defined and constant particle radius and does not account for the complex and changeable morphology. It lies in the nature of the electroacoustic method that not all of the charges contribute to the effective ζ potential measured. It can be assumed that with increased cluster size a greater portion of the inner surface charge is overlooked in the electroacoustic measurements. This loss of active surface charge is smaller when the agglomerate decomposes in smaller units, as it is the consequence of coarsening. Thus, not only the pronounced variation of the ζ-potential finds its explanation in the agglomeration: even the slight decrease in ζ-potential observed after and before an agglomeration step may be qualitatively explained by the superimposed coarsening, emphasizing the inhomogeneous nature of the dispersions. At some points in time an abrupt decay of the ζ-potential is occurring (around 200 and 1000 min). This effect can arise in the course of an aggregation of several medium-sized clusters of which fewer but larger cluster are created.

Dynamic light scattering (DLS) is also used on composite electrolytes to get further insight into the effective particle size as well as on detailed structural aspects of particle aggregates. One typical result is shown in Figure 26.
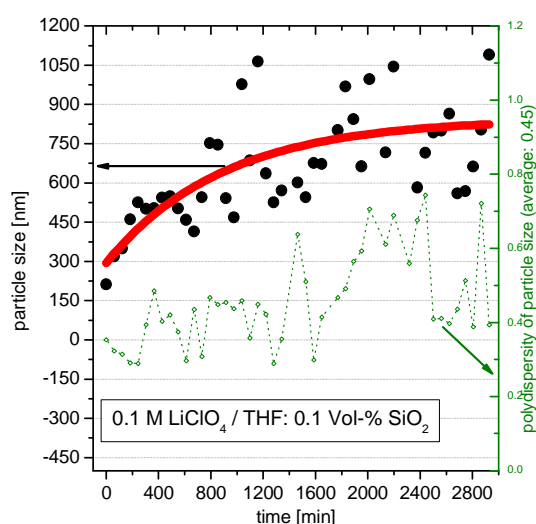

Fig. 26: Dynamic Light Scattering results of (0.1 M LiClO$_4$ + THF): 0.1 Vol-% SiO$_2$, fitted with a two-parametric exponential function.

The recorded time-dependent data again indicate agglomeration which is in good agreement with the corresponding conductivity, CFM and Zeta potential data. In spite of the pronounced scatter, the data suggest (red curve) that particles are initially homogeneously dispersed and subsequently agglomerate as time elapses. The particle size reaches steady state after several thousand minutes, in rough agreement with the plateau in the σ measurements. The results show a strong variation of the cluster size, corresponding to the highly dynamic processes during reversible cluster formation. The time-dependent development of the particle size measured using DLS as well as ionic conductivity measurements indicate a diffusion limited aggregation process due to the weakly pronounced coarsening effects which are only relevant at a late point in time during the measurement. The conducting pathways grow continuously creating a network with a tenuous structure. According to the DLA theory, this is due to the fact that approaching particles readily adhere to other particles as a consequence of which the interior of the clusters are screened from particle penetration. This indicates that the interparticle bonds are strong and might even have a chemical character to a significant part (e.g. hydrogen bonding).[107] As the particle content is low cluster-cluster aggregation plays a dominant role when fractal clusters are formed. As a result of the cluster-cluster aggregation with a DLA character, the fractal dimension d_f is reduced due to the fact that two fractals connect almost instantaneously with each other when they meet. Therefore widely spread and loosely packed structures are produced.

As previously given results and interpretations are of fundamental interest not only in the case of soggy-sand electrolytes, but also in other technological and scientific fields where particle network formation plays an important role it is worthwhile to investigate network formation in the context of composite liquid-solid systems also by means of theoretical studies. For this purpose a Monte Carlo 2D simulation is applied.

The ratio between the ionic conductivity in the space charge zone at a nanoparticle and the ionic conductivity in the unaffected bulk electrolyte is a fixed parameter that is estimated by Equation (34) as usually done in cases in which this ratio is high. Here, the β-factor (which measures not only how much of the filler material percolates but also how much of the connected interfacial area contributes to the transport in the direction of measurement) in the investigated composite solid electrolytes can be assumed to be $\beta_L = 0.5$.[37] With the powder density ($\rho = 2.400 \; g \cdot cm^{-3}$) and the BET surface ($537.9 \; m^2 \cdot g^{-1}$) of the SiO$_2$ particles

typically used in the preparation of Soggy-sand electrolytes, Ω is found to be $\Omega = 1.84 \cdot 10^9 \ m^{-1}$. If the ion exchange capacity values of SiO_2 in water are used to assess Σ [44], $\Sigma = 3.7 \cdot 10^{-3} \ mol \cdot m^{-2}$ is obtained. To estimate the ionic mobility previous work by Muhuri et. al. [108] is used where the equivalent conductivity of 0.09 M $LiClO_4$ in 1,2-Dimethoxyethane (DME) was determined to be $\Lambda \left(Li^+ \ in \ 0.09 \ M \ LiClO_4 + DME \right) = 2.80 \ S \cdot cm^2 \cdot mol^{-1}$. DME has a very similar dielectric constant ($\varepsilon = 7.1$) compared to THF and it is reasonable to assume similar equivalent conductivities for 0.1 M $LiClO_4$ in THF. By setting the experimentally obtained value $\sigma_\infty = \sigma \left(0.1 \ M \ LiClO_4 + THF, t = 0 \right) = 5.2 \cdot 10^{-5} \ S \cdot cm^{-1}$ as a reference for the ionic conductivity of the bulk, the estimated relationship between the conductivity at the oxide particle surface and the bulk for these systems is calculated to be 190:1. This value is set as a simulation parameter. The influence of the presence of nanoparticles on the ionic conductivity in the bulk will be discussed in chapter 3.2.3. The value of 190:1 shows that the conductivity is significantly enhanced in the space charge zone. Compared with the conductivity differences in the bulk and at the grain boundary of solid-solid composites which often reach five to seven orders of magnitude the obtained enhancement in the solid-liquid case is much less pronounced. This leads to the conclusion that here a certain bulk conductivity always has to be taken into account and complete percolation is not absolutely required. Such a behavior can also be observed from the Monte Carlo (MC) simulation combined with numerical FEM calculations shown below (Figures 27 a1-e2).
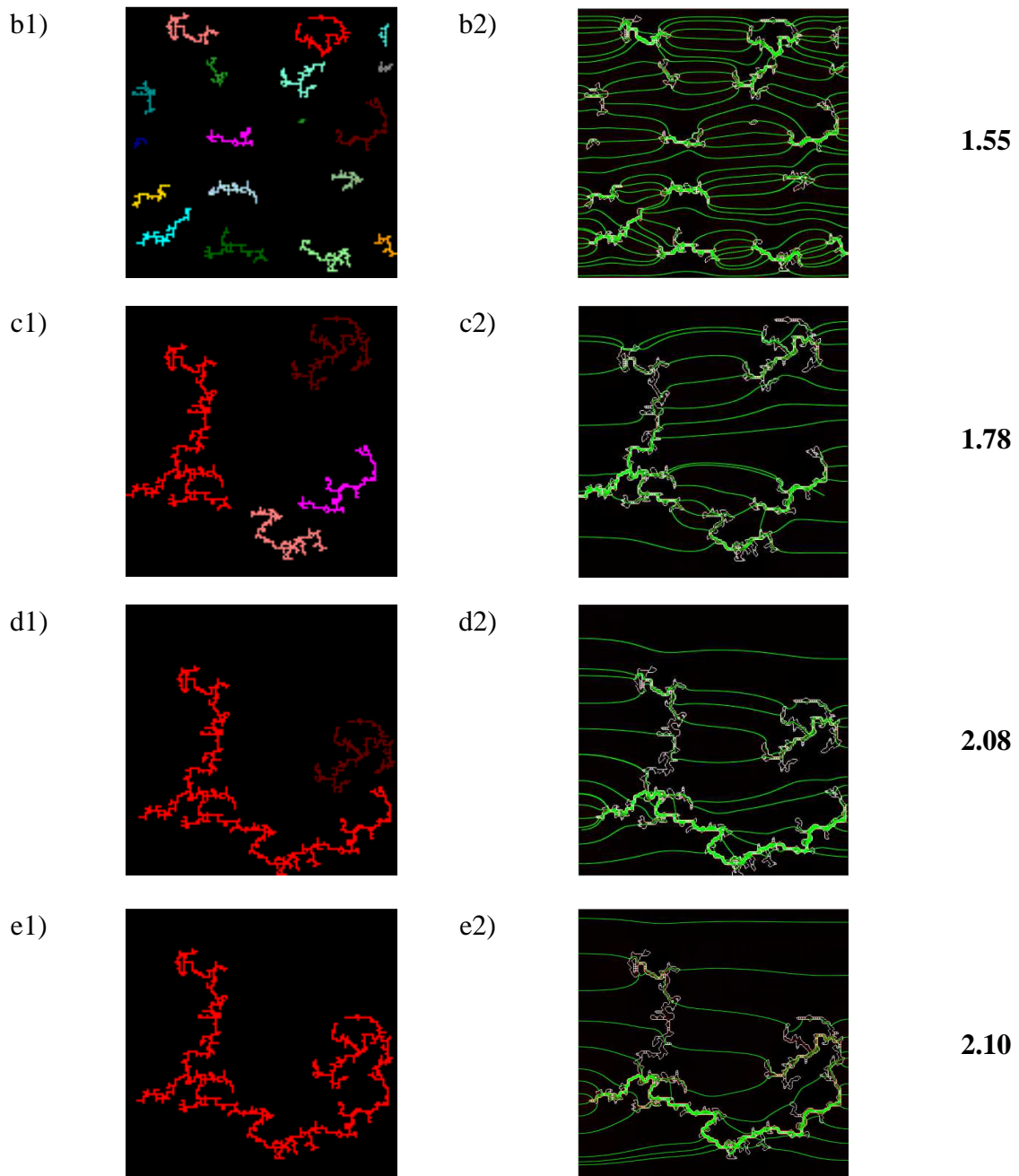
$\sigma / \sigma_{initial}$

a1)

a2)

1
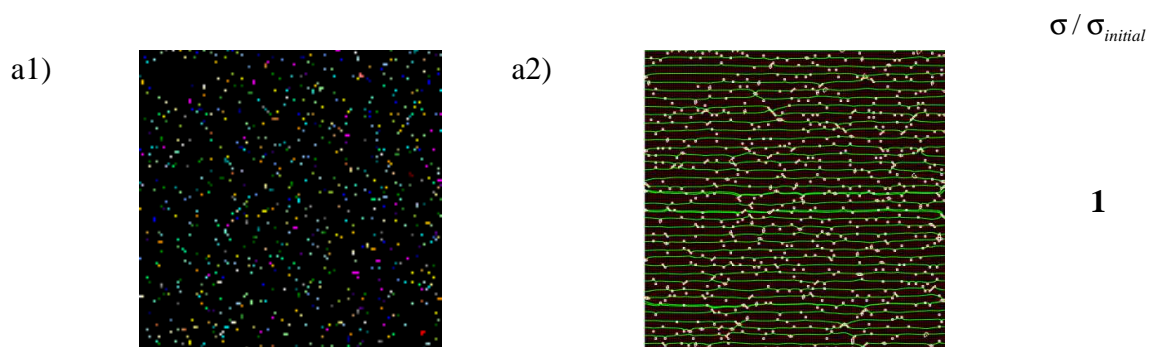
Fig. 27: Results from MC Simulation (cluster structure, a1-e1) and subsequent FEM calculation (current density streamlines, a2-e2). The relative increase of conductivity for each structure compared to the initial state (a2) is given.

Fig. 27 shows the results of a typical Monte Carlo simulation (first column) and subsequent FEM calculation (second column) for very low oxide particle volume fractions on the two dimensional lattice. Several situations are compared concerning the present structure of the clusters as well as the qualitative change in conductivity (third column) ranging from the

initial state (mostly colloidal solution, Fig. 27 a1) to the situation where a large percolating cluster is formed (Fig. 27 e1). Fig. 27 b1 shows the formation of small clusters which is due to statistical occupation of lattice sites. The corresponding current density streamlines (Fig. 27 b2) are slightly bent and distributed rather equally over the whole lattice. Here and in the following FEM calculations, the (electrical) flow line density is proportional to the current density (magnitude controlled). For simplicity's sake, the layer thickness is chosen to be identical to the pixel size and the conductivity therein is assumed to be constant. The latter approximation is less severe as lateral conductivity effects are not relevant.

The situation changes when fewer but larger clusters are present (Figs. 27 c1, d1) with current density streamlines being more strongly bent towards the clusters (Figs. 27 c2, d2). It can be noticed that already at this stage the number of current density streamlines per area in the bulk phase is higher the shorter they are corresponding to the preference of the pathway (Fig. 27 c2). Finally an advanced state is reached with just one almost completely percolating network (Fig. 27 e1). In that case (Fig. 27 e2), almost all current density streamlines are going along the percolation pathway. Interestingly it can still be recognized that some streamlines are bridging spaces where no particles are present. This is due to the finite bulk conductivity in the liquid state. The ionic conductivity increase from the initial to the final state is around 2.10. This value is lower than experimentally observed (conductivity increase of up to 5 times, Fig. 22) due to influences such as the 2D approximation, different final states and simplifying assumptions used in the Monte Carlo simulations. However, the simulation clearly shows that a percolating cluster in an electrolyte is much more favorable than the respective homogeneous dispersion or an accumulation of spatially isolated small clusters.
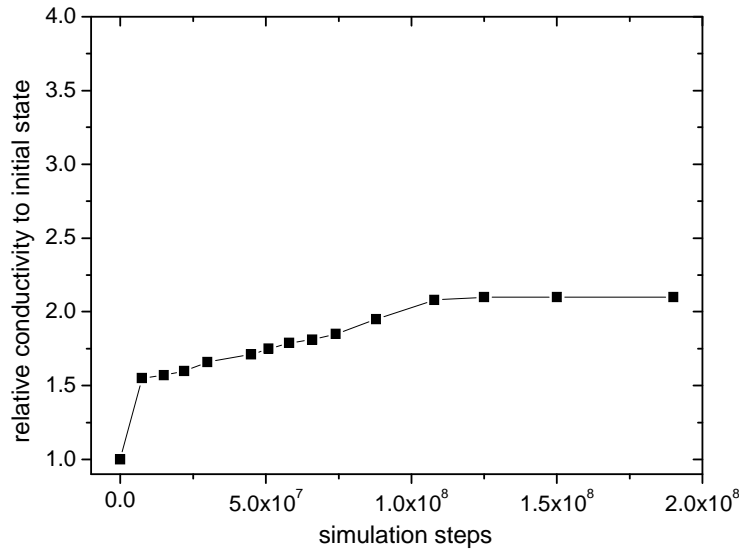
Fig. 28: Relative increase of conductivity for the formed structures during aggregation compared to the initial state $t = 0$. The final σ / σ_0 ratio is 2.1.

Figure 28 represents the evolution of the overall conductivity upon particle aggregation obtained by 2D Monte Carlo simulation. The transition from simulation steps to simulation time is rather unproblematic as confirmed from investigations on multiple network formation simulations (respective results are not shown here). The conductivity steeply increases at the beginning of the simulation. Subsequently, in a certain time period the conductivity is further enhanced almost linearly before reaching a steady state. Obviously, the occurrence of linear segments reflects various time intervals in which different cluster sizes are predominant. As already mentioned, this is explainable by the fact that the mobility of the cluster is strongly size dependent. Starting then from isolated particles of same size, double-sized particles occur on collision and it takes quite a time, in fact until all the single particle events have occurred before double-sized particle collision events occur. The shape of the σ-t curve resembles the experimentally determined conductivity curve (Fig. 22). In total it can be concluded that the experimentally obtained conductivity curves can be reproduced well by the application of the Monte Carlo simulation with adjacent FEM calculations. This again confirms the proposed mechanism of cluster growth leading to expanded space charge zones which enable a fast ionic transport through the electrolyte even when the formed network is not completely percolating.

59

3.2 Soggy-Sand Electrolytes in the Steady State

3.2.1 Quantitative Estimate of the Ionic Conductivity and Lithium Transference Number (system: $LiClO_4$ + THF)

In the previous considerations it was shown how to superimpose bulk and space charge conductivities to the overall value. In this section the local conductivity effects themselves are calculated based on mass action constants for ion pair association.

As already mentioned before, the conductivity increase is significantly dependent on the type of solvent. In less polar systems more ion pairs are present that can be broken up, simultaneously the space charge zones are more extended owing to lower bulk conductivity and lower dielectric constant. For non-polar solvents overlap of double layers is probable and can be found already at very low volume fractions.[48] As for tetrahydrofuran containing samples fundamental literature data can be referred to, it is even possible to estimate the achievable overall conductivity and transference number enhancements whose consistency with the obtained experimental data can be checked. For that purpose it is useful to reconsider the ideal parallel switching model. The error made in this context due to the bulk contribution is not too high as the dielectric constant of tetrahydrofuran is 7.5 still leading to a pronounced difference between the bulk conductivity and the space charge layer conductivity. The relevant estimation of the conductivity using of the parallel switching model is given by [48]

$$\sigma_m = (1-\varphi)\sigma_\infty + \beta_L\Omega\varphi(2\varepsilon\varepsilon_0 RT)^{1/2} u c_0^{1/2} = (1-\varphi)\sigma_\infty + \beta_L\Omega\varphi\Sigma uF \tag{40}$$

which represents a more detailed notation of Equation (2) in the introductory section. The product uFc_∞ is the bulk conductivity, the product $uF\sqrt{c_0 c_\infty}$ is the average conductivity in the space charge zone when referring to the same conducting species and is valid as long as mobility variations and contributions from the adsorbed ions can be ignored. In Equation (40) the bulk conductivity has cancelled out as the mean effective concentration in the space charge zone is $\sqrt{c_0 c_\infty}$ while the thickness of the space charge zone is proportional to $c_\infty^{-1/2}$.[48]

The surface charge density Σ is expressed by the term $(2\varepsilon\varepsilon_0 RT)^{1/2} c_0^{1/2}$. If all surface groups are active, it can be obtained from the ion exchange capacity (IEC) and Ω via [48]

$$|\Sigma|/F = IEC \cdot \rho / \Omega. \tag{41}$$

The assumptions given above are supported by the temperature dependent measurements that were carried out for the filler-free electrolyte as well as for the composite electrolyte containing 0.1 Vol-% SiO_2 particles (Figure 29).
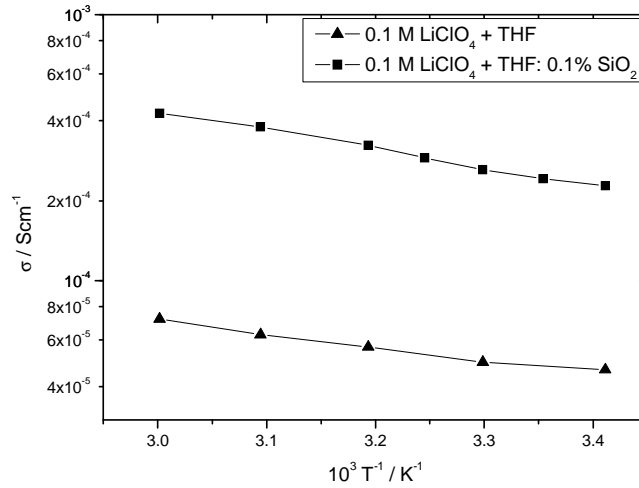

Fig. 29: AC conductivity as function of temperature for filler-free and filler-containing $LiClO_4$/THF electrolytes.

It can be recognized that the conductivity increase in this case lies in the range of half an order of magnitude while the slopes of the conductivity curves (determined by the activation energies for ionic transport) are very similar indicating that no fundamentally different transport mechanisms seem to play a role.

According to Barthel et. al. [54] the mass action constant for the ion association of $LiClO_4$ in THF is

$$K_A \equiv K\left\{Li^+ + ClO_4^- \leftrightarrow LiClO_4\right\} = 3.7 \cdot 10^7 \, mol^{-1} \cdot dm^3 = \frac{\left[LiClO_4\right]}{\left[Li^+\right]\left[ClO_4^-\right]} \qquad (42)$$

whereby the square brackets denote the molar concentrations of the species. Without significant failure they can be used instead of the respective ionic activities. Obviously the system is characterized by a very high tendency of ion pairing. Yet this means that also triple ion species created from an ion with an ion pair such as $Li(ClO_4)_2^-$ or $Li_2ClO_4^+$ might play a role in this consideration. From literature it is known that the triple pair formation constant is $K_T = 36 \, mol \cdot dm^{-3}$ for $m = 0.1 \, mol^{-1} \cdot dm^3$. Yet it can be shown by consideration of the respective mass action laws of anionic and cationic triple pair formation together with electroneutrality and mass balance equations that the triple pair contributions are negligible, here it helps that the ionic mobility of triple ions is smaller than that of single ions.[48]

Consequently, it can be stated that only a small fraction of ions is free to move, namely $[Li^+]$ = $[ClO_4^-]$ $\approx 5 \times 10^{-5}$ mol·dm^{-3}.[48]

With the introduction of nanoparticles an overall conductivity enhancement of up to 5 times is observed. On the local scale, this can be attributed to the adsorption of anions on the particle surface. For very strong adsorption, the concentration of anions in the adsorption layer can be estimated to be 5 anions per nm^2 while the thickness of the adsorption layer is assumed to be 0.1 nm. Hereby it is worthwhile to note that the solubility limit with such a high lithium concentration is not surpassed as the anionic concentration is decreased by the same factor due to adsorption.[48] With the estimations given above, the conductivity enhancement can be predicted. However this is valid only in the case when the contact surface area is much higher than the particle surface area that can be presumed from the applied microscopy techniques. Indeed, the measured BET surface area is 270 m^2·g^{-1}. From this value the effective particle size is derived to be $\approx$1 nm. However, the BET surface area is not necessarily identical to the actually available particle surface for ion adsorption. A more direct way is given by the measurement of the ion exchange capacity via titration (For this purpose, the oxide fillers were dispersed in a 0.1 M aqueous NaCl solution and stirred for 1 h. A defined amount of a 0.01 M NaOH solution was added to each sample and the slurry was then titrated back with a 0.01 M HCl solution). The observed value for the IEC is 1.47 mmol·g^{-1}. Inserting this value into Equation (41) results in a calculated BET surface area of 219 m^2·g^{-1} which is in good agreement with the directly measured BET value. In the IEC-approach another approximation is hidden. What is experimentally measured is the proton exchange capacity. Nonetheless it reveals the number of active hydroxyl surface groups which – with a high likeliness – is very similar to the number that leads to anion adsorption.

The conductivity difference between the bulk and the composite can then be rewritten as

$$\Delta\sigma_m \approx \beta\Omega\varphi u |\Sigma| \approx \beta\varphi u \cdot IEC \cdot F\rho \tag{43}$$

If β is on the order of 1, then Equation (43) delivers a maximum overall conductivity enhancement $\Delta\sigma_m / \sigma_\infty$ of about 30 is consistent with the experimental results that show a maximum conductivity increase of 5 for $\varphi = 0.1\%$. As already mentioned the activation energies are very similar (Fig. 29) suggesting analogous ion transport mechanisms and simplifying the analysis. Naturally in this approach numerous assumptions are made that can explain the deviation between the experimental and the predicted value. The most probable

reason for the difference of the conductivity enhancements is that β is significantly lower than 1 due to the fact that by far not all particles within the network actually contribute to the newly formed conducting pathways (another one is that the number of active particle surface groups is smaller in the clusters than predicted by the IEC value being valid for individual particles). Ascribing the deviation solely to β as a result of the comparison between theory and experiment, only around 20% of the particles are taking part in completely continuous percolation which represents a rather realistic image of the whole situation. This is in particular the case as large contributions stem from the inner open porosity of the agglomerates that is not trivially connected throughout the network.[48]

Eventually it can be concluded that the space charge model of parallel resistances is able to explain the observed Soggy-sand effects in a nice way, solely through concentration enhancement. Yet additional mobility effects originating from possible contributions of the particle surface OH-groups cannot fully be excluded. In principle a good way to study them would be further temperature dependent Impedance Spectroscopy investigations. However it is expected that the β factor, representing in a way the particle network morphology, changes with temperature in a non-trivial way.

The fact that the reversible destruction of the network by ultrasonic treatment of the sample leads to a conductivity decrease followed by a recreation excludes the decisive influence of impurities such as water. Such effects are anyway improbable as the solvent has been distilled and as the salt as well as the filler particles have been dried under vacuum whereas the sample preparation has been performed under argon atmosphere. Moreover, slight water addition corresponding to the formation of a monolayer of introduced water cannot lead to the experimentally observed conductivity enhancement effects. This is also confirmed by the research of Barthel et. al.[54] Accordingly a conductivity increase of such an order of magnitude would require substantially larger water concentrations. Yet it is still not possible to fully exclude specific solvation effects at the interface.

Regarding the possible applicability of Soggy-sand electrolytes in lithium batteries the lithium transference number always remains a crucial factor for the quality of electrolytes. As already mentioned and also shown in previous investigations the addition of SiO_2 filler particles leads to the immobilization of anions at their surface and thus to an increase of the lithium transference number. Within the same model of parallel switching a connection between the

total conductivity enhancement and the Li^+ transference number of the SiO_2-free electrolyte ($t_+ \equiv \sigma_+ / \sigma$) and the composite electrolyte ($t_{m+} \equiv \sigma_{m+} / \sigma$) is given as [36, 48]

$$t_{m+} \equiv \frac{\Delta\sigma_m / \sigma_\infty + t_+}{1 + \Delta\sigma_m / \sigma_\infty} \tag{44}$$

By performing polarization experiments the lithium transference numbers

$$t\left(Li^+,\ 0.1\ M\ LiClO_4 + THF\right) = t_+ = 0.13$$

and

$$t\left(Li^+,\ \left(0.1\ M\ LiClO_4 + THF\right): 0.15\%\ SiO_2\right) = t_{m+} = 0.41$$

are determined. When the observed conductivity enhancements $\Delta\sigma_m / \sigma_\infty \approx 150\%$ for 0.15% SiO_2 are introduced into Equation (44) this results in a t_{m+} value of 0.65 which is reasonably comparable to the experimental value as Equation (44) ignores non-idealities in the particle distribution and that the experimental results refer to different samples with distinct network morphologies. The relative conductivity increase of 150% taken corresponds to a sharp maximum and any deviations would lead to smaller $\Delta\sigma_m / \sigma_\infty$ and – as a result of this – to smaller t_{m+} values.[48]

3.2.2 Advanced Oxide Materials as Soggy-Sand Filler Particles with Special Morphologies

As shown in the previous section on a fundamental basis, the performance of a composite electrolyte for a given type of salt and solvent depends on the amount of particles but, even more important, on their chemical nature and morphology. Without a strong interaction between the particles, the formed clusters and finally networks would be much denser due to the inevitable coarsening which occurs the more easily the more reversible interparticle bonding is. As then the solvent is not able to interpenetrate the clusters in a sufficient manner, favored network sedimentation is the consequence of the higher mass density. Apart from creating a stable network it should always be the aim to establish as many percolation pathways as possible. Hereby a problem has to be faced even when the interaction between the particles is strong, e.g. for small particles with a high BET surface area originating from the difficulty of controlling the network formation process. This is caused by poorly

controlled initial situations in the composite electrolytes as well as by the statistical particle movement and their aggregation. This results in different network structures for the same sample composition not only aggravating the reproducibility of experimental data but also preventing the purposeful development of an optimal network structure for a given composition. Naturally one has to work on the surface chemistry of the particles and not merely on the sheer surface area to solve this problem. Actually attempts were made to synthesize particles with specific surfaces in order to influence the network formation process and eventually the resulting network morphology. One approach in this context was done by Das et. al. [109] who synthesized so-called Janus particles, i.e. particles with two different functional surface groups on each hemisphere. Particularly, one hemisphere is kept with hydroxyl groups whereas on the other hemisphere the hydroxyl groups are capped by methyl or octyl groups. The choice of these functional groups allows for the formation of a lower number of network morphologies as the interactions between particles (H-bonding and Van-der-Waals interactions) are not isotropic but depend on the direction of their approach. As observed by Impedance Spectroscopy the conductivity with functionalized particles is lower than with non-functionalized ones. Obviously the modified surface not only leads to weaker aggregation and as a result to less stable and expanded networks but possibly also to a negatively influenced ion dissociation and ionic transport along the particle surface. Nevertheless an approach of network structure control based on the idea of surface modification remains promising especially when the attachment of polar surface groups is considered. They are not only able to strongly bond the particles but also do the job of enhancing the percentage of dissociated ions.

For many years a lot of research activities have focused on the synthesis of particles with certain non-spherical structures and special surface morphologies.[59, 110] While these materials cover a large field of possible applications such as for chemical sensors or chromatography, they have also been considered to be suitable for composite electrolytes as ionic transport might be directed along intended pathways or special network morphologies that can be formed.[111] However respective investigations by Sann et. al. [111] on mesoporous SBA-15 amongst others did not reveal any conductivity enhancements. This has been ascribed to the quick particle sedimentation due to their large size. Even while stirring the samples, their conductivities are not enhanced according to the given results. However, the materials class of mesoporous cross-linked silica particles remains interesting as filler candidates as through a

synthesis, a large variety of particle morphologies can be created with a large variety of conductivity properties. This is why in the following study possible reasons for the observed mechanical and electrical properties of mesoporous silica containing electrolytes are discussed.

In contrast to the previous investigations by Sann et. al. [111] a periodic mesoporous silica with crystal-like benzene bridges between silicon atoms (denoted as B-PMO) is used in this work which was synthesized in the group of Prof. Fröba (Hamburg University) by Jürgen Morell. The synthesis procedure is described in [59, 110] and schematically shown in Fig. 30 together with the resulting particle structure.
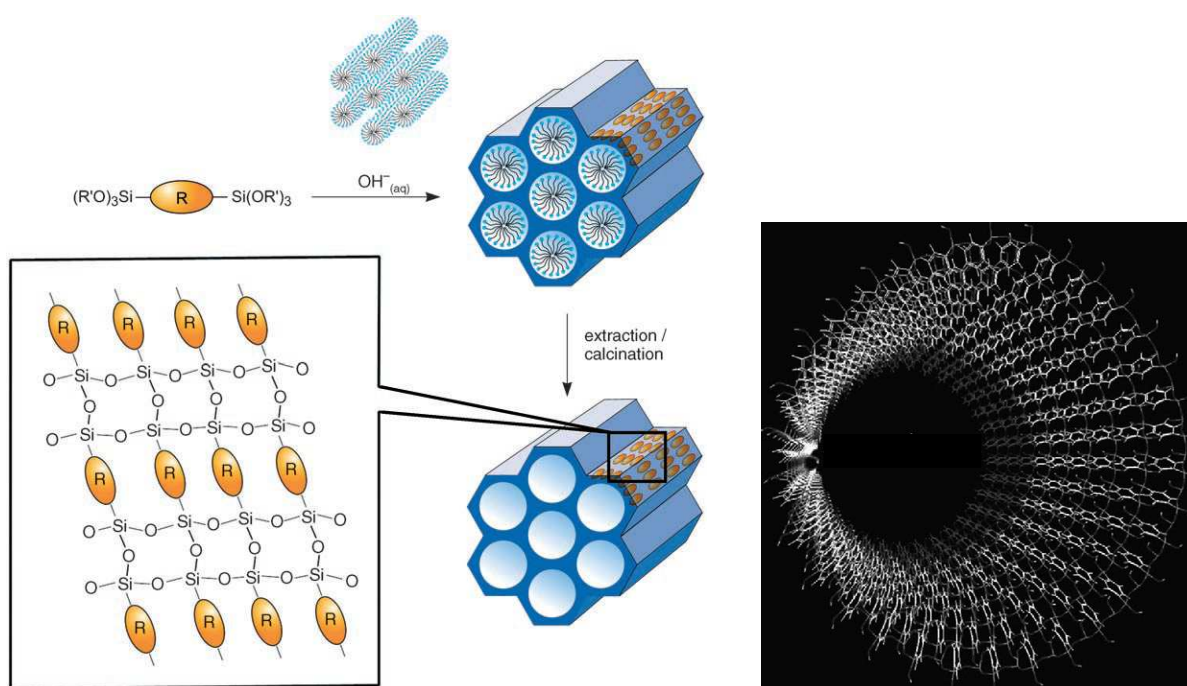
Fig. 30: Left: Synthesis procedure and structure of a typical benzene-bridged periodic mesoporous organosilica. **Right:** Model of the pore surface of a mesoporous benzene-bridged organosilica. The benzene molecules are arranged circularly along the pore and are embedded between the silica layers bordering both sides. The pore surface of the silica is saturated with silanol groups. The benzene and silica layers are arranged alternately along the pore axis.

As observed by SEM the particles are around 12 μm long and consist of a hexagonal tunnel-like structure with a pore width of 6 nm.[59, 110] When looking at such morphology it can be expected that ions released from ion pairs by the adsorption of their counterpart on the inner or outer surface might be able to travel quickly along the outer surface or inside the additional tunnels provided by the particles. To further characterize the particles, BET measurements were performed and pore size distribution was calculated as shown in Fig. 31.
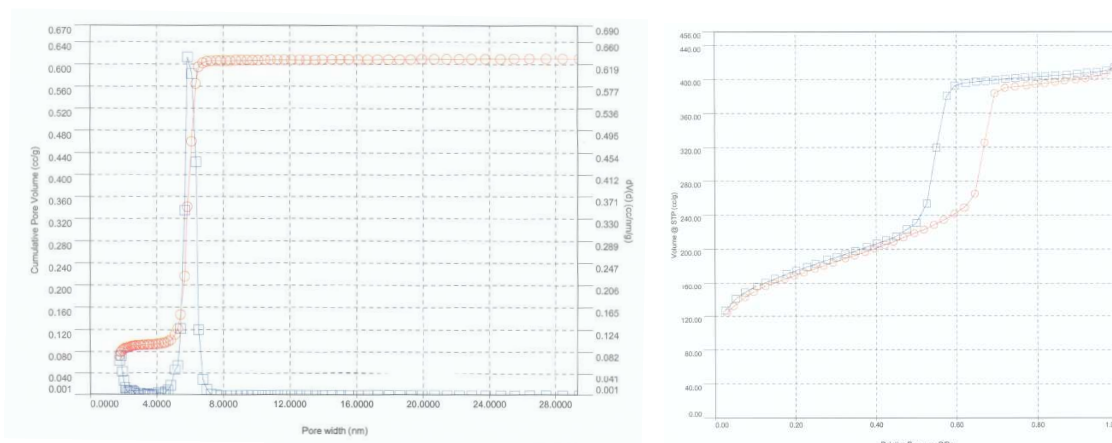
Fig. 31: Left: Cumulative pore volume of B-PMO obtained from the DFT analysis of N_2 at room temperature. Red curve: volume, blue curve: derivative. **Right:** BET isotherms of B-PMO. Red curve: adsorption, blue curve: desorption.

BET surface area is determined to be 570 m^2 g^{-1} almost as high as the surface area of fumed silica (605 m^2 g^{-1}) featuring a much lower particle size of just 7 nm. This leads to the assumption that the potential for ionic adsorption on the surface is very high.

Another promising filler is MCM-41 (Mobil Crystalline Materials, originally produced at Mobil Corporation laboratories) which is a type of a mesostructured silica with a unit cell size of 4.6 nm (TEM and HRTEM in Fig. 32 a,b). The selected section and the corresponding depth profile are shown in Fig. 33.
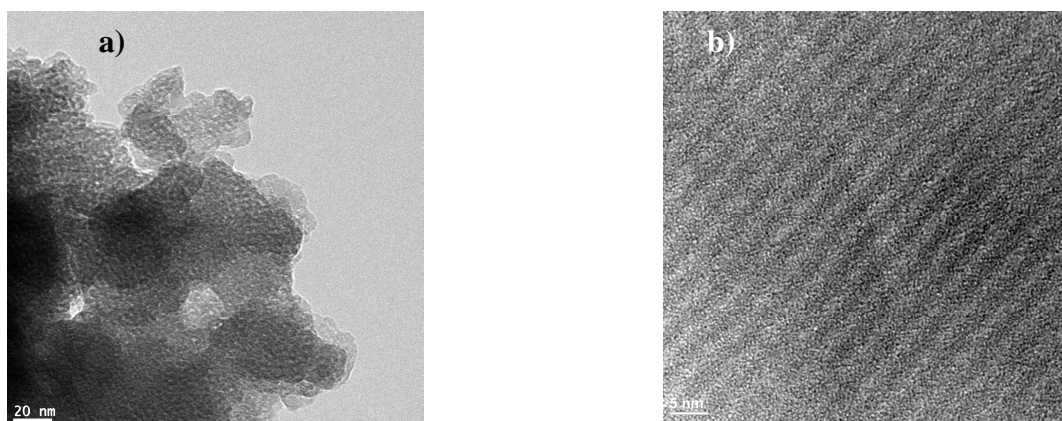
Fig. 32: a) TEM and **b)** HRTEM micrographs of MCM-41.
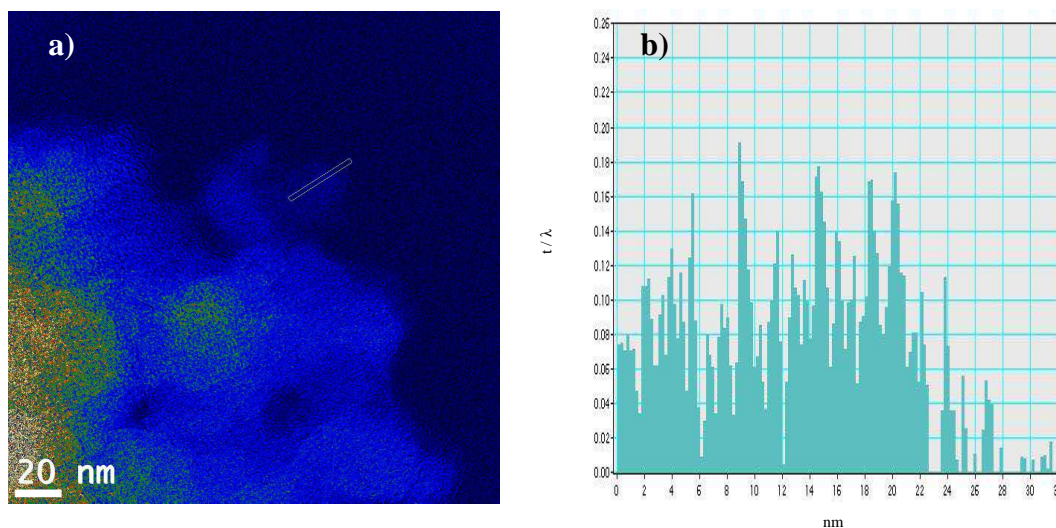

Fig. 33: a) Thickness map with the chosen section for the depth profile shown in Fig. 31 (MCM-41). Thickness maps were obtained by acquiring unfiltered and zero-loss filtered images, where only elastically scattered electrons with no energy loss contribute to the second one. The logarithm of the ratio of these images is displayed which is a measure of the specimen thickness. **b)** Typical depth profile of a MCM-41 layer, λ=114.5 nm.

It can be observed (Fig. 32 a) that a long-range order in the solid state is absent while the higher resolution micrograph (Fig. 32 b) shows well developed sub 5 nm wide porous channels. With the additionally recorded depth profiles, the uniformity of the silica particles is evaluated (Figs. 32 c and 33); micrographs as well as the depth profile reveal a non-symmetric alternation of silica and pores. The actual particle size is difficult to determine due to the strong deviation of the particle shape from a model sphere. Furthermore the particle's pore volume of 0.98 cm^3 g^{-1} and its pore size of 2.3-2.7 nm were determined by DFT analysis of the nitrogen adsorption isotherm shown in Fig. 34.
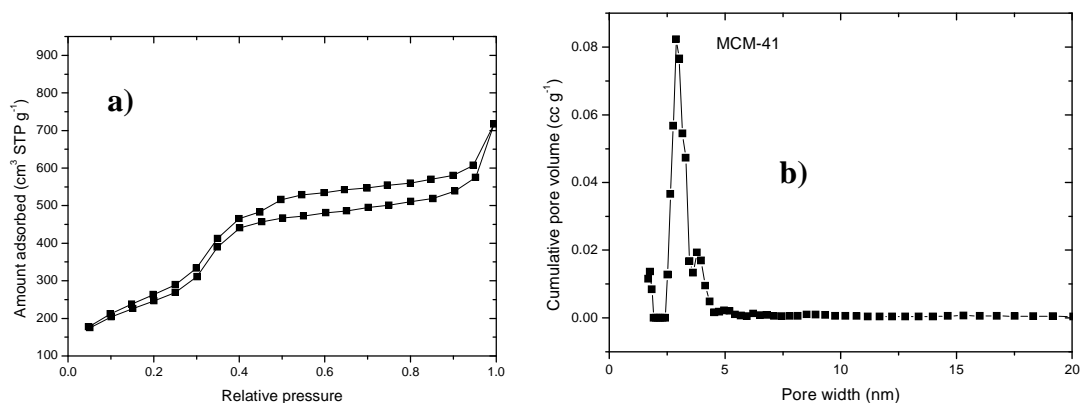
Fig. 34: a) BET isotherm of MCM-4. **b)** Pore size distribution of MCM-41 obtained from the DFT analysis of the nitrogen adsorption isotherm.

Remarkably the BET surface area (Fig. 34, black curve) of MCM-41 reaches a value of 990 m^2g^{-1} which leads to the expectation of high ionic adsorption degree. However the non-uniformity of the particles is not a good pre-condition for the formation of stable and expanded silica networks.

The third tested filler type, MSU-H (originally synthesized at Michigan State University, hexagonal structure) represents a much more ordered structure, shown in Fig. 35 with the respective depth profile displayed in Fig. 35.
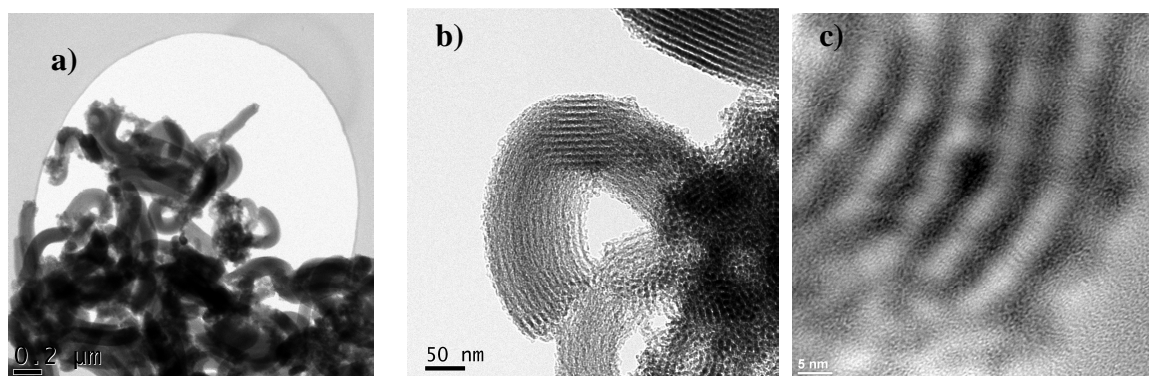

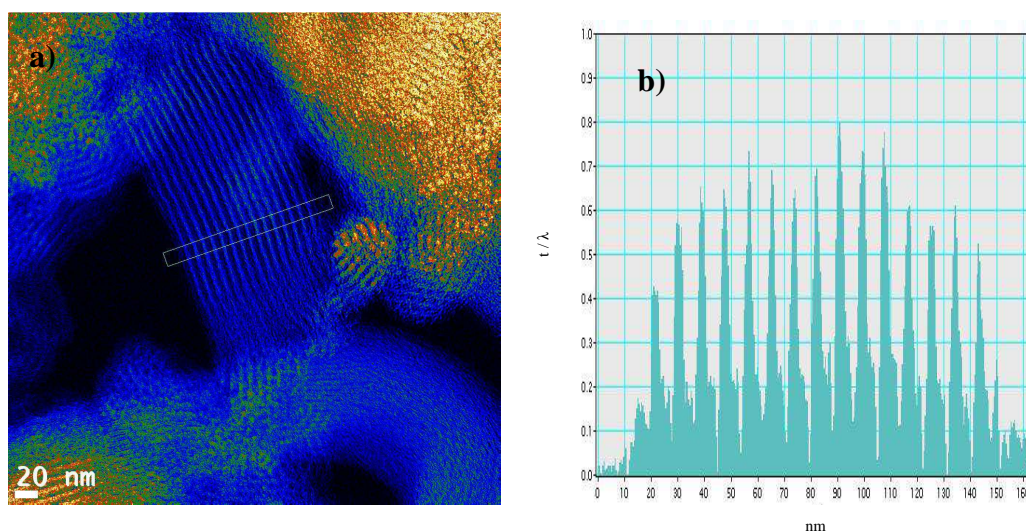**Fig. 35: a)** TEM, **b)** HR-TEM micrographs of MSU-H and **c)** HR-TEM micrograph, visible pores

Fig. 36: a) Thickness map with the chosen section for the depth profile shown in Fig. 7d (MSU-H). Thickness maps were obtained by acquiring unfiltered and zero-loss filtered images, where only elastically scattered electrons with no energy loss contribute to the second one. The logarithm of the ratio of these images is displayed which is a measure of the specimen thickness. **b)** Typical depth profile of a MSU-H layer, $\lambda = 114.5$ nm.

It can be seen from the micrographs that the particles show more uniform morphologies and accordingly long range two-dimensional hexagonal structures with parallel pores within the particles. This is corroborated by the symmetrical depth profile for a typical MSU-H layer (Fig. 36b). The analysis reveals worm-like particles with average size of ≈ 250 nm. From Fig. 37a, the BET surface area can deduced to be 764 m^2g^{-1} which – together with the two different pore sizes of 7 nm and 15 nm (determined from the N_2 adsorption isotherm in Fig. 37b). The existence of bimodal pore size distribution arises from the intrinsic feature of MSU-H –inter-particulate textural mesopores coming from the regions between the fundamental domains. [112] Hereby the predominant pore size is substantially larger in comparison with MCM-41 (15 nm pores, Fig. 37b) with only a small amount of smaller mesopores (7nm) in each individual particle.
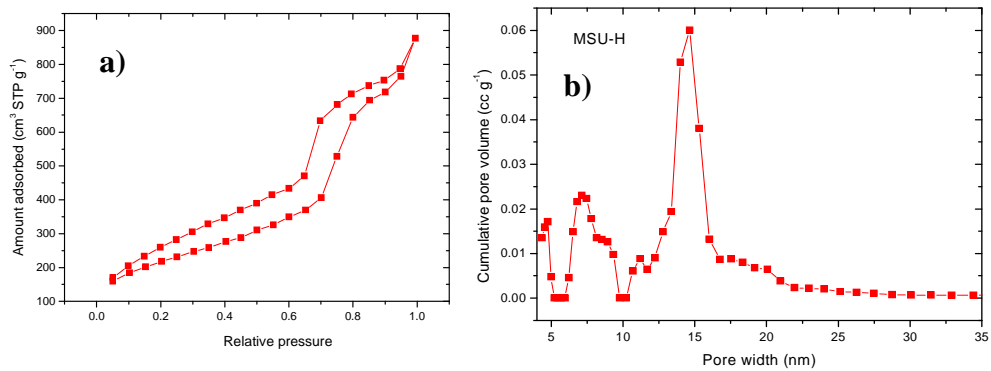
Fig. 37: a) BET isotherm of MSU-H. **b)** Pore size distribution of MSU-H obtained from the DFT analysis of the nitrogen adsorption isotherm.

The surfaces of both MSU-H and MCM-41 are covered exclusively with hydroxyl groups (Si-OH) which is revealed by the Infrared Spectra in Fig. 38.
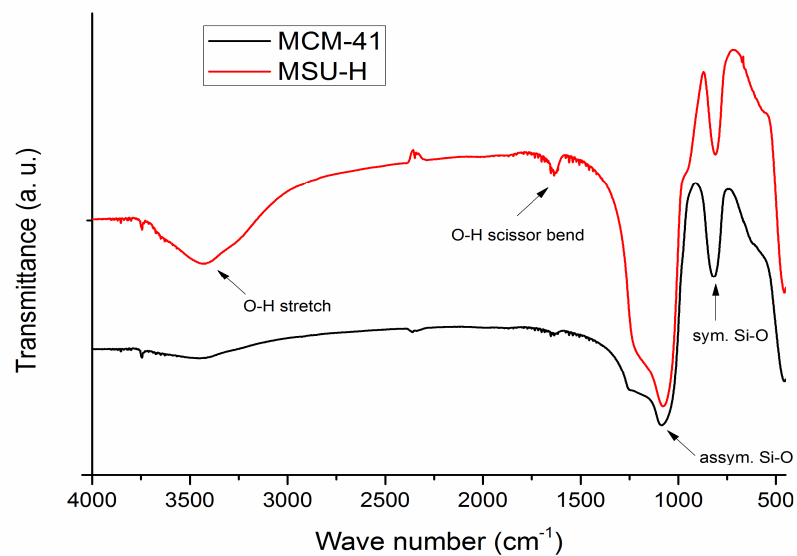

Fig. 38: Infrared spectra of MCM-41 and MSU-H.

According to the powder analysis all three filler types have the potential to lead to improvements of the electrical and/or mechanical properties of electrolytes. To test the characteristics of the resulting composites, lithium triflate is used as a typical salt together with DMSO or PEG-150 as solvents.

An initial hint towards the ability to adsorb ions on the surface is the composite electrolyte's Zeta potential as a function of φ. As an effective and complex value it not only gives insight into the individual particle's capability of ion adsorption but also sheds light on the

interparticle aggregation and the resulting stability of the dispersion. In the context of lithium battery electrolytes one aims at negative Zeta potential values denoting the preferential anion adsorption. This has often been observed with conventional filler types such as fumed silica.[30] The results for B-PMO containing samples with 1M LiOTf + PEG-150 are shown in Fig. 39.
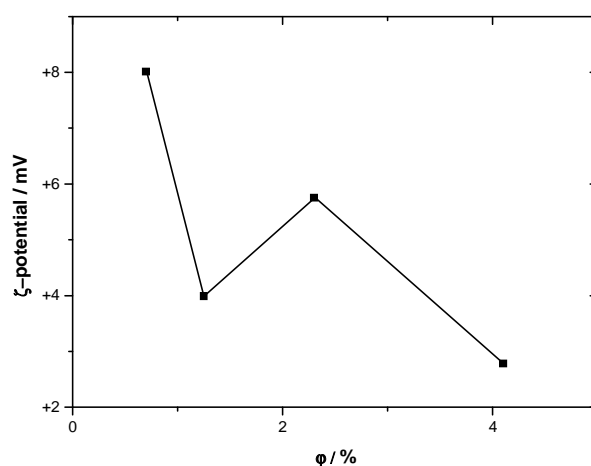

Fig. 39: Zeta potential of B-PMO containing 1 M LiOTf / PEG-150 as a function of φ(B-PMO).

Surprisingly the Zeta potential has positive values for all particle volume fractions, an unusual behavior for Soggy-sand fillers. Yet the typical decrease of the absolute value of the Zeta potential is often observed and arises from the particle aggregation and the resulting lower surface area being relevant for ion adsorption. The positive sign denotes a preferential cation adsorption at the surface which, at least for lithium ion battery electrolytes, is a disadvantageous phenomenon. Obviously the silanol groups at the outer and inner surface of B-PMO are not capable of adsorbing the large anions either due to weak interaction or due to steric reasons. Rather the lithium ions are adsorbed more easily even though there are no electron-rich accessible functional groups present at the particle surface. This leads to the conclusion that the lithium ions are attracted by the benzene rings which are a structural element of the porous morphology. The formed Li^+-benzene-π-complexes are well known to be stable.[113] In any case the preferential cation adsorption is unfavorable and involves no real benefits from the rather high BET surface area of B-PMO. The rather low absolute values of the Zeta Potential give a strong indication of the kinetic instability of the dispersions finally leading to particle sedimentation. This could be a consequence of the unfavorable/insufficient

wetting of the organosilica particles. Simply by the naked eye the sedimentation tendency can be observed rather quickly after the sample preparation (Fig. 40).

Fig. 40: Sedimented B-PMO (2.8 Vol-%) in 1 M LiOTf / PEG-150 after 2 hours.

In the case of non-occurring gel formation together with the observed low absolute values for the Zeta potential it is reasonable to state that the aggregation is occurring in a spherical way leading to clusters which, as a result, simply resemble a super-particle of a correspondent larger size. In such as unfavorable situation sedimentation is unavoidable (cf. to Equation (4)). Furthermore it is probable that even the non-aggregated particles coagulate as their size is 40-50 times larger than those of MCM-41 and MSU-H. This fact together with preferential cation adsorption can explain the non-satisfactory conductivity behavior by Sann et. al.[111] Yet as the particle type is not exactly comparable to the previous investigations the AC conductivity for a typical sample (1 M LiOTf + PEG-150: B-PMO (2 Vol-%)) is measured and set in comparison to the filler-free solution (Fig. 41).
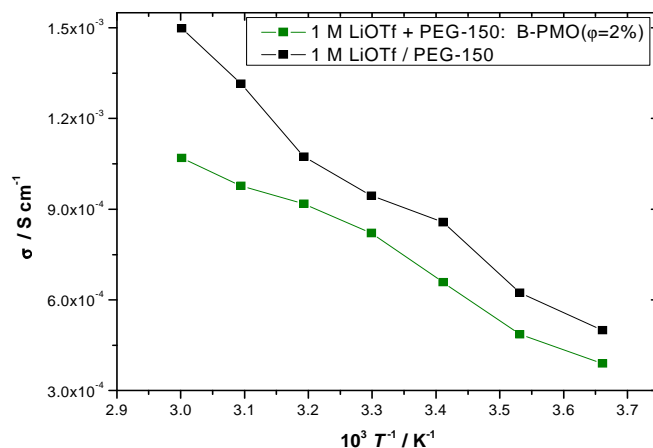
Fig. 41: Conductivity as a function of temperature in a typical B-PMO sample.

For this filler type no favorable conductivity increase is obtained in the measured temperature range which is also valid for other B-PMO volume fractions. The low total conductivity is the consequence of the low *IEC* value of 0.377 mmol·g^{-1} indicating small adsorption strength despite the high BET value. With the previously shown results of the Zeta potential one comes to the conclusion that the aggregates are not stable which is probably caused by the effective low outer surface-to-volume ratio of the particles. The contact area between two tubular particles is rather small leading to weak Van-der-Waals interactions and hence to pure statistical alignment of the particles. Therefore stable networks cannot be expected. This however also means that the advantages of the additional ionic conduction do not show up because of bad percolation. Even if the ionic diffusivity within one particle/pore is high, further transport is hindered by the statistical particle arrangement. This is also valid for similarly shaped particles of a comparable size (several micrometers) with more suitable functional groups for ionic dissociation. However, the approach to increase the particle porosity and thus increase the numbers of channels for ion transfer remains promising and is not investigated in detail, especially in the context of nano-sized particles.

As MCM-41 particles are much smaller and provide an even higher BET surface area more suitable Zeta potential and conductivity data are expected to be obtained. When looking at the Zeta potential (Fig. 42) for 1M LiOTf + PEG-150 and 1M LiOTf + DMSO, a rather familiar Zeta potential vs. φ relationship is recognized.
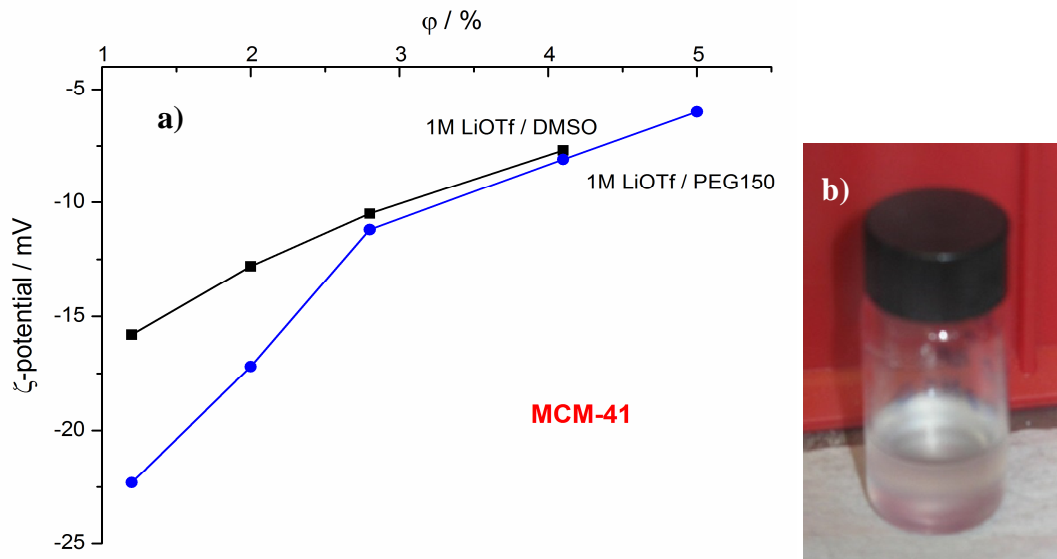
Fig. 42: a) Zeta potential of MCM-41 containing samples as a function of φ(MCM-41). Measurements were made at room temperature. **b)** Stored sample of 1 M LiOTf / PEG-150 /MCM-41 (2 Vol-%) after 1 day.

The preferential anion adsorption is indicated by negative Zeta potential values. Furthermore the absolute values remain rather high up to $\varphi = 0.028$. Especially in this regime one can expect kinetic stability of formed networks in which enough particle surfaces are spatially available for ion adsorption. When comparing the two solvents DMSO and PEG-150 it can be stated that the absolute values for the DMSO containing samples are lower (in particular for lower volume fractions) while the decrease of Zeta potential for higher volume fractions is less steep than for the PEG-150 containing samples. This indicates that in PEG-150 the ion dissociation effect in the diffusive layer around the particles in relation to the bulk is stronger due to the lower dielectric constant of PEG-150 resulting in higher amount of ion pairs compared to DMSO. At the same time it can be observed even by the naked eye that gelation is more pronounced for PEG-150 containing samples reflecting higher absolute Zeta potential values for large φ. Probably due to the missing long-range order of the particles the prepared composite electrolytes are only mechanically stable for few days.

As a result of the previous observations, MSU-H might as well be a good candidate for a soggy-sand filler fulfilling both conditions of high surface area due to high porosity as well as the low tendency of sedimentation due to nano-sizing of the particles. The respective Zeta potentials for 1M LiOTf + PEG-150 and 1M LiOTf + DMSO (Fig. 43), the values are also negative and slightly higher absolute values can be noticed for large volume fractions in PEG-150 based electrolytes compared to the situation of MCM-41.
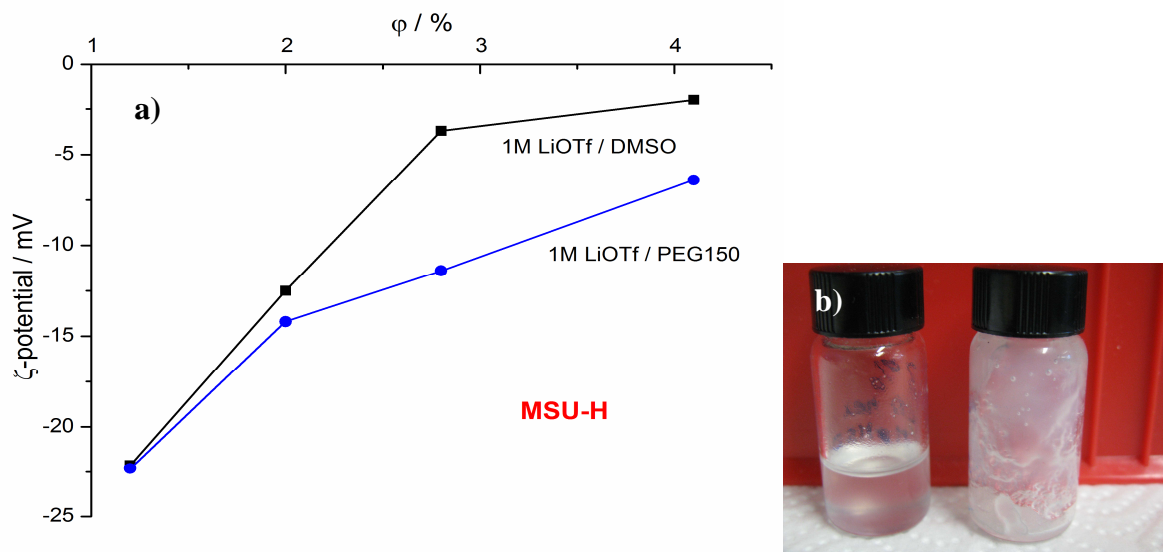
Fig. 43: a) Zeta potential of MSU-H containing samples as a function of φ(MSU-H). Measurements were made at room temperature. **b)** Stored samples of 1 M LiOTf / PEG-150: MSU-H ($\varphi = 2\%$, left) and 1 M LiOTf / PEG-150: MSU-H ($\varphi = 2.8\%$, right) after 5 days.

On the contrary, for small volume fractions, the MCM-41 containing samples show higher absolute Zeta potential values. This is understandable as MCM-41 shows a higher BET surface area compared with MSU-H. As a result, in the typical situation for low φ of few expanded clusters being present, the ion adsorption capability of MCM-41 particles is slightly higher. In further comparison of the samples containing each filler sort by naked eye, it can be observed that the MSU-H containing samples show a strong tendency of gel formation (Fig. 43b). For the same volume fraction in 1M LiOTf + PEG-150 they feature a semi-solid character whereas the MCM-41 containing samples are still liquid. This obviously has to do with the existent long-range order of MSU-H particles and leads to a steeper decrease of the Zeta potential caused by the spontaneous cluster formation. As far as the difference of the results between the two used solvents is concerned a very similar trend is observed as for MCM-41 containing electrolytes. Again by introducing particles to the electrolyte, more ion pairs can be broken in the case of PEG-150 as its dielectric constant is lower leading to a higher effective Zeta potential, in particular for higher volume fractions. In summary, it can be stated that the values of Zeta Potential are not too high so that interparticle repulsion prevents agglomeration due to the high surface charge on each individual particle overcoming the attractive Van-der-Waals forces. On the other hand it is still large enough in absolute values to impede sedimentation over a longer time period (Fig. 43b) allowing for improved mechanical properties of the electrolytes. While the sample containing φ (MSU-H) = 2% is a

viscous liquid, the sample characterized by φ (MSU-H) = 2.8% already features the characteristics of a gel. Additionally, when the samples were heated after a first measurement of the Zeta potential at room temperature to 80°C and cooled down again to room temperature, the measured Zeta potential stayed nearly invariant indicating that the surface properties and probably also the network structure hardly change upon heating/cooling

To investigate the mechanical properties of the composite electrolytes with the two filler types MCM-41 and MSU-H, rheology represents a powerful tool as this technique not only determines the viscosity of the sample but can also confirm the presence of a non-Newtonian liquid if the dynamic viscosity is measured as a function of the shear rate. The respective results for samples with various particle volume fractions are shown in Fig. 44.
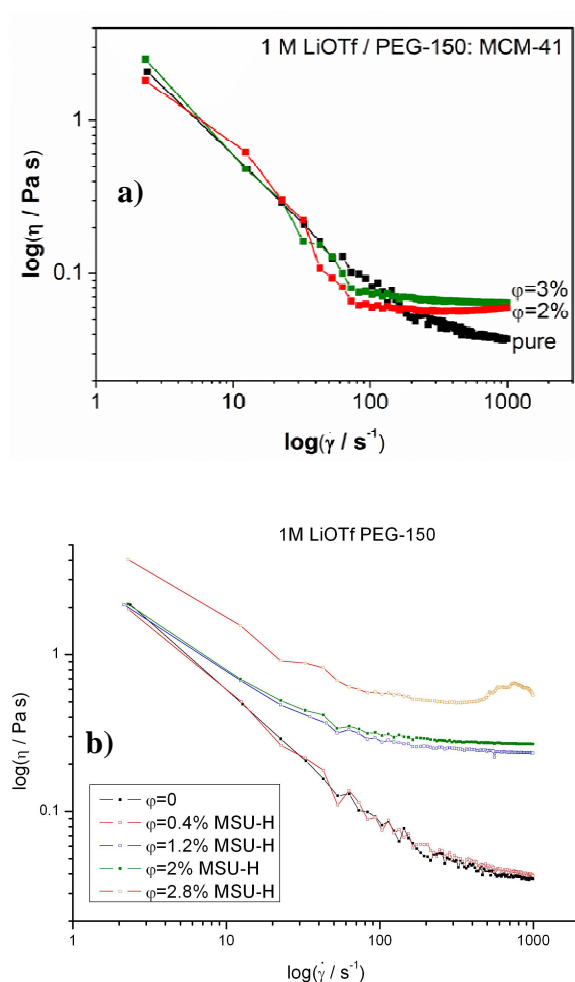

Fig. 44: Viscosity as a function of the shear rate for **a)** MCM-41 and **b)** MSU-H containing samples.

In the case of low volume fractions for both filler types, the viscosity decreases systematically with the increasing shear rate. Such non-Newtonian, shear-thinning behaviour indicates the presence of coherent networks and is typical for pseudoplastic materials.[114] For MCM-41

containing Soggy-sands (Fig. 44a), the viscosity increase is not distinct, in particular for lower shear rates (below 100 s^{-1}). Even though networks of MCM-41 particles might exist, they seem not to be stable and to expand over the whole electrolyte to form a gel. For MSU-H containing composite electrolytes (Fig. 44b) however, the viscosity strongly increases, particularly with $\varphi > 1$ Vol-% which is in good agreement with naked eye observations. Additionally, for higher volume fractions (2.8 Vol-%) the viscosity firstly decreases and then increases at higher shear rate (over 500 s^{-1}). This can be attributed to a transition from shear-thinning to shear-thickening behavior according to previous investigations [30] where this effect has been ascribed mutual hindering of broken network parts. As a result, the viscosity dynamically increases.

Naturally, it is crucial to see how the observed local properties influence the overall conductivity of the composite electrolytes. As both filler types lead to far more favorable Zeta potential values than the B-PMO containing electrolytes and they do not sediment, an advantageous impact on the AC conductivity is also expected. For that purpose temperature dependent Impedance Spectroscopy has been carried out (Fig. 45) with a focus on MSU-H as filler as it shows more promising mechanical properties.
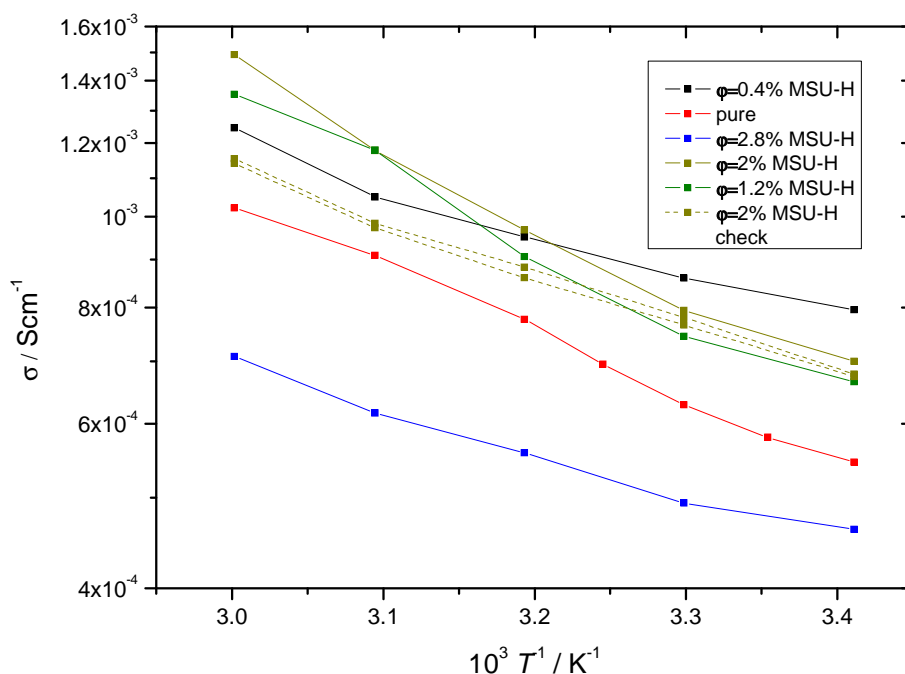

Fig. 45: Temperature dependent AC conductivity for 1 M LiOTf + PEG-150 and MSU-H as filler material with different volume fractions.

Increased conductivities are observed for all electrolytes containing MSU-H with a volume fraction $\varphi(MSU-H) \leq 2$ Vol-% . Interestingly, the relative conductivity increase reaches up to 45%, which is comparable to PEG-150 based electrolytes with fillers which are much smaller in size such as 10 nm sized silica or even fumed silica (7 nm).[30] This can be attributed to the additional internal pathways provided by the particles themselves. The graphs are highly reproducible upon heating and cooling revealing a good kinetic stability of the formed network. However the reproducibility in terms of sample composition is not very high as indicated by the scatter of the effective activation energies as well as by an additional measurement of a newly prepared sample with $\varphi(MSU-H) = 2\%$ in Fig. 45. The conductivity behavior for both samples (1M LiOTf + PEG-150: 2 Vol-% MSU-H) is comparable up to 40°C above which the conductivity in the firstly prepared sample reaches higher values probably due to the different structure of the formed particle network.

In contrast to what would be expected (lower conductivity in the cooling cycle due to coarsening effect), the conductivity for the cooling cycle lies slightly above the one for the initial heating cycle. This is of fundamental interest as it shows in the case of MSU-H that the created networks do not rearrange in an unfavorable manner – described by the coarsening concept – and macroscopically remain stable and able to favorably influence the ionic transport throughout the entire electrolyte. The reason for this might lie in the fact that the particle "sliding" along the network surface – a typical mechanism in the context of coarsening – is hindered by the internal porosity and the resulting interparticle contact area.

For $\varphi(MSU-H) = 2.8\%$, the overall conductivity is reduced. This is a typical behavior of Soggy-sand electrolytes at higher volume fractions due to the fact that a high amount of particles leads to partial blocking of percolation pathways. Furthermore, inhomogeneous wetting and salt adsorption/exhaustion can occur in such systems which will be discussed in a later section (chapter 3.2.4). The blocking effect obviously overcompensates the strong porosity effect which increases the number of possible percolation pathways. Nonetheless, the total conductivity for such a semi-solid material (Fig. 45) is still high considering the fact that the particle size is around 10-20 times larger than fumed silica nanoparticles with a similar surface chemistry. Obviously the porosity effect dominates.

Another crucial parameter for the applicability of a lithium battery electrolyte is its lithium transference number t_{Li^+} . As a result of the observed anion adsorption via the Zeta potential

measurements, a significant t_{Li^+} increase is expected. As a reference, t_{Li^+} of the pure liquid electrolyte (1 M LiOTf + PEG-150) has been determined to be t_+ (1 M LiOTf + PEG-150) = 0.22. At first glance, such value reveals the dominance of anion conductivity. The actual individual contributions to the overall conductivity will be investigated in more detail in a later section (chapter 3.3).

Looking at the composite electrolytes – again with a focus on MSU-H as filler material and PEG-150 as a solvent – different transference numbers are observed. Typical polarization curves are shown in Fig. 46 representing the basis for determining the transference number together with AC conductivity data measured before and after the polarization process with lithium electrodes. It has to be kept in mind when considering the non-monotonic curve shapes that the mesoporous particles probably interact chemically with the highly active lithium electrodes in an unfavorable way which has a certain influence on the measurement. The lithium transference number t_{m+} (1 M LiOTf + PEG-150: φ (MSU-H) = 2%) = 0.49 of the composite electrolyte (with φ (MSU-H) = 2% is more than twice as high compared to the filler-free electrolyte (t_+ = 0.22) which confirms the model of anion adsorption and locally enhanced lithium diffusivity. Furthermore, in the composite electrolyte with φ (MSU-H) = 2.8% the transference number t_{m+} (1 M LiOTf + PEG-150: φ (MSU-H) = 2.8%) = 0.30 is enhanced in spite of the reduced overall conductivity (Fig. 46).
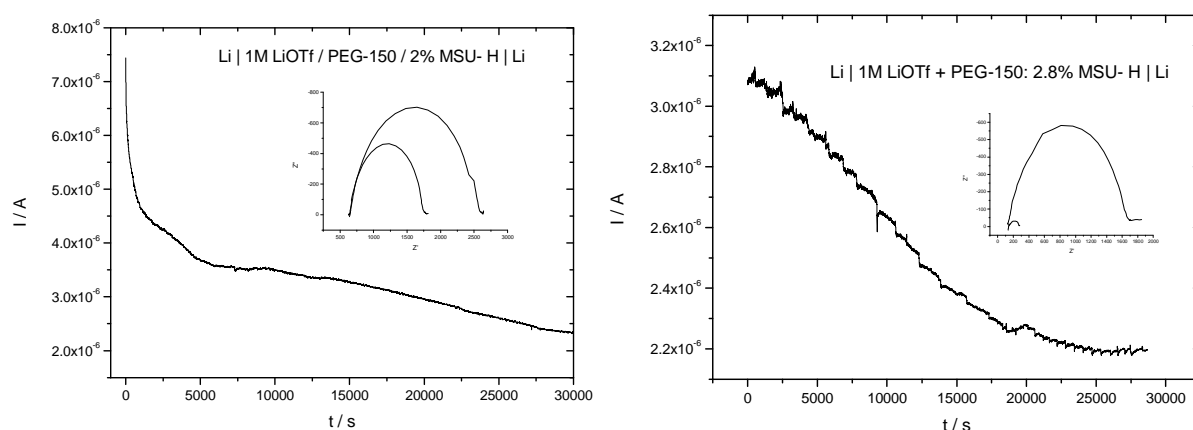

Fig. 46: Electric current as a function of time at room temperature for different MSU-H containing electrolytes. The DC measurements were carried out potentiostatically at 10 mV across the symmetric cell. Left: 1 M LiOTf / PEG-150 / 2% MSU-H, Right: 1 M LiOTf / PEG-150 / 2.8% MSU-H. The lithium metal electrodes are blocking the anions such that in the steady state only lithium ions flow (cf. section 2.2.6).

The latter can be attributed to the fact that even if the ions are not able to be transported throughout the electrolyte due to the blocking effect there is still enough network surface present to enhance the ion pair dissociation leading to an enhanced conductivity in the vicinity of the network for a short range transport.

As shown in chapter 3.2.1, the transference number can be linked with the conductivity enhancement according to Equation (44). With the assumption that due to the increase of σ_+ and decrease of σ_- at one SiO$_2$ content the cation transference number in the space charge zones can be regarded to be close to unity, Equation (2) leads to [115]

$$t_{m+} = \frac{\sigma_{m+}}{\sigma_m} = \frac{\sigma_\infty^+ + \varphi\alpha\sigma_{scl}}{\sigma_\infty + \varphi\alpha\sigma_{scl}} \tag{45}$$

where α stands for the volume ratio of the space charge layer to silica particle and σ_{scl} is the average conductivity over the space charge layer. Using Equation (44) the transference number for the (1M LiOTf + PEG-150): 2 Vol-% MSU-H composite can be estimated to be $t_{m+} = 0.37$ which is in reasonable agreement with the measured one (0.49). This result has to be taken with a pinch of salt as the experimental determination of the transference number contains an absolute uncertainty of around 10%. Furthermore possible deviation of the predicted t_{m+} is related to the fact that Eq. (44) is no longer well fulfilled if the mobile ion pairs are present. This will be discussed in section 3.3. Note that the $\sigma_m(\varphi)$-curve increases with φ initially and after having reached a maximum decreases due to blocked pathways. The sample with this volume fraction already shows an increased conductivity, but beyond the volume fraction of the maximum. Obviously blocking effects solely have an impact here. This aspect is not taken into account in Equation (44). Especially for φ (MSU-H) = 2.8% however, bulk path blocking cannot be neglected anymore as the overall conductivity is lower than $(1-\varphi)\sigma_\infty$. As a consequence $\Delta\sigma_m / \sigma_\infty$ becomes negative. For the purpose of estimating the lithium transference number also in this case, the additional bulk percolation efficiency factor β_∞ has to be considered (Note that blocking factors do not explicitly appear in Eq. (45)). Therefore σ_∞ is replaced by $\beta_\infty\sigma_\infty$ leading to the more accurate expression

$$t_{m+} = \frac{\beta_\infty (t_+ - 1) + 1 + \dfrac{\Delta\sigma_m}{\sigma_\infty}}{1 + \dfrac{\Delta\sigma_m}{\sigma_\infty}} \qquad (46)$$

To be precise, β_∞ needs to be multiplied by $(1-\varphi)$.[115] Yet the deviation of the latter term from 1 is negligible. For the (1M LiOTf + PEG-150): 2.8 Vol-% MSU-H sample a reasonable value for β_∞ = 0.74 is obtained when the experimentally observed values for $\Delta\sigma_m/\sigma_\infty$ and t_{m+} are inserted in the Eq. (46). Accordingly, around ¼ of the possible percolation pathways are blocked here. The above assumption that space charge percolation is more sensitive to non-ideal silica distribution than bulk percolation is able to explain the maximum appearing in the lithium transference number vs. φ relation.[31] Such a behavior is highly probable as network interruption directly leads to interruption of the space charge pathways but not of the bulk pathways. Blocking effects that affect bulk and space charge layer identically would not affect the effective transference number as such blocking factors would cancel out in Equation (46). If only bulk pathways are blocked an increase of t_{m+} would be the consequence which is indeed confirmed for high particle volume fractions (Table 3 and Fig. 47).

Sample	t_{m+} (exp.)= t_{pol+}
1 M LiOTf + PEG-150	0.22
1 M LiOTf + PEG-150: MSU-H ($\varphi = 2\%$)	0.49
1 M LiOTf + PEG-150: MSU-H ($\varphi = 2.8\%$)	0.30
1 M LiOTf + PEG-150: MSU-H ($\varphi = 5\%$)	0.27
1 M LiOTf + PEG-150: MSU-H ($\varphi = 8\%$)	0.30
1 M LiOTf + PEG-150: MSU-H ($\varphi = 10\%$)	0.49

Table 3: Lithium transference number values for (1M LiOTf + PEG-150) electrolytes with different MSU-H volume fractions.
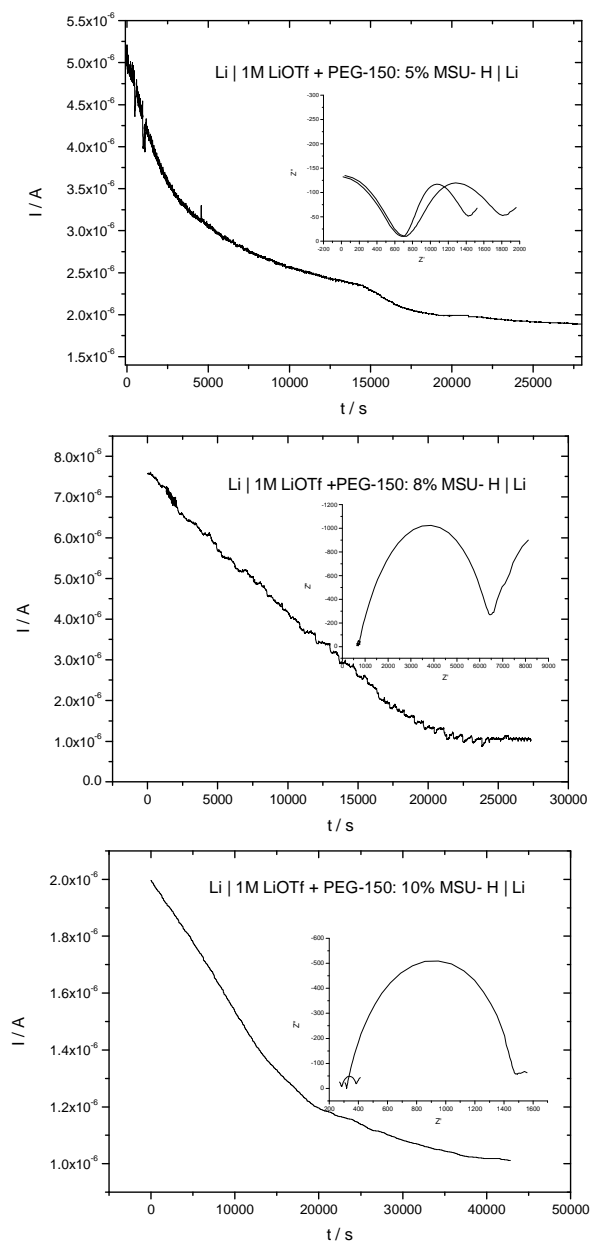
Fig. 47: Electric current as a function of time at room temperature. The DC measurements were carried out potentiostatically at 10 mV across the symmetric cell (lithium electrodes). Top left: 1 M LiOTf + PEG-150: 5 Vol-% MSU-H, Top right: 1 M LiOTf + PEG-150: 8 Vol-% MSU-H, Bottom: 1 M LiOTf + PEG-150: 10 Vol-% MSU-H.

Additional AC conductivity results with DMSO as a solvent are shown in Figure 48.
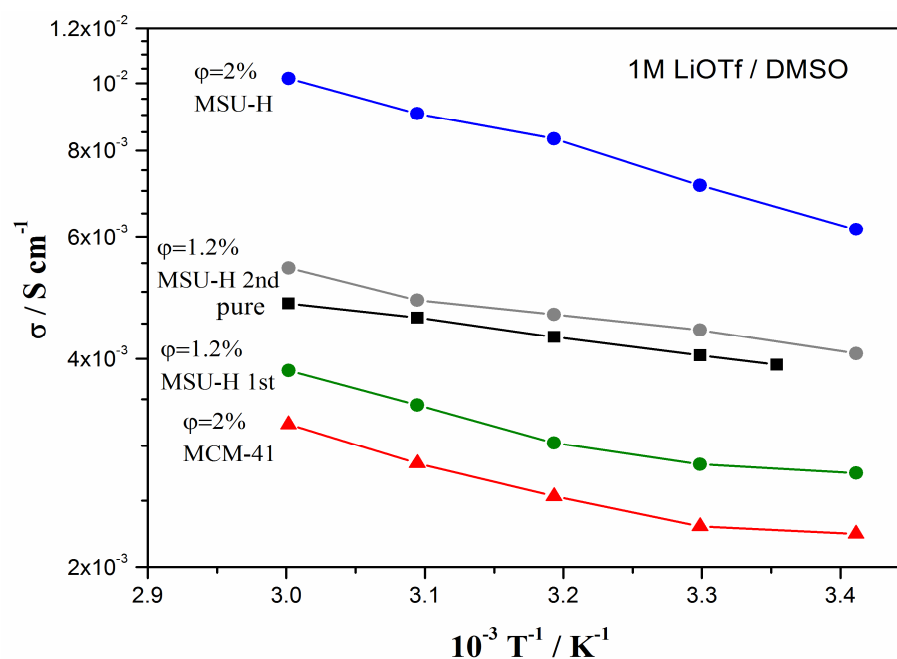
Fig. 48: AC conductivity as a function of temperature for 1 M LiOTf + DMSO and different volume fractions of MSU-H/MCM-41 as filler materials.

As can be seen the conductivity enhancement for most composite electrolytes is lower than in the case of PEG-150. This is well expected due to the higher dielectric constant of DMSO leading to a degree of dissociation which is already high in the pure solution. Therefore, the particles addition cannot enhance this value much further. For φ(MSU-H) = 1.2 Vol-% of MSU-H the conductivity is not easily reproducible for different samples as the first sample (green curve) leads to a decrease in conductivity whereas the second sample (gray curve) shows a slight increase. This is a consequence of the statistical network formation in a liquid electrolyte. In the case of φ (MCM-41) = 2 Vol-% (red curve) the conductivity is lower than for the filler-free sample. Here, the particles seem to disturb the good conductivity that is provided by the high amount of free ions. Interestingly, for φ (MSU-H) = 2% an enhanced conductivity is obtained. Simultaneously, the activation energy for this sample is slightly higher compared with the other samples. This might be due to the competing effects of increased principal ionic mobility of lithium due to lower electrophoretic hindrance by the anion in the space charge zone of the additional pores and the stronger solvation by the solvent molecules to enable transport especially inside the pores. Due to the small diameter of

the pores the fraction of space charge conductivity within them compared with the bulk conductivity is high in contrast to the situation at the outer edge of a particle. One could tend to assume that the conductivity could be hindered by the size of the solvation shell for lithium ions when it cannot be completely formed within the pores. However the diameter of typical solvation shells of dissolved Li in organic solvent is ~0.4 nm which is sufficiently smaller compared to even micropores.[116]

In summary, the pore size (2.5 nm for MCM-41 vs. predominantly 15 nm for MSU-H) and morphology of the particles has a predominant influence whereas the specific surface area only plays a minor role in the ability of filler's ionic adsorption and consequently enhancement of the ionic transport. The anions seem to be adsorbed preferably at the outer surface of the MCM-41 particles whereas the diffusion of the solvated ion pairs and ions into the pores seems to be slow in the case of MCM-41 due to the smaller pore size and a non-uniform pore distribution as observed by depth profile compared with MSU-H. This is additionally supported by the different ion exchange capacities of MCM-41 (IEC(MCM-41) = 0.497 mmol g^{-1}) and MSU-H (IEC(MCM-41) = 0.842 mmol g^{-1}). With the IEC of MSU-H reaching almost double the IEC value of MCM-41 in view of the smaller BET surface area the pores seem to be more easily accessible for the electrolyte. To explain the similar Zeta potential values (Figure 43a and 44a) it is reasonable to assume that the adsorbed ions within the pores of MSU-H are not sufficiently contributing to the overall measured Zeta potentials. Obviously, the special structure of MSU-H containing interconnected pores of sufficient size is crucial for good ionic transport. For this special filler, the amount of φ (MSU-H) = 2% in the PEG-150 solvent seems optimal for creating numerous percolation pathways combined with a negligible blocking effect of particles that do not directly enhance the ionic conductivity. It is promising in terms of applicability that in PEG-150 which has a similar dielectric constant and viscosity to the typically used Li battery solvent 1:1 EC/DMC [111] it is possible to achieve increased conductivities while the composite gel-like electrolyte remains mechanically stable for weeks.

3.2.3 Numerical Modeling of Soggy-Sand Electrolytes in the Steady State

Apart from the numerical investigations of the network formation and coarsening kinetics it is of great use to apply the simulation to the steady state situation in a Soggy-sand electrolyte as well.

Especially in the case of Soggy-sand electrolytes it is important to be able to roughly predict which external parameters (type and amount of particles, solvent, salt concentration) have to be adjusted to achieve a certain conductivity enhancement in a composite electrolyte compared to the particle-free electrolyte. Additionally it is not only the conductivity that is of interest but in terms of mechanical stability also the fractal dimension (co-domain between 1 and 2) of the cluster, the average amount of neighbors for each particle (maximal 4 due to two-dimensional lattice) and even the percolation probability (co-domain between 0 and 1) give a hint on the "quality" of a formed network. Thereby the percolation probability is defined as the time span with full percolation divided by the total number of simulation time. By this definition percolation is only recorded if it is permanently stable. For the purpose of determining these values, the developed simulation needs to investigate the cascade external parameters-network structure-physical properties. As a result the simulation is helpful in selecting materials as to achieve beneficial properties.

In the simulation the concentrations vary from 0.056 to 0.25. Due to the two-dimensional approach and other assumptions arising from the nature of Monte Carlo simulation these values do not quantitatively correlate with an experimental particle volume fraction. It has been observed experimentally in many composite electrolytes that beyond a volume fraction of 0.10 the particles are not wetted homogeneously and the electrolyte appears to be solid rather than gel-like which results in very low conductivities. However the theoretically investigated concentrations cover the range from very low to high volume fractions. Furthermore the attractive particle interaction potential $V_{attractive}$ in close proximity is varied from 50 meV to 150 meV. In the following typical physical values are investigated as a function of the outer parameters of particle concentration and $V_{attractive}$.

Figure 49 shows the average connectivity for each particle as a function of time until the steady state. It can be seen that the number of neighbors decreases with increasing interaction energies. Here the effect is observed that the attractive interaction energy of a specific particle

to another particle to which it initially sticked is too high to be overcome even though the total energy for this particle in another environment with a higher number of surrounding particles would be even lower.
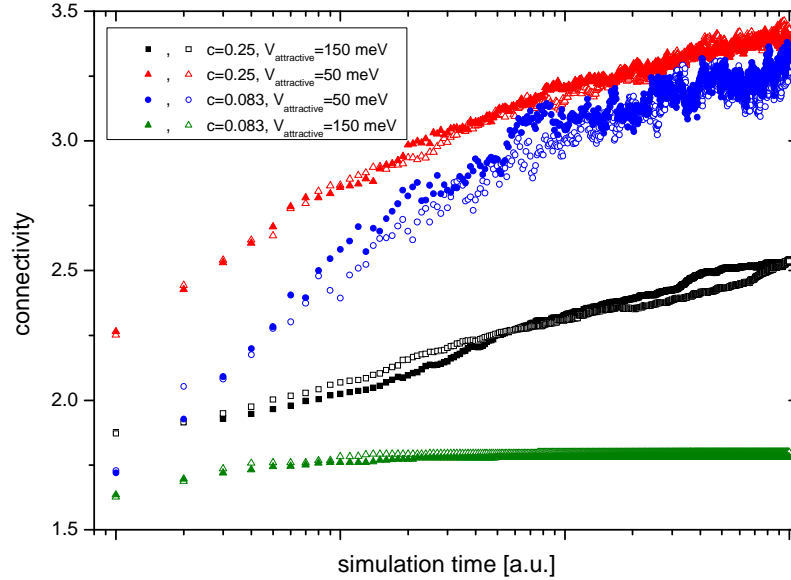

Fig. 48: Average connectivity of particles for different particle concentrations, surface diffusion factor: 0.3 (cf. section 2.3.2). For each set of parameters two simulations are shown to visualize the scattering.

The resulting clusters for high attractive interaction energies are highly fractal and to a large extent keep their structures over time. This is due to the fact that the coarsening as a competing event to the initial interaction is of medium strength which allows the particles to just slowly diffuse into the core of the network. Of course the average amount of neighbors is higher for higher concentrations. It increases continuously due to aggregation and network restructuring. For low concentrations few large clusters are formed if the interaction energy is high (green dots). This is the situation in the experimentally observed behavior (Fig. 26 in chapter 3.1). Low interaction energies (blue dots) however lead to numerous small clusters that are not stable and therefore hardly influence the conductivity. Furthermore in this situation the reproducibility is worse compared to the highly concentrated sample with low $V_{attractive}$ (red dots). It is important to notice that the densification of the cluster is both a result of the coarsening effect reflecting the surface diffusion and low particle interaction energies mainly reflecting the bonding and debonding of an additional particle at the network as they are not independent from each other.

The repulsive double-layer interaction thereby obviously not only decelerates the particle aggregation due to repulsion of the equally charged surfaces but also favors the unhindered diffusion of a particle into the network where it eventually will bond.

The described effect of the interaction energy is also observed in the graph of the percolation probability displayed in Fig. 50.
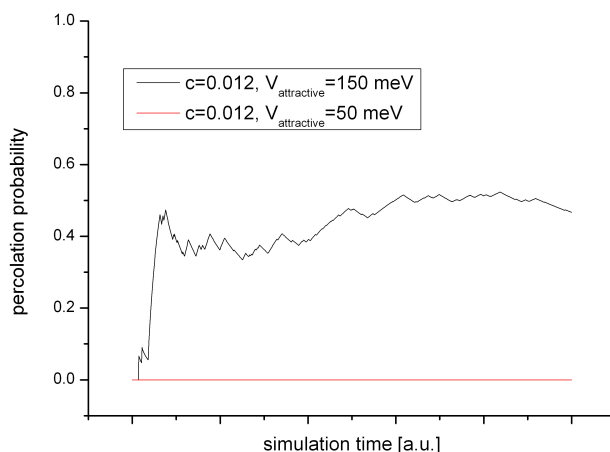

Fig. 50: Percolation probability in dependence of $V_{attractive}$.

Obviously percolation is highly dependent on the interaction energies with respect to the same dilution. In case of low interaction energies percolation is not detectable in the complete time interval. Additionally percolating clusters are not necessarily stable even at higher interaction energies (black curve) as sub cluster branches can break off easily when not attached to the network by several particle bridges. The total percolation from one electrode to the other can already be interrupted by a small network rearrangement or the loss of few particles in the cluster. This sensitivity can be clearly seen in the black curve of Fig. 49. It has been observed in various simulation runs as well as in AC conductivity experiments that the formation of percolating clusters can happen in different ways even when the external parameters are the same whereby reproducibility remains a problem in experimental investigations of composite electrolytes. This is due to the predominant statistical network formation. Therefore it is worthwhile to create morphologically stable template structures in a chemical way (e.g. electrically insulating nanofibers with a suitable surface connected to the electrode) or to use at least strongly bonding nanoparticles to achieve good conductivities in a rather well reproducible manner.

In summary percolation is of course more probable for higher particle concentrations, but percolation can occur also in composite electrolytes with lower particle volume fractions. For this, more time is necessary and the realization of the percolation event depends on various parameters such as sufficient interaction energy, slow particle diffusion along the surface, DLA dominating behaviour. Certainly there will be a minimum volume fraction below which a percolating cluster cannot be formed. Yet (as seen in section 3.1) this value is very low for small particle sizes.

However these networks are mechanically easier to stabilize (lower tendency of sedimentation) by the solvent as it has more contact sites with the particles. Monomeric solvents like THF or DMSO can penetrate the cluster and stabilize it at the individual contact sites. Polymer solvent molecules such as polyethylene glycol can enclose the cluster at certain positions and stabilize it in this way. Additionally the clusters in the lower concentration regimes contain less "dead" areas in which the ions are accumulated and do not contribute to ion conduction. So it is on the one hand probable that lots of percolation pathways are formed in case of high volume fractions. The conductivity on the other hand is only locally enhanced as expressed by the higher transference number (see e.g. chapter 3.2.2) even though the overall conductivity due to blocking and insufficient particle wetting effects might be lowered (AC conductivity). A simulation result in good agreement with the experimental data is shown in Fig. 51.
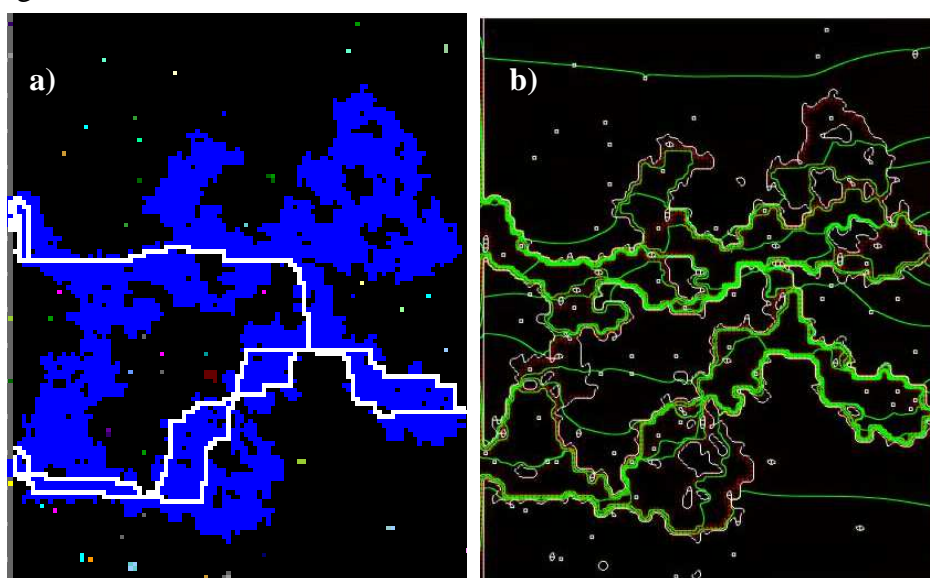

Fig. 51: Example for a kinetically stable cluster, set parameters: c=0.25, strong particle surface diffusion, $V_{attractive} = 100$ meV . Fig. 51a shows several percolation pathways automatically detected by the Monte Carlo simulation while the current density streamlines in Fig. 51b represent the preferential ionic conduction pathways.

Despite the high amount of particles and the numerous principal percolation pathways (Fig. 51 a) the current density streamlines are almost exclusively arranged along the edge of the large cluster (Fig. 51 b) where the solvent is still present. Therefore when particles are not porous themselves, the amount of effective percolation pathways is strongly reduced due to insufficient wetting. By this the maximum in the plot of conductivity vs. particle volume fraction [30] is explainable. In the region of low particle volume fractions the amount of pathways is low. However, here, the blocking effect of particles for conducting pathways is negligible. The resulting effect is a slight increase in conductivity. The conductivity is further enhanced by the creation of more conducting pathways with increasing particle volume fraction until the conductivity reaches a maximum. In the region of even higher particle volume fractions the blocking effect reduces the number of pathways while additionally favoring sedimentation of the network due to worse mechanical stabilization by the solvent. An important characterizing value for the network structure is the fractal dimension (Fig. 52).
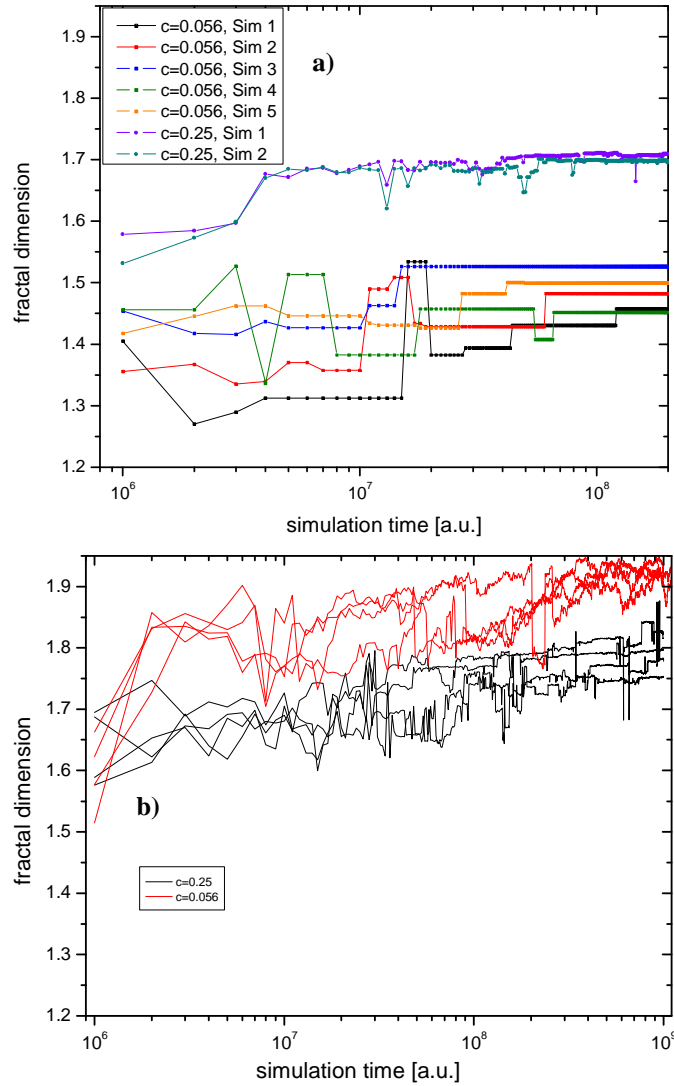
Fig. 52: Fractal dimension as a function of simulation time (several simulation runs). **a)** parameters: $V_{attractive} = 150\ \text{meV}$, low particle surface diffusion factor, **b)** parameters: $V_{attractive} = 70\ \text{meV}$, low particle surface diffusion factor, four simulations for each particle concentration.

In the case of high interaction energy (Fig. 52 a) the resulting clusters feature a high fractal dimension due to a higher particle volume fraction ($c = 0.25$). The reproducibility is very good in spite of the partial statistical characteristics of the simulation. For very low volume fractions ($c = 0.056$) particle networks are shaped differently leading to a more greatly scattered fractal dimension. In this case few large clusters are formed. Compared to the higher particle concentration the statistical influence on aggregation is more pronounced. When considering low interaction energy (Fig. 52 b) the statistically caused scattering of the fractal dimension is also pronounced in the case of high volume fraction ($c = 0.25$). One detects

smaller networks of statistical shape which can easily break and be restored in a different way. Only after a longer simulation time the fractal dimension stabilizes to a greater extent. For low volume fractions ($c = 0.056$) only small clusters are formed that are almost isolated from each other. The probability of complete restoration is low and also the effect on conductivity is negligible.

In summary, the simulation is indeed able to further explain the experimentally observed conductivity features and also give hints as to the materials choice. Thereby major parameters are the interaction energies of the particles with the anions and with each other as well as the kinetic barriers for surface diffusion. A composite electrolyte requires an amount of filler particles that on the one hand allows for the formation of many percolation pathways but on the other hand does not lead to large blocking effects. The particles themselves apart from a high concentration of suitable functional groups on their surface need to show strong Van der Waals interactions with each other while the surface diffusion within a network should be kinetically hindered (mechanism of diffusion limited aggregation, DLA).

3.2.4 Further Analysis of the Particle Surface Chemistry via IEC and the Impact of Ion Adsorption at the Particle Surface on the Overall Ionic Conductivity

In the previous chapters the Ion Exchange Capacity (IEC) has been used to estimate the capability of a particle type to adsorb ions. Compared with the BET data, this method is more meaningful (see chapter 3.2.2) as the latter just gives evidence of the surface area which is available to N_2 gas without further insight of what might happen when the particle surface is introduced to the liquid systems. Here one has to distinguish between the ion exchange capacity under neutral conditions that measures the amount of electrolyte protons of the SiO_2 surface. The standard method of measuring the IEC is to disperse a defined amount of particles in 0.1 M NaCl aqueous solution (double distilled water) under stirring and to titrate it by 0.01 M NaOH to the neutral point. If one is interested in the IEC under basic conditions, i.e. the number of protons that can be detached by offering NaOH thereafter, a defined amount of 0.01 M NaOH aqueous solution is added before the dispersion is back-titrated with a HCl aqueous solution of 0.01 M up to the neutral pH value. From the required volume of the HCl solution the IEC is determined. As described in chapter 3.2.2, for MCM-41 this latter

IEC value of 0.497 mmol·g^{-1} is obtained whereas MSU-H features an IEC value of 0.842 mmol·g^{-1}. The number of acid protons is two orders of magnitude below. The systematic results are summarized in Table 4 with MCM-41 and MSU-H as filler types.

#	Measurement Procedure	Filler Type	IEC / mmol·g^{-1}
1	Dispersion: filler in 0.1 M NaCl, addition of excess 0.01 M NaOH, back-titration with 0.01 M HCl to the neutral point	MCM-41	0.497
		MSU-H	0.842
2	Dispersion: filler in 0.1 M NaCl, titration with 0.01 M NaOH to the neutral point	MCM-41	$7.51 \cdot 10^{-3}$
		MSU-H	$1.69 \cdot 10^{-2}$
3	Dispersion: filler in 0.1 M NaCl, removal of filler by centrifugation, titration of the remaining solution with 0.01 M NaOH to the neutral point	MCM-41	$7.87 \cdot 10^{-3}$
		MSU-H	$1.36 \cdot 10^{-2}$
4	Dispersion: filler in 0.1 M NaCl, addition of excess 0.01 M NaOH, removal of filler by centrifugation, back-titration of the remaining solution with 0.01 M HCl to the neutral point	MCM-41	0.477
		MSU-H	0.848
5	Dispersion: filler in double distilled water, addition of excess 0.01 M NaOH, back-titration with 0.01 M HCl to the neutral point	MSU-H	0.490
		MSU-H	0.828
6	Dispersion: filler in double distilled water, addition of excess 0.01 M NaOH, removal of filler by centrifugation, back-titration of the remaining solution with 0.01 M HCl to the neutral point	MCM-41	0.434
		MSU-H	0.805
7	Dispersion: filler in double distilled water, titration with 0.01 M NaOH to the neutral point	MCM-41	$6.36 \cdot 10^{-3}$
		MSU-H	$1.01 \cdot 10^{-2}$

Table 4: IEC values of MCM-41 and MSU-H obtained for different measurement procedures

With all procedures MSU-H turns out to be the filler type with a higher capability of ion exchange. However by applying the different measurement procedures the surface chemistry at the particles is elucidated in more detail. By dispersing the filler in the aqueous NaCl solution, protons are released to the bulk lowering the pH value (procedure #1, standard procedure for determining the IEC value). When excess NaOH is added to the dispersion, a part of the hydroxide anions is neutralized by the protons. The remaining hydroxyl ions are then back-titrated by HCl to the neutral point. The resulting IEC values determined by this titration are rather large (procedure #1). Yet NaOH obviously cannot fully deprotonate the surface OH-groups if pH is lower than 7 as the direct titration with NaOH leads to smaller

IEC values in procedure #2 compared with procedure #1. This is also valid when the filler is removed from the solution after the NaCl addition (procedure #3). Obviously an excess amount is required for fully deprotonating the surface. When the particles are centrifuged off the solution before the back-titration (procedure #4) almost the same IEC values for the two particle types are observed compared with procedure #1. This confirms the accuracy of the results of procedure #1 whereby no other protons apart from the ones which originated from the particle surfaces are present in the solution. As expected NaCl is not initially required to remove the protons from particle surface as the sole addition of excess NaOH (procedure #5) leads to very similar results as with procedure #1 and #3. The confirmation that the protons in the solution are actually neutralized comes from the fact that with particle removal after the NaOH addition leads to well comparable IEC values (procedure #6). The direct titration of the dispersion with adjacent removal of the particles by centrifugation (procedure #7) again does not give the actual IEC values due to insufficient deprotonation of the surface with this method.

Even though the ion exchange capacity is measured in aqueous solution based on the principle of surface deprotonation its order of magnitude also gives a hint on the capability of adsorbing ions on the surface of the particles. First of all it can be stated that in the organic solvent used protons can be safely assumed not to be released. Rather than injecting positive ions in order to achieve a negative Zeta potential one has to assume anions to be adsorbed in agreement with the expectations. Furthermore the results give information on the bulk concentration changes on SiO_2 addition. Especially in the case of a high IEC value the question arises if the ionic adsorption perceptibly affects the bulk conductivity. Consequently the dependence of the ionic conductivity of a given composite system (here 0.1 M $LiClO_4$ + THF with MSU-H as filler) is determined as a function of φ when the particles are removed by centrifugation beforehand (Fig. 53).
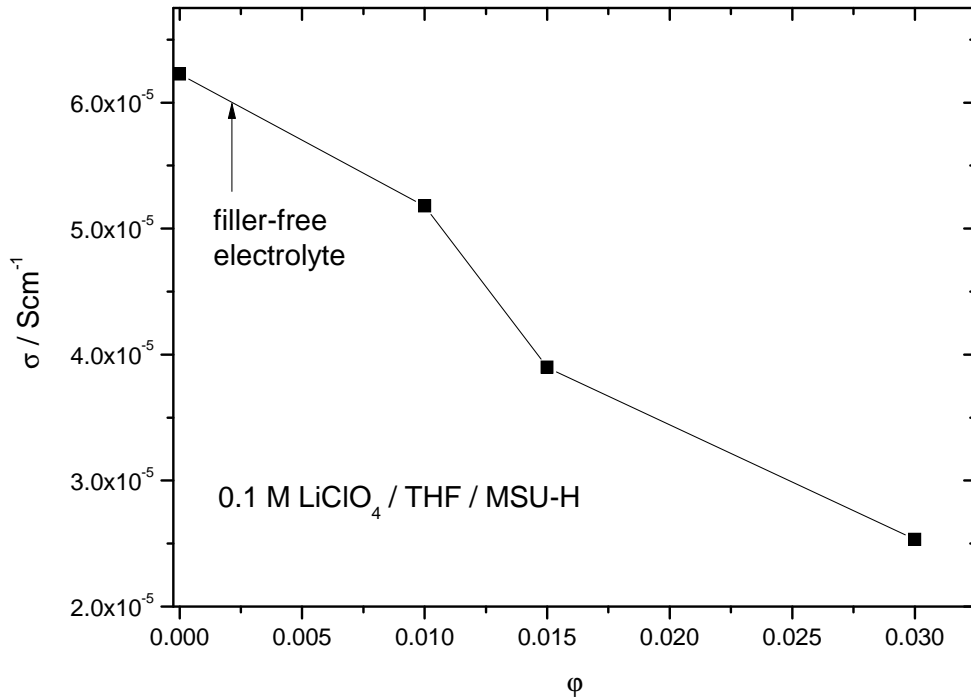
Fig. 53: Room temperature conductivity of 0.1 M LiClO$_4$ + THF: MSU-H composite electrolyte after removal of all particles with help of centrifugation.

An almost linear decrease of σ with φ is observed. This indicates a strong anion adsorption at the particle surface. When the particles are removed the cations in the diffusive cloud stay in close proximity to fulfill the electroneutrality condition. The remaining filler-free electrolyte is significantly depleted of ions and its conductivity markedly lower. This effect of salt exhaustion naturally becomes more pronounced with increasing φ.

The concentration change in the bulk by adsorption is given by [36]

$$\frac{\Delta c(\varphi)}{c(0)} = \frac{a}{c(0)} \frac{6}{R} \frac{\varphi}{1-\varphi} \approx \frac{6a(\varphi/R)}{c(0)} \approx \frac{\Delta\sigma(\varphi)}{\sigma(0)} \tag{47}$$

This equation assumes strong saturated adsorption such that the amount of adsorbed particles (*a*) is independent of bulk concentration. Eq. (47) explains the linearity of Fig. 53 and predicts *a* to be 2 / (nm)^2. This is about 1/5 of the value of the number of protons on the surface as concluded from IEC. A higher value would result, but also a deviation from the linearity if dependence of *a* on c is introduced.[36]

To investigate the impact of the salt exhaustion effect on the composite electrolytes in more detail, the room temperature conductivity of LiClO$_4$ + THF: MSU-H is measured as a function of φ for three different concentrations of LiClO$_4$ (Fig. 54).
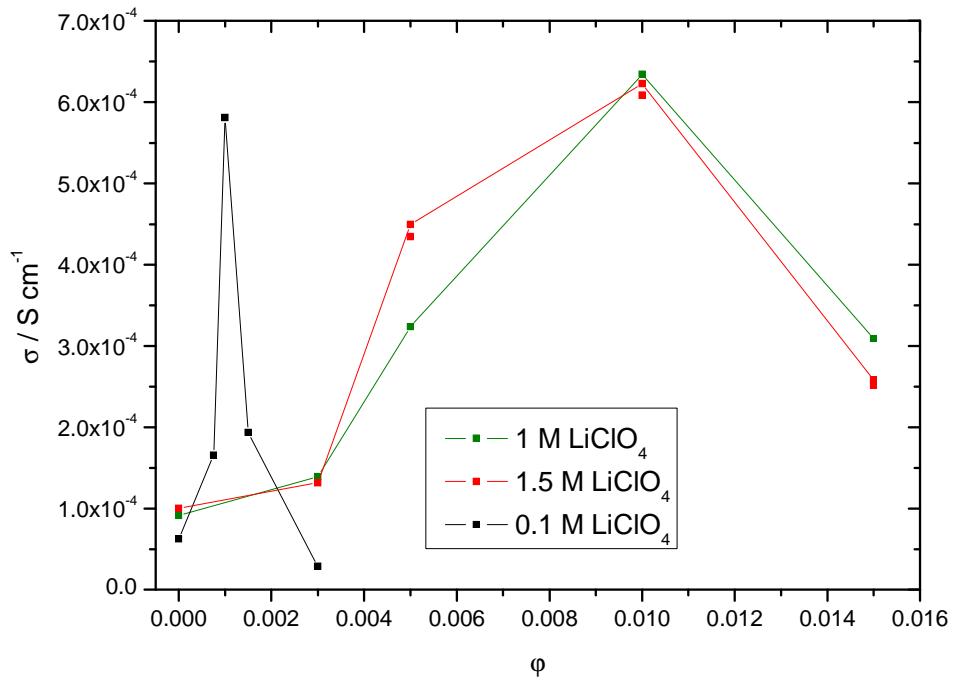
Fig. 54: Conductivity as a function of φ(MSU-H) for three concentrations of LiClO$_4$ in THF

It is observed that the volume fraction at which the conductivity maximum appears is strongly shifted from low to high salt concentrations. Additionally the maximum is developed much broader for high salt concentrations. For 0.1 M LiClO$_4$ the conductivity soon decreases when the salt concentration is low as obviously a significant part of the salt anions are adsorbed at the surface consequently with the cations in the diffusive cloud. For this low volume fraction the network pathway interruption is not expected to play a role whereby the strong decrease after the maximum is mainly a result of the salt exhaustion. The bulk conductivity thereby is very low for all investigated volume fractions and is further decreased by the salt exhaustion effect. The salt depletion does not play such an important role for higher salt concentrations in the composite electrolyte as enough salt ions remain practically unaffected by the addition of particles and the subsequent ion adsorption. Therefore the maxima for the 1 M LiClO$_4$ and 1.5 M LiClO$_4$ containing samples are shifted to much higher volume fractions whereby the decreases following the conductivity maxima are less steep. Here the decrease of the conductivity after the maximum is mainly a result of the coarsening and already described blocking effects.

In summary for the interpretation of the typical φ vs. σ plots in the context of Soggy-sand electrolytes the salt exhaustion effect needs to be considered apart from the already known

other phenomena leading to the dome-shaped curves especially for low salt concentrations and electrolytes with a low filler-free ionic conductivity.

3.2.5 Local Ionic Conduction in Systems with High Particle Volume Fractions

In chapter 3.2.4 it could be stated that the overall ionic conductivity for high φ not only drops due to the previously known phenomena of network pathway blocking by particles or coarsening but also substantially due to salt exhaustion in the course of extensive ion adsorption. All in all, a rather steep conductivity drop is observed for these particle amounts whereby the conductivity further decreases with increasing φ. In terms of the lithium transference number a different image has to be drawn. In the applied quasi-parallel switching model in which for a given SiO$_2$ content an increase of σ_+ and a decrease of σ_- is predicted, it is reasonable to assume the cation transference number in the space charge zones being close to unity.[36] It has been shown by A. Jarosik et. al. [31] that this model with the further assumption that space charge percolation is more sensitive to non-ideal silica distribution than bulk percolation is able to explain the maximum in the lithium transference number vs. φ relation. The initial increase on SiO$_2$ addition is due to the local space charge effects percolating through a expanded particle network. First blocking owing to non-favorable SiO$_2$ distribution results in lower effective transference numbers as a consequence of a preferential perturbation of space charge conductivity. If the blocking effects affect bulk and space charge layer identically this would hardly influence the effective transference number as such blocking factors cancel out in $\Delta\sigma_m / \sigma_\infty$ (cf. Equation (46)). Simultaneously the salt-exhaustion effect is not of great influence on the transference number as it was the case for the conductivity itself.

For very high volume fractions a transformation of bulk pathways into space charge pathways is expected. Hence in that regime almost exclusively space charge contributions exist. If the blocking effect mainly affected the bulk pathways, an increase of t_{m+} would be expected. This behavior has been already observed for MSU-H containing samples for high φ (chapter 3.2.2) and is also reflected by further results on composite electrolytes containing fumed silica (Fig. 54, $\varphi = 0.10$ and $\varphi = 0.12$, the results for lower φ are given in Ref. [29]).
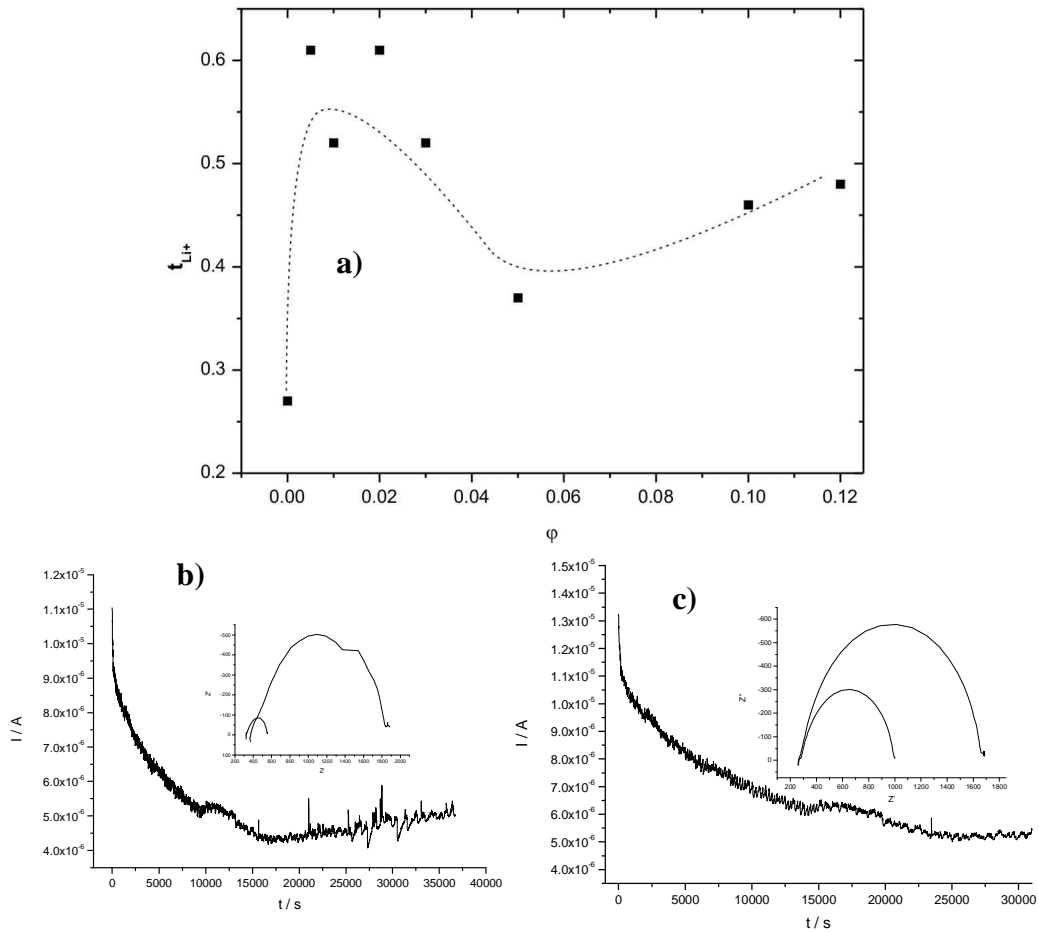
Fig. 54: a) Lithium transference number as a function of φ for 1 M LiClO$_4$ / PEG-150 / SiO2 (7 nm, fumed). Dashed line shows the overall trend of t_{Li^+} increase determined by DC polarization (**b)** and **c)**) recorded potentiostatically at 10 mV for φ=0.10 and φ=0.12.

As observed, t_{Li^+} reaches values larger than 0.6 for well-percolating space charge layers at low φ values. The blocking effect leads to a decrease of t_{Li^+} (decrease in $\Delta\sigma_m / \sigma_\infty$). Obviously with increasing φ the bulk pathways become more and more narrow whereby the space charge zones can overlap. As a consequence, t_{Li^+} is enhanced again (0.45).

A high lithium transference number might be attainable even at high φ-values even when σ_m of the composite electrolyte reaches values lying below the filler-free value σ_∞.

3.2.6 Ionic Conduction in Ionic Liquid Based Composite Electrolytes

The conventional polymer and liquid electrolytes used for lithium batteries still feature many drawbacks such as the comparably low room temperature conductivity on the one hand and the poor mechanical, thermal and chemical stability on the other. In recent years a relatively new class of materials has come into focus having the potential to overcome such problems. These are ionic liquids, i.e. room temperature molten salts which exclusively consist of the ions of which at least one is of organic nature showing rather high ionic conductivity values and good thermal stability.[117] Until now, very little is known about the exact ionic liquid conduction mechanism, especially when an additional lithium salt is introduced to the system. Equation (1) derived from the Stokes-Einstein rule and describing the ionic conductivity of a liquid system is not always applicable to ionic liquids due to the correlated motion of cations and anions (N, the number of charge carriers, is not easily definable here). If we assume that the model ionic liquid system consists entirely of ions then it is probable that some ions of opposite sign are sufficiently close to form relatively stable aggregates, they may be regarded as neutral species which cannot be charge carriers. At least one may expect that different ion-ion interaction in various ionic liquid mixtures leads to the formation of different ionic aggregates.[58] In an even more complex situation, when a lithium salt with the same anion is introduced, the dissolution of $[Li^+][X^-]$ in ionic liquid $[A^+][X^-]$ leads to the ternary structure $[Li^+]_m[A^+]_n[X^-]_{(m+n)}$ where a higher viscosity, lower conductivity and lithium transference number are observed compared to conventional lithium electrolytes.[26, 58]

Nevertheless, several approaches towards the preparation of composite systems have been made including ionogels (ionic liquid/polymer), ternary systems (ionic liquid/polymer/oxide particle) and hybrid electrolytes (ionic liquid tethered oxide particles) whereby most of the attempts have not led to improved ionic conductivities.[24, 58] In this context, a logical question that arises is if the concept of Heterogeneous Doping can be applied to ionic liquids to improve their electrical and mechanical properties. Furthermore, from a fundamental point of view, effects observed upon addition of SiO_2 nanoparticles can give insight in the conduction mechanism within the bulk ionic liquid. To keep the composite electrolyte as simple as possible as to allow for easier analysis and interpretation of the obtained data, here an ionic

liquid was chosen that contains the same anion as the previously used lithium salt (lithium triflate, LiOTf), 1-ethyl-3-methylimidazolium trifluoromethane sulfonate (EMIM OTf).

As a starting point, the temperature dependent ionic conductivity is investigated when only LiOTf is introduced (Fig. 55a). The results are complemented by DSC measurements (Fig. 55b) performed from -50°C to 20°C (scan rate 1 K / min).
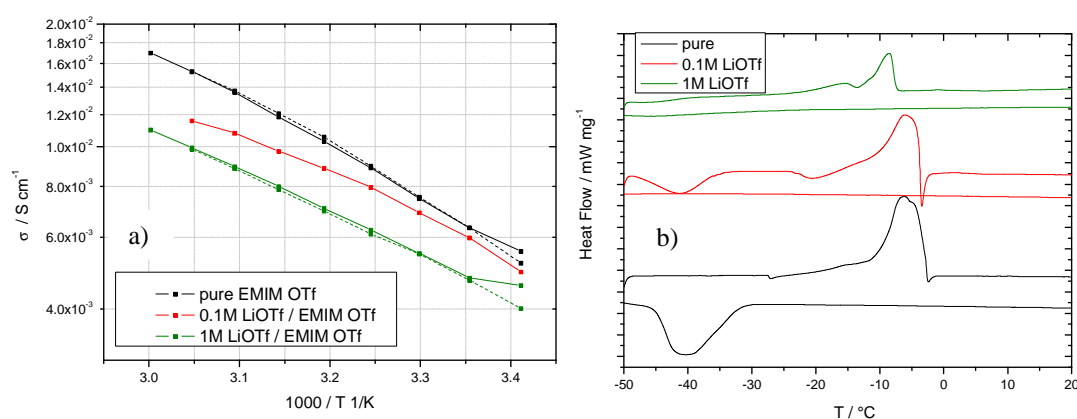

Fig. 55: a) Temperature dependent ionic conductivity for pure EMIM OTf and LiOTf containing EMIM OTf with different concentrations (heating cycle: solid line, cooling cycle: dashed line) **b)** DSC thermograms of the respective samples.

The overall ionic conductivity significantly drops upon salt introduction as obviously the salt ions hinder the ionic transport within the ionic liquid. The lithium ions seem not to be transported effectively as otherwise at least an unchanged conductivity is expected due to their small size. The strength of the salt impact on the ionic liquid is seen from the DSC data. EMIM OTf crystallizes around -30°C (cooling cycle minimum) and starts to melt at -10°C (heating cycle maximum). The melting peaks shift upon salt addition while the crystallization peak almost completely vanishes when the salt concentration is increased.

The same system is further investigated in terms of heterogeneous doping by SiO_2 (7nm, fumed) and Al_2O_3 is added as a filler (Fig. 56). In the case of Al_2O_3 (10 nm, Fig. 56 c), the conductivity is strongly reduced.
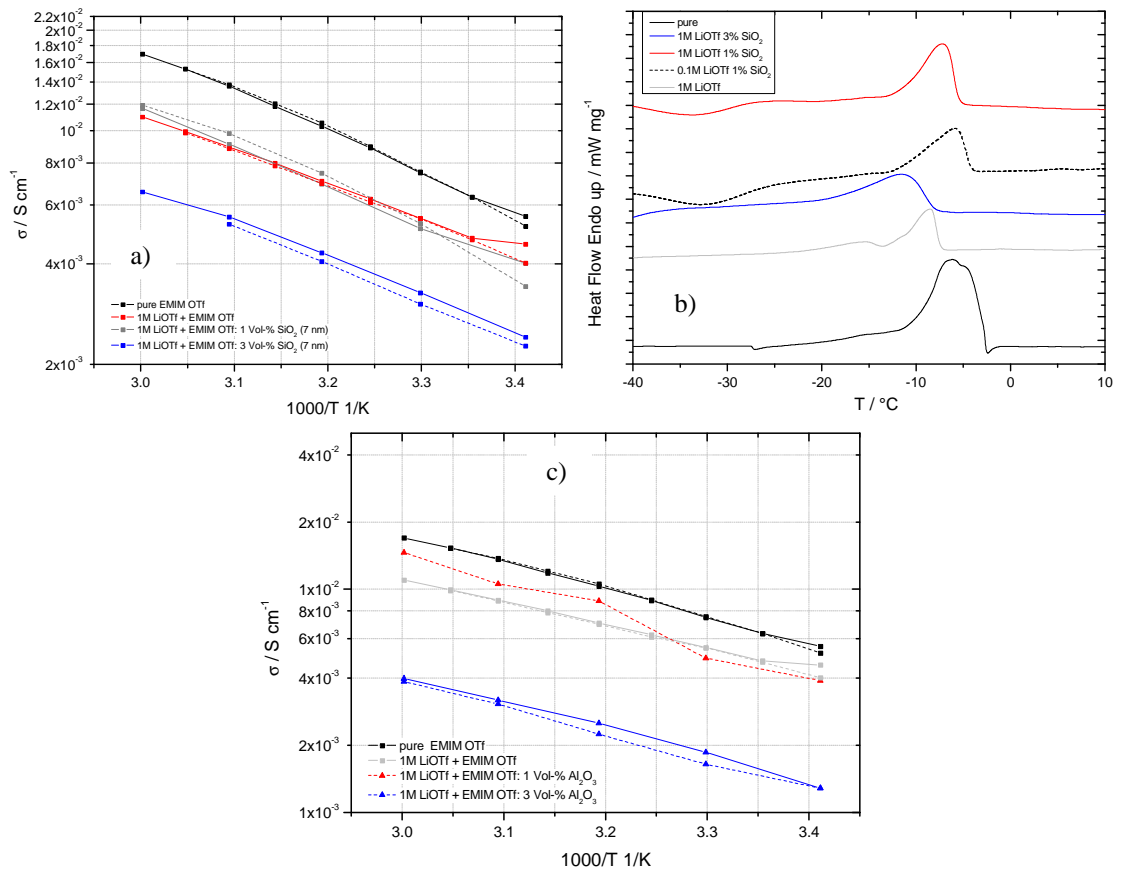
Fig. 56: a) Temperature dependent ionic conductivity for pure EMIM OTf, LiOTf containing EMIM OTf and ternary systems including SiO_2 (7 nm, fumed) (heating cycle: solid line, cooling cycle: dashed line). **b)** DSC thermograms of the respective samples. **c)** Temperature dependent ionic conductivity for pure EMIM OTf, LiOTf containing EMIM OTf and ternary systems including Al_2O_3 (10 nm) (heating cycle: solid line, cooling cycle: dashed line).

Here it is observed that for a certain particle volume fraction (1 Vol-%) the conductivity stays constant compared with the filler-free salt containing sample. However, the overall conductivity is still significantly lower compared with the pure ionic liquid. For higher φ (3 Vol-%) the relative conductivity drop is even higher, around 40%. The DSC experiments show a shift of the melting temperature also more pronounced for increasing φ. Conversely, the particles have a strong effect, even by naked eye a much more viscous electrolyte is observed. In total it must be stated that the desired effects of at least keeping the conductivity intact whereby the viscosity of the electrolyte is increased can hardly be achieved with this type of composite electrolyte.

The situation becomes more interesting when the salt is left out from the composite electrolyte (Fig. 57).
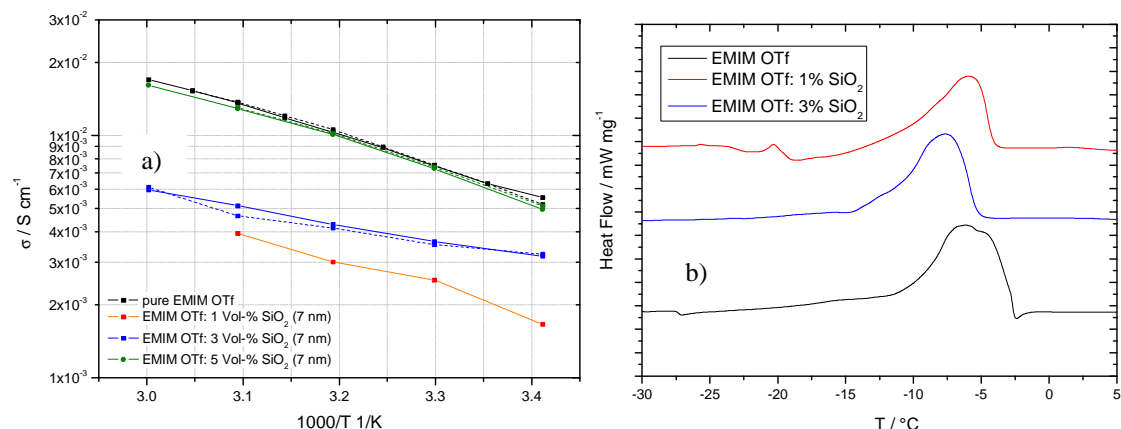

Fig. 57: a) Temperature dependent ionic conductivity for pure EMIM OTf, and EMIM OTf containing SiO_2 (7 nm, fumed) (heating cycle: solid line, cooling cycle: dashed line). **b)** DSC thermograms of the respective samples.

It is observed that for increasing particle volume fractions the conductivity values reach the values for the filler-free electrolyte. For $\varphi = 5$ Vol-% the differences are almost non-existent. With respect to DSC thermograms, upon doping with SiO_2 only a slight shift of the melting curve is observed. Rheological experiments are additionally performed on the samples with $\varphi = 3$ Vol-% and $\varphi = 5$ Vol-% (Fig. 58).
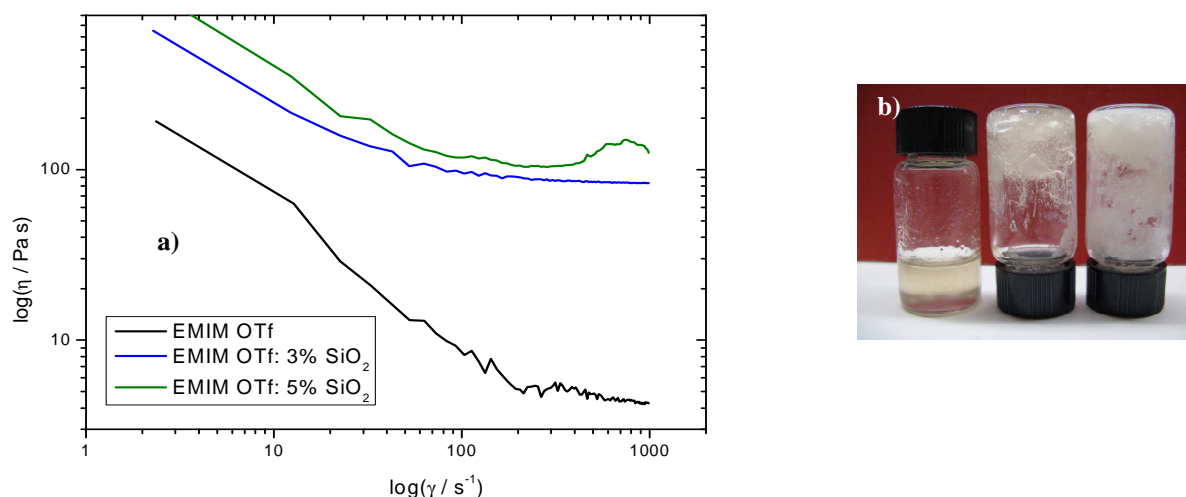

Fig. 58: a) Viscosity as function of the shear rate for 3% and 5% SiO_2 in EMIM OTf. **b)** Images of pure EMIM OTf, EMIM OTf: 3% SiO_2, EMIM OTf : 5% SiO_2 (from left to right).

The viscosity strongly increases in both composite electrolytes compared to the filler-free ionic liquid. For $\varphi = 5$ Vol-% SiO_2, a transition from shear thinning to shear thickening behavior is also observed. All samples show a substantially different consistency than

conventional liquid electrolytes (Fig. 59b). In the case of particle addition a glue-like gel is obtained.

Presented results are highly promising also in terms of the applicability of these composite electrolytes as they in some cases (EMIM OTf: 5 Vol-%) nominally show the same conductivity with strongly enhanced mechanical stability.

3.3 Individual Contributions of the Ionic Species to the Ionic Conduction

In electrolytes, the assumption is often made that the mass transport current is exclusively caused by charged species. Yet the influence of ion pairs and higher aggregates on the ionic conduction should not be neglected. Especially in the case of polymer electrolytes, little is known about the exact conduction mechanisms. Certainly in the case of not too high dielectric constants of the solvents and an unfavorable interaction between the solvent molecules and the salt ions, the number of ion pairs is high. They often strongly interact with the present salt ions. This can lead to the formation of higher aggregates such as triple ions for high salt concentrations. Stolwijk et. al. [118] revealed a significant ion pair contribution in LiI + PEO. Their PFG-NMR results on solid polymer electrolytes also show a dominant anion conductivity in certain cases. In many ionic liquid electrolytes lithium transference numbers lower than 0.5 are found. According to their work the Li tracer transport seems to be carried out mainly in form of ion pair transport as the lithium ion itself is often strongly bond to the oxygen atoms (usually 4 to 5 as shown by molecular dynamic simulations) of the polymer backbone. Following the work on coupled ion/electron motion in solids,[118] a mechanism can be anticipated in which the effective lithium ion transport is ensured by the diffusion of ion pairs to one of the electrodes and a countermotion of the anions to the other electrode (Fig. 59). [103, 118, 119]
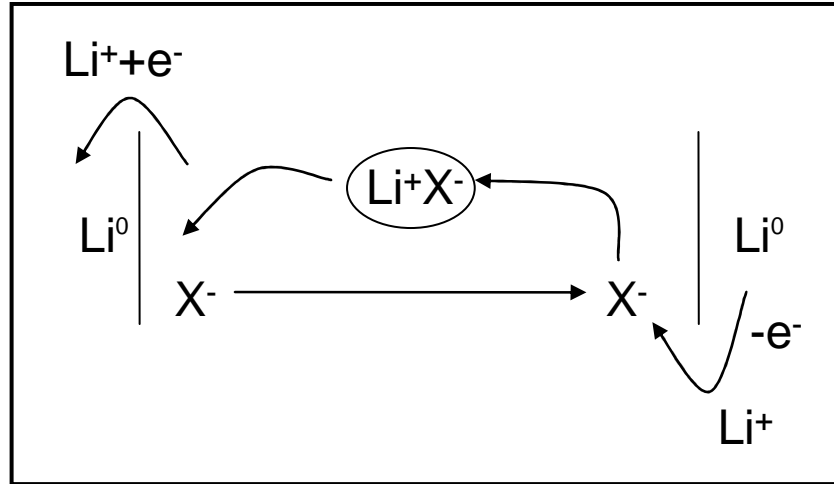
Fig. 59: Vehicular transport mechanism for lithium ions from one electrode to its counter electrode.

This thus represents a cooperative motion (vehicular transport) based on the chemical diffusion due to a concentration gradient and allows for a steady-state transport between two lithium electrodes (DC polarization experiment) even if $\sigma_+ \equiv \sigma_{Li^+} = 0$.[103, 120-124] When the ion pair releases a lithium ion to the electrode where it is discharged, it frees an anion that diffuses to the counter electrode where it is loaded with a new lithium ion. This way an uninterrupted stationary transport is maintained provided that the dissociation/association reactions are fast.[103]

As mentioned, the aspect of motion of two charge carriers in an electrochemical cell under certain boundary conditions whereby the species are able to rapidly react to another species which also shows a certain diffusivity, has already been treated theoretically for the solid state in the Concept of Conservative Ensembles.[103, 121-124] In that context the ionic species consisted of ionic defects and electrons, yet this concept can be applied to the isomorphic problem of determining the lithium transference numbers in Li-salt-containing polymers.[125] The effective conductivity (σ_{pol}) derived from $I_{(t \to \infty)}$ is not simply σ_+ but also features contributions from the anion (σ_-) and the ion pair (s). The latter represents the diffusivity of the ion pair in units of the ionic conductivity. It can be derived from the Nernst-Einstein Equation

$$s = \frac{ce^2}{k_B T} D \qquad (48)$$

with D being the self-diffusion coefficient. The effective conductivity in the steady state of the dc polarization then follows as[103]

$$\sigma_{pol} = \sigma_+ + \frac{s \cdot \sigma_-}{s + \sigma_-} = \sigma_+ + \left(\frac{1}{s} + \frac{1}{\sigma_-}\right)^{-1} \tag{49}$$

When the true transference number is given as

$$t_+ = \frac{\sigma_+}{\sigma_+ + \sigma_-} \tag{50}$$

whereas the measured transference number that ignores the ion pair contribution needs to be written as

$$t_{pol+} = \frac{\sigma_{pol}}{\sigma_+ + \sigma_-} = \frac{\sigma_{pol}}{\sigma} \tag{51}$$

it follows that[103]

$$t_{pol+} = t_+ + (1 - t_+)\frac{s}{s + \sigma_-} \tag{52}$$

The first term of Equation (52) refers to the mechanism reflected by the standard Equation $t_+ = \frac{\sigma_{pol}}{\sigma}$ whereas the second term represents the contribution by the vehicular transport mechanism for $s, \sigma_- \neq 0$. For very large s values $\sigma_{pol} = \sigma$ results meaning that no polarization occurs. Thus the equalization of experimentally obtained $t_{pol+} = 1$ with $t_+ = 1$ is mechanistically grossly wrong even though in applied battery research a lack of polarization often just satisfies.[103] To apply Equation (49) to determine the individual contributions of ionic species to ionic conduction, Li-tracer diffusion experiments are required as they cover all present Li atoms (denoted by s_{Li}^* denoting the diffusivity of all lithium containing species in units of the ionic conductivity). Converting in the same way the tracer diffusion coefficient D_{Li}^* to a quantity s_{Li}^* via

$$s_{Li}^* = \frac{c_{Li}F^2}{RT}D_{Li}^*. \tag{53}$$

In terms of individual contributions s_{Li}^* is given by

$$s_{Li}^* \equiv s + \sigma_+ \tag{54}$$

Together with

$$\sigma = \sigma_+ + \sigma_- \tag{55}$$

originating from AC conductivity experiments at high frequencies and Equation (49), the desired parameters σ_{Li^+}, σ_{X^-} and s follow from the measurable parameters σ, σ_{pol} and s_{Li}^* as[103]

$$\sigma_{Li^+} = \sigma_{pol} - F$$
$$\sigma_{X^-} = \sigma - \sigma_{pol} + F \tag{56}$$
$$s = s^* - \sigma_{pol} + F$$

whereby

$$F = \sqrt{\left(s_{Li}^* - \sigma_{pol}\right)\left(\sigma - \sigma_{pol}\right)} \tag{57}$$

Note that these considerations refer to the filler free situation. Equally s, σ_- and σ_+ can be obtained from AC experiments and two PFG experiments, ^{7}Li and ^{19}F PFG-NMR, according to

$$s = \frac{1}{2}\left(s_{Li}^* + s_X^* - \sigma\right)$$

$$\sigma_{X^-} = \frac{1}{2}\left(s_X^* - s_{Li}^* + \sigma\right) \tag{58}$$

$$\sigma_{Li^+} = \frac{1}{2}\left(s_{Li}^* - s_X^* + \sigma\right)$$

allowing for a worthwhile consistency check. To test the applicability of the just given concept, PEG-150 is used in which lithium triflate as conductive salt is dissolved with the concentrations 0.1 M, 0.5 M and 1 M. The salt features fluorine atoms enabling the analysis by Equations (58). In terms of potentiostatic polarization experiments the standard routine for determining the transference number is carried out in a cell for which the cell constant is known. This is necessary for additionally obtaining the actual value of σ_{pol}. PFG-NMR and AC conductivity measurements are done in the temperature range of 20-60°C.

The respective polarization curves are shown in Fig. 60. Together with AC measurements beforehand and afterwards, σ_{pol} as well as t_{pol+} can be calculated.
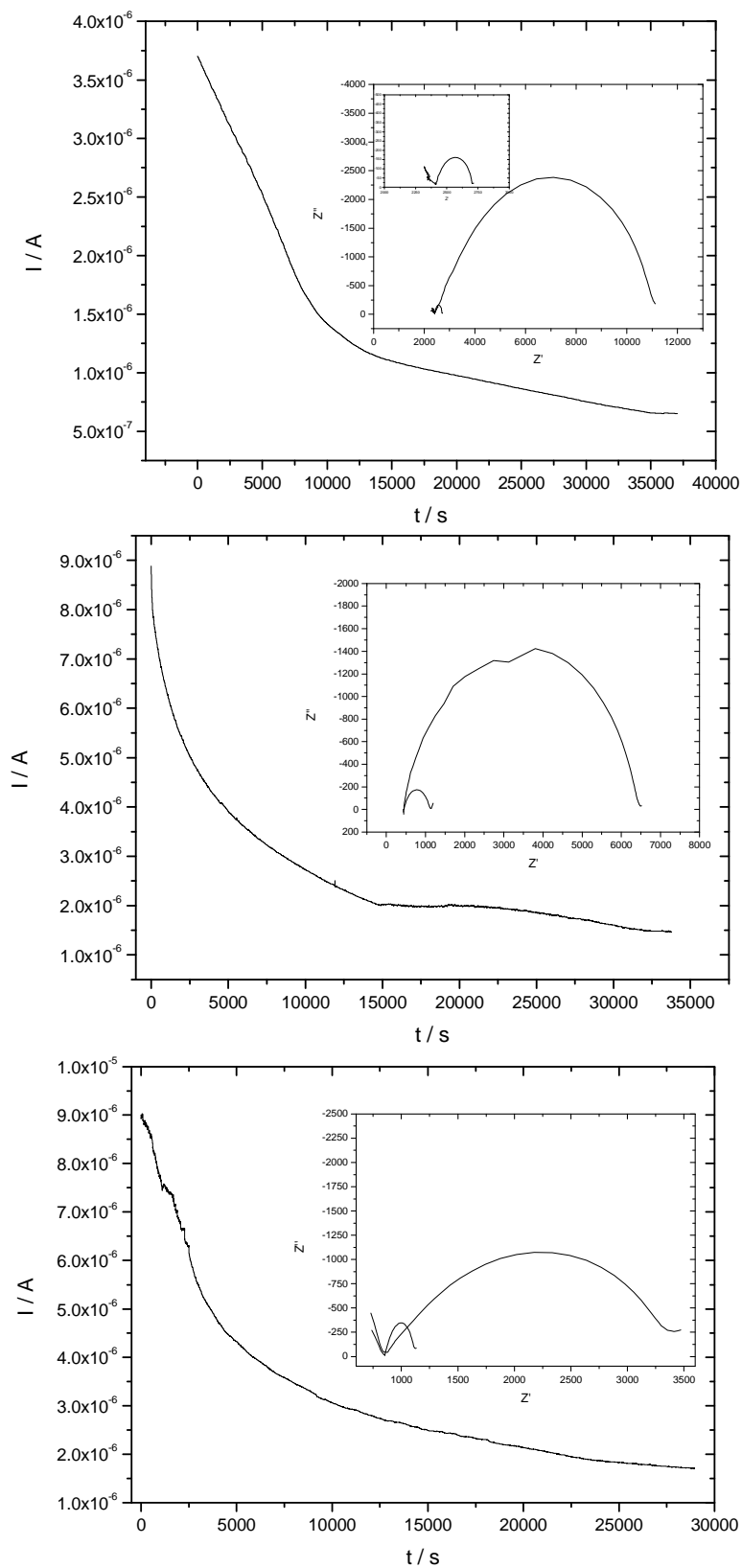
Fig. 60: DC Polarization curves and respective AC curves for **a)** 0.1 M LiOTf + PEG-150, **b)** 0.5 M LiOTf + PEG-150 and **c)** 1 M LiOTf + PEG-150. Measurements were carried out potentiostatically at 10 mV.

The latter parameter is calculated with help of Equation (22) which takes into account the influence of the SEI formation at the lithium electrodes during the polarization process. The temperature dependent diffusion coefficients which are determined by PFG-NMR are shown in Fig. 61.
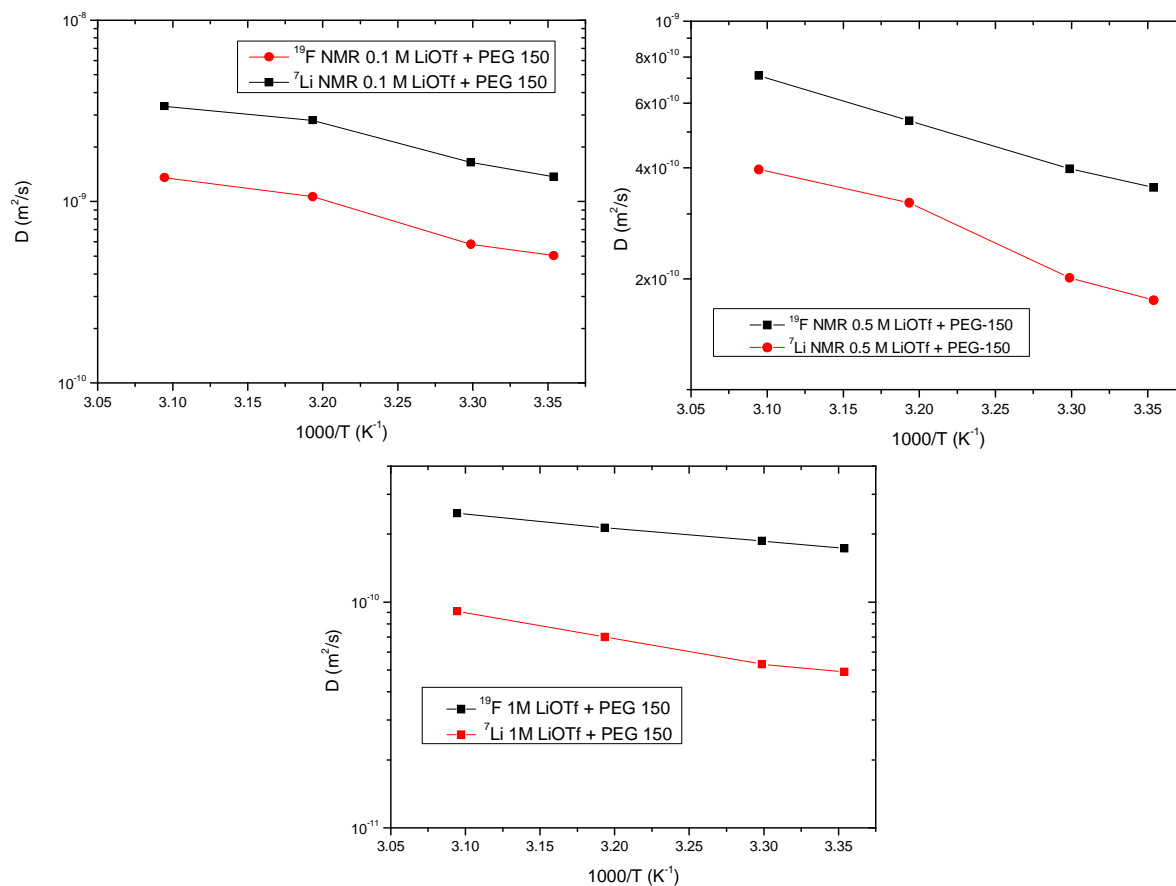

Fig. 61: Temperature dependent Diffusion coefficients for LiOTf + PEG-150 determined with help of PFG-NMR.

As expected the diffusivity of the anion is higher for all three salt concentrations. Together with the room temperature AC conductivity data determined with help of blocking electrodes (Fig. 62) the desired parameters are accessible with help of the Equations given above.
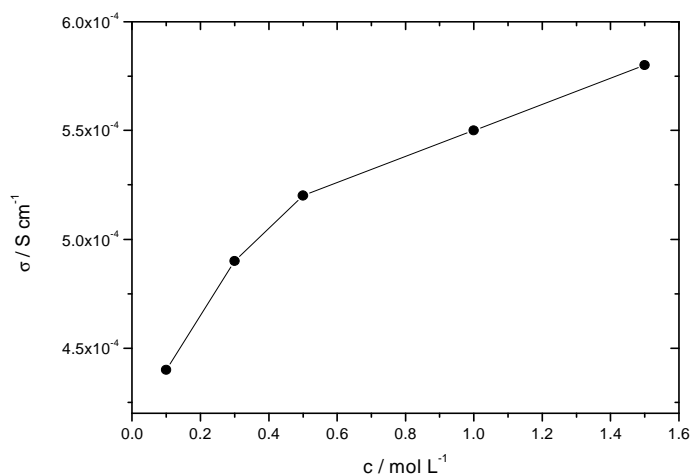
Fig. 62: Room temperature conductivity as a function of the salt concentration

After an almost linear increase with the salt concentration the conductivity curve shows a saturation that has often been found for conventional electrolytes. The obtained results are compared with those of the Soggy-sand electrolyte 1M LiOTf + PEG-150: 1 Vol-% SiO_2 (7 nm, fumed) which are shown in Fig. 63.
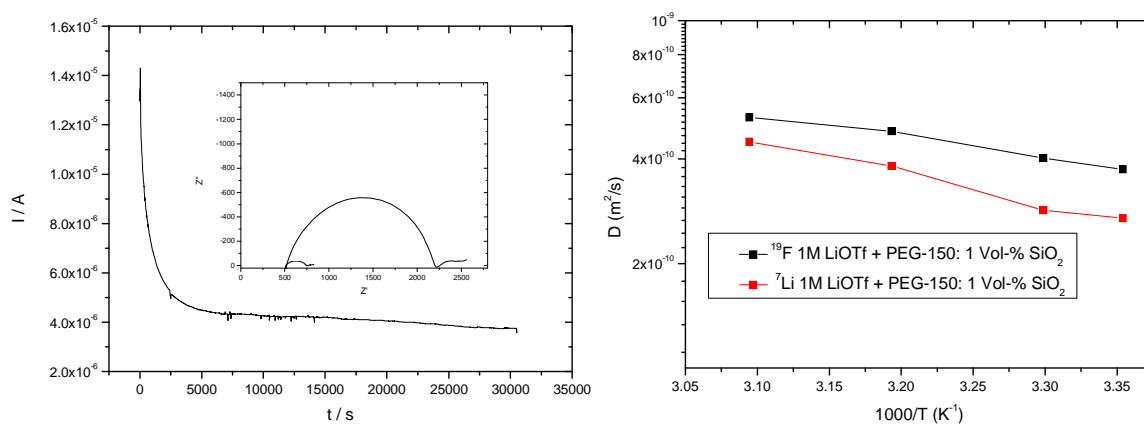

Fig. 63: a) DC Polarization curve and respective AC curves for 1M LiOTf + PEG-150: 1 Vol-% SiO_2 (7 nm, fumed). Measurements were carried out potentiostatically at 10 mV. **b)** Temperature dependent diffusion coefficients for LiOTf + PEG-150: 1 Vol-% SiO_2 (7 nm, fumed) determined with help of PFG-NMR.

Table 5 summarizes the experimental results of such a multi-technique approach and the individual transport contributions evaluated according to Eq. 56 and 58.

c	s_{Li}^{*}	s_{F}^{*}	σ	σ_{pol}	σ_{+}	σ_{-}	s	F	σ_{ind}	t_{pol+}^{BE}	$t_{+}^{calc.}$
mol/L	S/cm	S/cm	S/cm	S/cm	S/cm	S/cm	S/cm	S/cm	S/cm		
0.1	$1.9 \cdot 10^{-4}$	$5.18 \cdot 10^{-4}$	$4.4 \cdot 10^{-4}$	$1.6 \cdot 10^{-4}$	$6.83 \cdot 10^{-5}$	$3.72 \cdot 10^{-4}$	$1.22 \cdot 10^{-4}$	$9.17 \cdot 10^{-5}$	$9.2 \cdot 10^{-5}$	0.35	0.15
0.5	$3.3 \cdot 10^{-4}$	$6.63 \cdot 10^{-4}$	$5.2 \cdot 10^{-4}$	$2.5 \cdot 10^{-4}$	$1.03 \cdot 10^{-4}$	$4.17 \cdot 10^{-4}$	$2.27 \cdot 10^{-4}$	$1.47 \cdot 10^{-4}$	$1.4 \cdot 10^{-4}$	0.49	0.19
1	$1.6 \cdot 10^{-4}$	$6.52 \cdot 10^{-4}$	$5.5 \cdot 10^{-4}$	$1.3 \cdot 10^{-4}$	$1.78 \cdot 10^{-5}$	$5.32 \cdot 10^{-4}$	$1.42 \cdot 10^{-4}$	$1.12 \cdot 10^{-4}$	$1.2 \cdot 10^{-4}$	0.26	0.05
1: 1 Vol-% SiO$_2$ (7 nm fumed)	$4.8 \cdot 10^{-4}$	$7.05 \cdot 10^{-4}$	$7.9 \cdot 10^{-4}$	$4.0 \cdot 10^{-4}$	$2.83 \cdot 10^{-4}$	$5.08 \cdot 10^{-4}$	$1.98 \cdot 10^{-4}$	$1.08 \cdot 10^{-4}$	$1.77 \cdot 10^{-4}$	0.51	0.28

Table 5: Summarized data from PFG-NMR, AC conductivity and DC polarization measurements to determine the desired parameters σ_{+}, σ_{-} and s. t_{pol+}^{BE} indicates t_{pol+} determined with the method by Bruce and Evans described in chapter 2.2.6 whereas $t_{+}^{calc.}$ results from Eq. (52).

c	s_{Li}^{*}	s_{F}^{*}	σ	σ_{+}	σ_{-}	s	$\sigma_{pol}^{calc.}$	σ_{ind}^{NMR}
mol/L	S/cm	S/cm	S/cm	S/cm	S/cm	S/cm	S/cm	S/cm
0.1	$1.9 \cdot 10^{-4}$	$5.18 \cdot 10^{-4}$	$4.4 \cdot 10^{-4}$	$5.60 \cdot 10^{-5}$	$3.84 \cdot 10^{-4}$	$1.34 \cdot 10^{-4}$	$1.5 \cdot 10^{-4}$	$9.9 \cdot 10^{-5}$
0.5	$3.3 \cdot 10^{-4}$	$6.63 \cdot 10^{-4}$	$5.2 \cdot 10^{-4}$	$9.35 \cdot 10^{-5}$	$4.27 \cdot 10^{-4}$	$2.37 \cdot 10^{-4}$	$2.4 \cdot 10^{-4}$	$1.5 \cdot 10^{-4}$
1	$1.6 \cdot 10^{-4}$	$6.52 \cdot 10^{-4}$	$5.5 \cdot 10^{-4}$	$2.90 \cdot 10^{-5}$	$5.21 \cdot 10^{-4}$	$1.31 \cdot 10^{-4}$	$1.4 \cdot 10^{-4}$	$1.0 \cdot 10^{-4}$
1: 1 Vol-% SiO$_2$ (7 nm fumed)	$4.8 \cdot 10^{-4}$	$7.05 \cdot 10^{-4}$	$7.9 \cdot 10^{-4}$	$2.23 \cdot 10^{-4}$	$5.67 \cdot 10^{-4}$	$2.57 \cdot 10^{-4}$	$4.2 \cdot 10^{-4}$	$1.42 \cdot 10^{-4}$

Table 6: Data from PFG-NMR and AC conductivity measurement (blocking electrodes) with the derived values for σ_{+}, σ_{-} and s with help of Eq. (58) and the calculated overall conductivity in the polarized state with help of Eq. (49).

The analysis leads to self-consistent results. From the data it can be seen that the increase of the ionic conductivity in the non-polarized state (σ) when increasing salt-concentration is weakened with increasing salt concentration which is also confirmed by conductivity values for even higher concentrations such as 1.5 M ($\sigma = 5.8 \cdot 10^{-4}$ S cm^{-1}) indicating a saturation. The cationic conductivity contribution (σ_+) even runs through a maximum. In contrast the increase of the anionic conductivity (σ_-) flattens whereas ion pair contribution (s) stays rather constant. These deviations from proportionality must be ascribed to the concentration dependence of the mobility which is expected for these high salt contents. As a result, σ_{ind} is hardly changed for the chosen concentrations. However its value is rather high showing that the vehicular transport is important for this salt/solvent combination. Here the different degrees of solvation play a significant role. Lithium ions are strongly coordinated by the ether oxygen atoms of the polymer molecules which hinders their diffusion whereas the ion pair and especially the anion are more loosely surrounded by the solvent. Furthermore in the case of high salt concentrations the cations come into close proximity as the simplified estimation $d = (cN_A)^{-1/3}$ (d: distance between two lithium ions, N_A: Avogadro constant) shows. Here d is found to be 1 nm for 1 mol/L LiOTf in PEG-150 which indicates a correlated ionic movement with a reduced ionic mobility. This is in agreement with the respective $t_+^{calc.}$ which is strongly reduced compared to the lower salt concentrations. The non-linear effect of the concentration is also reflected by the variation of the overall viscosity in Fig. 64.
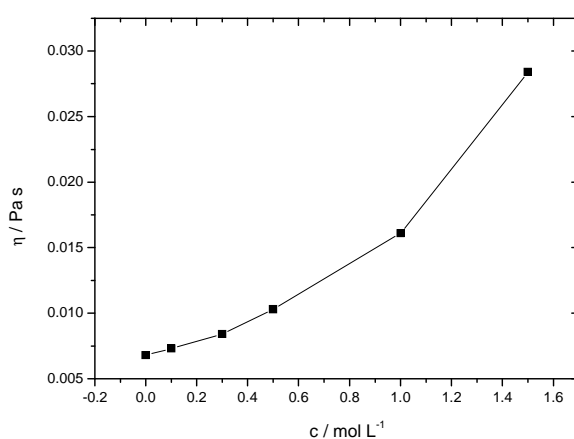

Fig. 64: Viscosity as a function of LiOTf concentration in PEG-150 (constant shear strain rate of 500 s^{-1}).

111

Let us now turn to the silica containing liquids. With addition of fumed silica the AC conductivity is significantly enhanced which is already known from previous investigations.[30] Here the strongest change is noticed for σ_+ as a result of the release of lithium ions due to anion adsorption which slightly reduces σ_- leading to a t_{pol+}^{BE} value of 0.51 and $t_+^{calc.}$ of 0.25 (t_{pol+}^{BE} indicates t_{pol+} determined with the method by Bruce and Evans described in chapter 2.2.6 whereas $t_+^{calc.}$ results from Eq. (52)). As already shown before the total conductivity of a composite electrolyte can be approximately (space charge layer: strongly enhanced cation concentration, depleted anion concentration, constant ion pair concentration) written as (σ_+^{SC}: cationic conductivity in the space charge layer)[103]

$$\sigma_{m,AC} = \varphi\beta\sigma_+^{SC} + (1-\varphi)\sigma_\infty \tag{59}$$

whereas the total conductivity in the polarized state is given by

$$\sigma_{m,pol} = \varphi\beta\sigma_+^{SC} + (1-\varphi)\sigma_{\infty,pol} \tag{60}$$

This assumes that the transference number in the space charge zones is close to 1. Here, as the salt concentration is high (1 mol/L) and the salt exhaustion effect only plays a minor role, the bulk conductivities in the unpolarized and polarized state can be approximately identified with the respective filler-free conductivities. When introducing the obtained values into Equations (59) and (60), similar results are found for σ_+^{SC} indicating their validity.

In summary it can be stated that for the first time individual contributions of ionic species – including the indirect ionic transport with help of ion pairs – could be explicitly extracted from a combination of AC, DC and tracer diffusion techniques. The influence of ion pairs on the ionic conductivity in the investigated system is strong due to the rather low dielectric constant of the solvent, the resulting high amount of ion pairs and the significant conductivity of the counter ion. In this and other systems with similar solvation properties the lithium transference can by no means exclusively be attributed to the single lithium transport as the vehicular mechanism plays a significant role. With filler particles the conductivity enhancement can be mainly attributed to the increased cationic conductivity in the space charge zones, while the polarization in the DC experiment mainly affects the bulk.

4 Conclusions

This work was devoted to the clarification of short-range and long-range effects in salt-containing liquid-solid composites. On one hand it deals with the classification of network kinetics as well as local and overall transport effects. On the other hand it was concerned with the question of how to generate corresponding materials suited for lithium battery electrolyte applications.

It could be shown that the network formation – a process of great importance for composite electrolytes as it codetermines the final physical and chemical properties – could be recorded in situ for low particle volume fractions in certain systems. Confirmations for the given conclusions thereby came from microscopic techniques which were applied for the first time in that research field as well as from electrochemical techniques. Monte Carlo simulations in combination with Finite Element analysis, developed together with Marcus Göbel, elucidated the phenomenon in greater detail and furthermore proved helpful to find proper composite electrolytes by investigating the interplay between network structure and physical properties. For this system even a quantitative estimate of the respective lithium transference numbers and conductivity enhancements was possible.

Further investigations in the context of ionic conduction were carried out which brought the salt exhaustion effect to light as an additional reason for the conductivity drop at high particle volume fractions and simultaneously indicated the strength of ionic adsorption at the particle surface by Ion Exchange Capacity measurements. It was moreover found for high particle volume fractions that space charge pathways transform to bulk pathways. With this result the dependence of lithium transference number on particle volume fraction became explainable. It was surprising to see that the local transference number could still be greatly enhanced compared to the filler-free solution even when overall conductivity had significantly dropped.

As far as applied research in terms of the Soggy-sand electrolytes is concerned, such composites using mesoporous solid particles improve the overall battery electrolyte performance by offering additional percolation pathways. It turned out in this context that it is the enhanced accessibility of ions to the particle network due to its favorable mesoporous morphology mesopores and not simply the specific surface area that leads to preferential ion adsorption and transport.

As a new approach ionic liquids are used as liquid component in the composites with a great potential of maintaining the high ionic conductivity and simultaneously improving the mechanical stability of these systems. Because of the higher stability they are more suitable for battery applications than previous systems.

With respect to transport phenomena therein, it could be shown that the application of a combination of various techniques (AC conductivity, DC conductivity and PFG-NMR) allows for the determination of individual contributions of ionic species to the ionic conductivity. The results show that the vehicular transport mechanism involving ion pairs and counter-motion of anions plays a significant role in Li-transference.

5 Outlook

The fundamental and applied interest in soggy-sand electrolytes is substantial as (i) a new tool-box for arriving at macroscopic properties is provided, (ii) the applicability potential in various fields is substantial. On the one hand, this class of electrolytes combines favorable electrical properties (high conductivity and lithium transference number) with excellent mechanical properties (mechanical stability, shapeability, wetting). On the other hand, due to the generality of the concept the variability of composing the actual system opens a wide field for achieving the desired physical properties. This includes the nature of solvents, salts and filler particles, but also size, shape, and surface chemistry of the fillers as well as the relative proportions, i.e., volume fraction as far as the filler is concerned and molar concentration as far as the salt is concerned. Yet, systematic research in that area is needed to a greater extent. The major weakness lies in the kinetic control of the morphology. This leads to significant problems in exactly reproducing overall conductivity effects or even getting them stationary during the window of operation. These intrinsic difficulties also appeared in the Monte-Carlo simulation.

It is to be expected that a better stationarity and thus a better reproducibility will be arrived at if a denser, percolating network is achieved. However, it is clear that the conductivity may severely drop at such high volume fractions. On the one hand there are various degrees of freedom in the preparation and sample composition to mitigate conductivity losses. On the other hand, looking at the conventional electrolytes, to enhance the overall conductivity is not the most important issue. What is more important, besides the mechanical advantages, is the substantial increase of the Li transference number.

Hence the challenge is to prepare composites with high filler fractions that are still homogeneous, locally electrically active (this may presuppose higher salt contents) and which exhibit a morphology with sufficient space charge percolation. For this purpose the idealized picture of a closely packed filler-sphere arrangement that would still offer percolation can serve as a long-term objective.

The intensification of research in that area could be more than worthwhile: viscous or solid-like but well-wetting electrolytes may be achievable with high conductivity and high transference numbers. Such electrolytes may make separators dispensable, strongly

simplifying the technology of battery fabrication. Such electrolytes can even be made transparent which is advantageous for photoelectrochemical applications.[36]

Glossary

Symbols

a   Minimum separation distance between ions

A   Surface area

B   Magnetic field strength

c   Concentration

C   Electric capacitance

d Dimensionality

d   Distance between electrodes

D Diffusion coefficient

e_0 Elementary charge

E Energy

F Faraday's constant

g   Gravitational constant

G   Strength of magnetic field gradient

i,I   Electric current

J Flux density

k Rate constant

k   Cell constant

K   Equilibrium constant

L   Length of d-dimensional space

M   Molecular mass

M Torque

m   Mass

n   Mole number

N   Number of particles

p   probability

P   Pressure

Q   Electric capacitance of a constant phase element

r   Particle radius

R   Electric resistance

s   Diffusivity of ion pairs ($D_{\pm}$) converted to conductivity units

S NMR signal intensity

t	Transference number
T	Absolute temperature
u	Ionic mobility
U	Electric voltage
V	Potential
W*	Non-Coulombic short range interaction energy
z	Ionic valence
Z	Electrical impedance
α	Degree of association / volume ratio of space charge layer to silica particle
β	Fraction of interfaces actually contributing to σ_m
γ	Gyromagnetic ratio
γ	Shear strain
δ	Mean distance between particles
δ	NMR pulse duration
Δ	Surface-to-surface distance
Δ	Time interval between two NMR pulses
Δ	Gradient
ε	Dielectric constant of the solvent
ε_0	Dielectric constant of vacuum
ζ	Zeta potential
φ	Volume fraction
η	Dynamic viscosity
κ	Reciprocal Debye length
λ	Wavelength
ρ	Gravimetric density
σ	(Ionic) conductivity
ν	Sedimentation velocity
ψ	Angle between cone and plate
ω	Frequency
μ	Electrophoretic mobility
Σ	Adsorbed charge density
τ	Relaxation time
τ	Shear stress
Ω	Surface-to-volume ratio of the particle

Indices

A	Ion pair association
b	Boiling
D	Double layer
diff	Diffusive
ex	Excess value over bulk contribution
f	Fractal
l	Liquid phase
L	Solid interphase
m	Overall
m	melting
p	Particle
pol	Polarized
s	Solid phase
S	Solvent
S	Anionic triple pair association
scl	Space charge layer
T	Cationic triple pair association
V	Volume
∞	Bulk
0	Adjacent to the particle
+	Cationic
$-$	Anionic
$\pm$	Neutral ion pair

Abbreviations

AC	Alternating current
BE	Bruce Evans method
BET	Particle surface area according to the Brunauer–Emmett–Teller technique
CPE	Constant phase element
CFM	Confocal Fluorescence Microscopy
CVI	Colloid vibration current
CVP	Colloid vibration potential

DLA	Diffusion limited aggregation
DLCA	Diffusion limited cluster aggregation
DLS	Dynamic light scattering
DMC	Dimethyl Carbonate
DMSO	Dimethyl Sulfoxide
DLVO	Derjaguin and Landau, Verwey and Overbeek theory
DSC	Differential Scanning Calorimetry
EC	Ethylene carbonate
EIS	Electrochemical Impedance Spectroscopy
HRTEM	High resolution transmission electron microscope
IEC	Ion exchange capacity
IVP	Ion vibration potential
PC	Propylene carbonate
PEG-150	Polyethylene glycol dimethyl ether
PEO	Polyethylene oxide
pzc	Point of zero charge
SEM	Scanning electron microscope
TEM	Transmission electron microscope
THF	Tetrahydrofuran

Bibliography

[1] J. M. Tarascon and M. Armand, *Nature* **2001**, *414*, 359-365.

[2] Kevin Kelly, http://kk.org/thetechnium/archives/2009/07/was_moores_law.php **2009**, visited February 13th 2014

[3] EMC Community Network and H. Crvelin, Quantum Backuptron: https://community.emc.com/people/ble/blog/2012/02/21/moores-law-limit-reached **2012**, visited February 13th 2014

[4] M. S. Whittingham, *Science* **1976**, *192*, 1126-1127.

[5] K. Mizushima, P. C. Jones, P. J. Wiseman and J. B. Goodenough, *Materials Research Bulletin* **1980**, *15*, 783-789.

[6] D. W. Murphy, F. J. Disalvo, J. N. Carides and J. V. Waszczak, *Materials Research Bulletin* **1978**, *13*, 1395-1402.

[7] M. Lazzari and B. Scrosati, *Journal of The Electrochemical Society* 1980, *127*, 773-774.

[8] Gaston Narada, *http://www.gaston-lithium.com/tech-certificates.html#e* **2005**, visited February 13th 2014,

[9] A. K. Padhi, K. S. Nanjundaswamy and J. B. Goodenough, *Journal of The Electrochemical Society* **1997**, *144*, 1188-1194.

[10] Byoungwoo Kang and Gerbrand Ceder, *Nature* **2009**, *458*, 190-193.

[11] V. S. Kolosnitsyn and E. V. Karaseva, *Russian Journal of Electrochemistry* **2008**, *44*, 506-509.

[12] J. Christensen, P. Albertus, R. S. Sanchez-Carrera, T. Lohmann, B. Kozinsky, R. Liedtke, J. Ahmed and A. Kojic, *Journal of The Electrochemical Society* **2012**, *159*, R1-R30.

[13] B. Scrosati, *Applications of Electroactive Polymers*; Chapman and Hall: London, **1993**

[14] P. M. Blonsky, D. F. Shriver, P. Austin and H. R. Allcock, *Solid State Ionics* **1986**, *18-19*, 258.

[15] S. Skaarup, K. West and B. Zachau-Christiansen, *Solid State Ionics* **1988**, *28-30*, 975-978.

[16] F. Capuano, F. Croce and B. Scrosati, *Journal of The Electrochemical Society* **1991**, *138*, 1918-1922.

[17] W. Wieczorek, Z. Florjanczyk and J. R. Stevens, *Electrochimica Acta* **1995**, *40*, 2251.

[18] F. M. Gray, *Solid polymer electrolytes: fundamentals and technological applications*; VCH Publishers, Inc.: Weinheim, **1991**.

[19] W. Xu and C. A. Angell, *Electrochimica Acta* **2003**, *48*, 2029-2035.

[20] Pierre-Jean Alarco, Yaser Abu-Lebdeh, Ali Abouimrane and Michel Armand, *Nature Materials* 2004, *3*, 476.

[21] H. J. Gores and J. Barthel, *Naturwissenschaften* **1983**, *70*, 495-503.

[22] Y. Ikeda, T. Kitade, S. Kohjiya, A. Hayashi, A. Matsuda, M. Tatsumisago and T. Minami, *Polymer* **2001**, *42*, 7225-7228.

[23] J. L. Schaefer, Y. Lu, S. S. Moganty, P. Agarwal, N. Jayaprakash and L. A. Archer, *Applied Nanoscience* **2012**, *2*, 91-109.

[24] M. Park, X. Zhang, M. Chung, G. B. Less and A. M. Sastry, *Journal of Power Sources* **2010**, *195*, 7904-7929.

[25] Y. H. Liang, C. Y. Hung and C. C. Wang, *Journal of Power Sources* **2009**, *188*, 261-267.

[26] N. Madria, T. A. Arunkumar, N. G. Nair, A. Vadapalli, Y. W. Huang, S. C. Jones and V. P. Reddy, *Journal of Power Sources* **2012**, *234*, 277-284.

[27] H. J. Gores and J. M. G. Barthel, *Pure And Applied Chemistry* **1995**, *67*, 919-930.

[28] J. E. Weston and B. C. H. Steele, *Solid State Ionics* **1982**, *7*, 75.

[29] A. J. Bhattacharyya, J. Maier, R. Bock and F. F. Lange, *Solid State Ionics* **2006**, *177*, 2565-2568.

[30] A. Jarosik, S. Hore, N. Kaskhedikar, C. Pfaffenhuber and J. Maier, *Electrochimic Acta* **2011**, *56*, 8115.

[31] A. Jarosik, C. Pfaffenhuber, A. Bunde and J. Maier, *Advanced Functional Materials* **2011**, *21*, 3961.

[32] A. Chandra and J. Maier, *Solid State Ionics* **2002**, *148*, 153.

[33] A. J. Bhattacharyya, M. Dolle and J. Maier, *Electrochemical and Solid-State Letters* **2004**, *7*, A432-A434.

[34] A. J. Bhattacharyya and J. Maier, *Advanced Materials* **2004**, *16*, 811-814.

[35] B. Kumar and S. J. Rodrigues, *Solid State Ionics* **2004**, *167*, 91.

[36] C. Pfaffenhuber, M. C. Goebel, J. Popovic and J. Maier, *Physical Chemistry Chemical Physics* **2013**, *15*, 18318-18335.

[37] J. Maier, *Progress in Solid State Chemistry* **1995**, *23*, 171.

[38] C. C. Liang, *Journal of The Electrochemical Society* **1973**, *120*, 1289.

[39] K. Shahi and J. B. Wagner, *Applied Physics Letters* **1980**, *37*, 757-759.

[40] J. Maier, *Physical Chemistry of Ionic Materials. Ions and Electrons in Solids.*; John Wiley and Sons Ltd.: Chichester, **2005**

[41] W. Wieczorek, K. Such, H. Wycislik and J. Plocharski, *Solid State Ionics* **1989**, *36*, 255.

[42] F. Croce, B. Scrosati and G. Mariotto, *Chemistry of Materials* **1992**, *4*, 1134-1136.

[43] B. Kumar and L. G. Scanlon, *Journal of Power Sources* **1994**, *52*, 261.

[44] S. Beyazyildirim, K. D. Kreuer, M. Schuster, A. J. Bhattacharyya and J. Maier, *Advanced Materials* **2008**, *20*, 1274-1278.

[45] H. P. Fritz, K. Stein and R. Herr, *Journal Of Power Sources* **1992**, *37*, 315-323.

[46] J. Fan and P. S. Fedkiw, *Journal of The Electrochemical Society* **1997**, *144*, 399.

[47] S. K. Das and A. J. Bhattacharyya, *The Journal of Physical Chemistry C* **2009**, *113*, 6699-6705.

[48] C. Pfaffenhuber and J. Maier, *Physical Chemistry Chemical Physics* **2013**, *15*, 2050-2054.

[49] J. N. Israelachvili, *Intermolecular and Surface Forces*, Academic Press **2010**.

[50] B. Derjaguin and L. Landau, *Progress in Surface Science* **1993**, *43*, 30.

[51] M. Smoluchowski, *Colloid and Polymer Science* **1916**, *18*, 48.

[52] T. A. Witten and L. M. Sander, *Physical Review Letters* **1981**, *47*, 1400-1403.

[53] T. A. Witten and L. M. Sander, *Physical Review B* **1983**, *27*, 5686-5697.

[54] J. Barthel, H. Krienke and W. Kunz, *Physical Chemistry of Electrolyte Solutions*; Steinkopff: Darmstadt, **1998**

[55] J. O. Besenhard, *Handbook of Battery Materials*; Wiley-Vch: **1999**

[56] K. Xu, *Chemical Reviews* **2004**, *104*, 4303-4418.

[57] T. P. Kumar, P. V. S. S. Prabhu, A. K. Srivastava, U. Bejoy Kumar, R. Ranganathan and R. Gangadharan, *Journal of Power Sources* **1994**, *50*, 283-294.

[58] M. Galinski, A. Lewandowski and I. Stepniak, *Electrochimica Acta* **2006**, *51*, 5567-5580.

[59] F. Hoffmann, M. Cornelius, J. Morell and M. Fröba, *Angew. Chem.* **2006**, *118*, 3290.

[60] L. Thiberville, S. Moreno-Swirc, T. Vercauteren, E. Peltier, C. Cave and G. B. Heckly, *American Journal of Respiratory and Critical Care Medicine* **2007**, *175*, 22-31.

[61] Light Microscopy Core Facility Duke University and Duke University Medical Center, http://microscopy.duke.edu/ **2013**, visited February 13th 2014.

[62] S. Brunauer, P. H. Emmett and E. Teller, *Journal of the American Chemical Society* **1938**, *60*, 309-319.

[63] Abragam, Oxford University Press London: **1985**.

[64] A. Telfah, University of Stuttgart, PhD Thesis: **2008**.

[65] D. A. Mac Innes and L. G. Longsworth, *Chemical Reviews* **1932**, *11*, 171-230.

[66] K. Kontturi, S. Mafe, J. A. Manzanares, J. Pellicer and M. Vuoristo, *Journal of Electroanalytical Chemistry* **1994**, *378*, 111-116.

[67] C. Wagner, *The Journal of Chemical Physics* **1950**, *18*, 62-68.

[68] M. H. Hebb, *The Journal of Chemical Physics* **1952**, *20*, 185-190.

[69] I. Yokota, *Journal of the Physical Society of Japan* **1961**, *16*, 2213-2223.

[70] J. Maier, *Zeitschrift Fur Physikalische Chemie Neue Folge* **1984**, *140*, 191-215.

[71] J. Evans, C. A. Vincent and P. G. Bruce, *Polymer* **1987**, *28*, 2324-2328.

[72] P. G. Bruce, J. Evans and C. A. Vincent, *Solid State Ionics* **1988**, *28-30*, 918.

[73] Paavan Kumar, P. C. Kapur and D. N. Saraf, *Colloid and Polymer Science* **1975**, *253*, 738-743.

[74] P. Debye and E. Hueckel, *Physikalische Zeitschrift* **1923**, *24*, 185-206.

[75] Andrei S. Dukhin and Philip J. Goetz, *Ultrasound for Characterizing Colloids. Particle Sizing, Zeta Potential, Rheology*; Elsevier B.V.: Amsterdam, **2002**

[76] A. S. Dukhin, H. Ohshima, V. N. Shilov and P. J. Goetz, *Langmuir* **1999**, *15*, 3445-3451.

[77] A. S. Dukhin, V. N. Shilov, H. Ohshima and P. J. Goetz, *Langmuir* **1999**, *15*, 6692-6706.

[78] F. Booth, *Proceedings of the Royal Society of London. Series A. Mathematical and Physical Sciences* **1950**, *203*, 533-551.

[79] R. W. O'Brien, *Journal of Fluid Mechanics Digital Archive* **1988**, *190*, 71-86.

[80] P. Prentice, I. Smithers Rapra Publishing: **1995**.

[81] N. Metropolis and S. Ulam, *Journal of the American Statistical Association* **1949**, *44*, 335-341.

[82] B. H. Kaye, *A Random Walk Through Fractal Dimensions*; VCH Verlagsgesellschaft: Weinheim (Germany), **1989**.

[83] S. Ulam and J. Von Neumann, *Bulletin of American Mathematical Society* **1945**, *51*, Abstract 165.

[84] Benoit B. Mandelbrot, *The Fractal Geometry of Nature*; W.H. Freeman and Company: New York, **1983**.

[85] D. A. Weitz and M. Oliveria, *Physical Review Letters* **1984**, *52*, 1433.

[86] W. Y. Shih, J. Liu, W. H. Shih and I. A. Aksay, *Journal of Statistical Physics* **1991**, *62*, 961-983.

[87] P. Meakin, *Physical Review Letters* **1983**, *51*, 1119-1122.

[88] M. Kolb, R. Botet and R. Jullien, *Physical Review Letters* **1983**, *51*, 1123-1126.

[89] W. C. K. Poon and M. D. Haw, *Advances in Colloid and Interface Science* **1997**, *73*, 71-126.

[90] A. Bunde, W. Dieterich and E. Roman, *Solid State Ionics* **1986**, *18-19*, 147-150.

[91] A. Bunde and S. Havlin, *Fractals and Disordered Systems*; Springer-Verlag Berlin: Heidelberg, **1991**

[92] A. Jarosik, U. Traub, A. Bunde and J. Maier, *Physical Chemistry Chemical Physics* **2011**, *13*, 2663.

[93] J. Maier, *Physical Chemistry of Ionic Materials*; John Wiley & Sons Ltd.: England, **2004**

[94] C. E. Goodyer, J. S. Fish, J. D. Fehribach, R. O'Hayre and A. L. Bunge, *Electrochimica Acta* **2011**, *56*, 9295.

[95] C. Pfaffenhuber, S. Beyazyildirim, K. Weichert, M. Bele, T. Mundinger, M. C. Goebel and J. Maier, *Journal of the American Chemical Society* **2011**, *133*, 14514.

[96] P. Meakin, *Physical Review A* **1983**, *27*, 1495-1507.

[97] P. Meakin, *Physical Review B* **1984**, *29*, 2930.

[98] W. B. Russel, A. B. Saville and W. R. Schowalter, *Colloidal Dispersions*; Cambridge University Press: New York, **1989**.

[99] F. Elsholz, E. Schoell and A. Rosenfeld, *Physica Status Solidi* 2007, *244*, 3639.

[100] W. K. Hastings, *Biometrika* **1970**, *57*, 97-109.

[101] N. Metropolis, A. W. Rosenbluth, M. N. Rosenbluth, A. H. Teller and E. Teller, *The Journal of Chemical Physics* **1953**, *21*, 1087-1092.

[102] M. Müller and K. Albe, *Beilstein Journal of Nanotechnology* **2011**, *2*, 40.

[103] J. Maier, *Advanced Functional Materials* **2011**, *21*, 1448-1455.

[104] M. Bele, O. Siiman and E. Matijevic, *Journal of Colloid and Interface Science* **2002**, *254*, 274-282.

[105] R. Notari and J. L. M. Abboud, *Pure and Applied Chemistry* **1999**, *71*, 645-718.

[106] V. N. Shilov, Y. B. Borkovskaja and A. S. Dukhin, *Journal of Colloid and Interface Science* **2004**, *277*, 347.

[107] S. R. Raghavan, H. J. Walls and S. A. Khan, *Langmuir* **2000**, *16*, 7920-7930.

[108] P. K. Muhuri, B. Das and D. K. Hazra, *Journal of Physical Chemistry B* **1997**, *101*, 3329-3332.

[109] S. K. Das, S. S. Mandal and A. J. Bhattacharyya, *Energy & Environmental Science* **2011**, *4*, 1391.

[110] J. Morell, M. Guengerich, G. Wolter, J. Jiao, M. Hunger, P. J. Klar and M. Fröba, *J. Mater. Chem.* **2006**, *16*, 2809.

[111] K. Sann, J. Roggenbuck, N. Krawczyk, H. Buschmann, B. Luerssen, M. Froeba and J. Janek, *Electrochimica Acta* **2012**, *60*, 1.

[112] S. Kim, A. Karkamkar and T. J. Pinnavaia, *Journal of Physical Chemistry B* **2001**, *105*, 7663.

[113] D. H. Barich, T. Xu, J. Zhang and J. F. Haw, *Angew. Chem. Int. Ed.* **1998**, *37*, 2530-2531.

[114] J. W. Goodwin and R. W. Hughes, *Rheology for Chemists. An Introduction.*; The Royal Society of Chemistry: Cambridge, **2000**.

[115] C. Pfaffenhuber, F. Hoffmann, M. Fröba, J. Popovic and J. Maier, *Journal of Materials Chemistry A* **2013**, *1*, 12560-12567.

[116] R. W. Impey, M. Sprik and M. L. Klein, *J. Am. Chem. Soc.* **1987**, *109*, 5900-5904.

[117] M. Armand, F. Endres, D. R. MacFarlane, H. Ohno and B. Scrosati, *Nature Materials* **2009**, *8*, 621-629.

[118] N. A. Stolwijk and S. Obeidi, *Physical Review Letters* **2004**, *93*, 125901.

[119] P. G. Bruce and C. A. Vincent, *Journal of Electroanalytical Chemistry* **1987**, *225*, 1.

[120] J. Maier, *Physica Status Solidi* **1984**, *123*, K89-K91.

[121] J. Maier, *Journal of the American Ceramic Society* **1993**, *76*, 1212-1217.

[122] J. Maier, *Journal of the American Ceramic Society* **1993**, *76*, 1218-1222.

[123] J. Maier, *Journal of the American Ceramic Society* **1993**, *76*, 1223-1227.

[124] J. Maier, *Journal of the American Ceramic Society* **1993**, *76*, 1228-1232.

[125] N. Kaskhedikar, J. Paulsdorf, A. Burjanadze, Y. Karatas, B. Roling and H. D. Wiemhofer, *Solid State Ionics* **2006**, *177*, 2699-2704.

Acknowledgements

Curriculum vitae

Christian Pfaffenhuber

Max-Planck-Institute for Solid State Research
Heisenbergstr. 1
70569 Stuttgart, Germany
Tel. 0711/6891725
Mobile: 0177/6031394
Fax: 0711/6891722
E-Mail: c.pfaffenhuber@gmx.de

Personal
Born on May 23rd 1985 in Passau, Germany
Married, one daughter

Education

12/2009-02/2014	Doctoral Degree at Max-Planck-Institute for Solid State Research in the Department of Prof. Maier and at the University of Stuttgart
10/2004-09/2009	Diploma Degree in Chemistry at the University of Regensburg in cooperation with the Max-Planck-Institute for Solid State Research in the Department of Prof. Maier, supervisor: Prof. Pfitzner, Topic: Investigations of Lithium ion conduction heterogeneous polyethylene glycol electrolytes

Employment

02/2008	Linde AG in München, Höllriegelskreuth, Occupation: Dimensioning of Batch-Reactors in a H_2-plant, development of a software to determine the performance-cost relationship for plant components
11/2007	Dechema-Seminar and internship in electrochemistry at the Karl-Winnacker-Institute in Frankfurt am Main, Occupation: Introduction to Impedance Spectroscopy, Material testing
08/2004	Wacker Chemie GmbH in Burghausen, Occupation: Assistance in synthesis procedures for special chemicals and in instrumental analytics
07/2004	Bayern-Chemie Protac in Aschau / Inn, Occupation: analytics of rocket fuel materials and assistance in processing of a large-scale synthesis process

Publications

A. Jarosik, S. Hore, N. Kaskhedikar, C. Pfaffenhuber, and J. Maier, *Electrochimica Acta* **56**(24), 8115–8121 (2011).

A. Jarosik, C. Pfaffenhuber, A. Bunde, and J. Maier, *Advanced Functional Materials* **21**(20), 3961–3966 (2011).

C. Pfaffenhuber, S. Sörgel, K. Weichert, M. Bele, T. Mundinger, M. Göbel, and J. Maier, *Journal of the American Chemical Society* **133**(37), 14514–14517 (2011).

C. Pfaffenhuber and J. Maier, *Physical Chemistry Chemical Physics* **15**(6), 2050–2054 (2013).

C. Pfaffenhuber, F. Hoffmann, M. Fröba, J. Popovic, and J. Maier, *Chemistry of Materials A* **1**(40), 12560-12567 (2013).

C. Pfaffenhuber, M. Göbel, J. Popovic, and J. Maier, *Physical Chemistry Chemical Physics* **15**(42), 18318-18335 (2013).

C. Pfaffenhuber, J. Popovic, C. Cavalca de Araujo, J. Melchior and J. Maier, *in preparation*.

Conferences

04/2013	3rd International Colloids and Energy Conference, Xiamen, China (poster)
08/2012	ISPE-13 XIII International Symposium on Polymer Electrolytes, Selfoss, Island (oral presentation)
07/2011	10th International Conference on Materials Chemistry, Manchester, Großbritannien (poster)
06/2011	110. Bunsentagung der Gesellschaft für Physikalische Chemie, Berlin (poster with award)
06/2011	85th Annual Symposium on Colloid and Surface Science, Montreal, Kanada (oral presentation)

06/2011   International Conference on Materials for Advanced Technologies, Suntec, Singapur (poster)